

NRL REPORT R-3358

COPY NO.

UPPER ATMOSPHERE RESEARCH
REPORT NO. V



PLEASE RETURN THIS COPY TO:

NAVAL RESEARCH LABORATORY
WASHINGTON, D.C. 20375
ATTN: CODE 2628

Because of our limited supply you are requested to return this copy as soon as it has served your purposes so that it may be made available to others for reference use. Your cooperation will be appreciated.

NDW-NRL-5070/2651 (Rev. 9-75)



NAVAL RESEARCH LABORATORY

WASHINGTON, D.C.

**APPROVED FOR PUBLIC
RELEASE - DISTRIBUTION
UNLIMITED**

UPPER ATMOSPHERE RESEARCH

REPORT NO. V

Compiled and Edited by
H. E. Newell, Jr. and J. W. Siry

June 17, 1948

Approved by:

Dr. J. M. Miller, Superintendent, Radio Division I



NAVAL RESEARCH LABORATORY

CAPTAIN H. A. SCHADE, USN, DIRECTOR

WASHINGTON, D.C.

**APPROVED FOR PUBLIC
RELEASE - DISTRIBUTION
UNLIMITED**

ABSTRACT

This report describes upper atmosphere research at the Naval Research

Laboratory during the last three quarters of 1947 and the first quarter of 1948. A detailed study of the solar spectra obtained during the V-2 flights of October 10, 1946, and March 7 and October 9, 1947, is given. The experiments performed in the missiles fired on May 15, July 10 and October 9, 1947, and January 22, 1948, are discussed. A description is provided of the experimental techniques and apparatuses which were employed. Results in cosmic ray research and pressure and temperature studies are presented. A mathematical analysis of the geometry of cosmic ray Geiger counter telescopes is given.

STATUS OF THE PROBLEMS

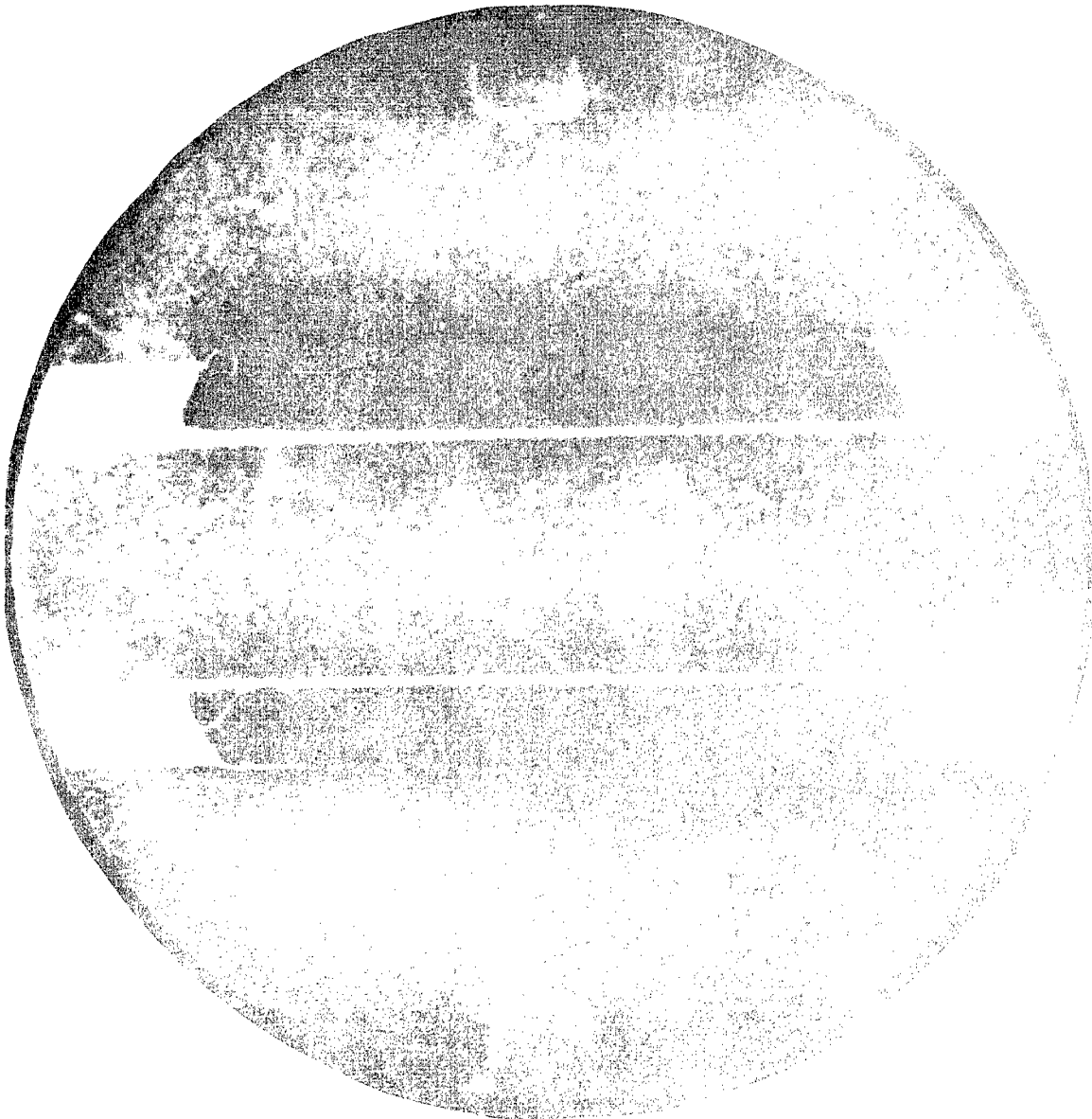
This is an interim report on the problems listed below; work on all these problems is continuing.

AUTHORIZATION

N26-02, P26-04, R10-20, R25-02, R25-01.

CONTENTS

	Page
Abstract	iv
Status of the Problems	iv
Authorization	iv
 INTRODUCTION	 1
CHAPTER I. THE FIFTH, SIXTH AND SEVENTH CYCLES OF V-2 FIRINGS	2
CHAPTER II. ANALYSIS OF THE FIRST ROCKET ULTRAVIOLET SPECTRA - E. Durand, J. J. Oberly and R. Tousey	7
CHAPTER III. THE V-2 AS A RESEARCH VEHICLE	29
Introduction	29
A. Instrumentation Techniques Employed in the V-2 Rockets Fired on May 15, and July 10, 1947 and January 22, 1948 - T. A. Bergstralh and C. P. Smith	29
B. Rocket Attitude Determination by Means of Gyroscopes - H. Spitz	38
CHAPTER IV. THE COSMIC RAY EXPERIMENTS	44
Introduction	44
A. The Counter Telescope Experiment of May 15, 1947 - B. Howland, G. J. Perlow and J. D. Shipman, Jr.	45
B. The Counter Telescope Experiment of July 10, 1947 - S. E. Golian and E. H. Krause	50
C. Electronics for the Counter Telescope Experiments - B. Howland, C. A. Schroeder and J. D. Shipman, Jr.	51
D. The Cloud Chamber - S. E. Golian, C. Y. Johnson, E. H. Krause and M. L. Kuder	58
E. Equipment for the Automatic and Remote Control of the Cloud Chamber - C. Y. Johnson, M. L. Kuder and C. A. Schroeder	65
1. The Automatic Control Equipment	65
2. The Remote Control Equipment	67
CHAPTER V. GEOMETRIC FACTORS UNDERLYING COINCIDENCE COUNTING WITH GEIGER COUNTERS - H. E. Newell, Jr.	71
CHAPTER VI. ATMOSPHERIC STUDIES AT VERY HIGH ALTITUDES	87
Introduction	87
A. A Wire Accelerometer - R. J. Havens and H. E. LaGow	88
B. The Pressure and Temperature of the Upper Atmosphere on January 22, 1948 - N. R. Best, D. I. Gale, R. J. Havens and H. E. LaGow	90



The first cloud chamber photograph ever taken at an altitude of 145 kilometers. This exceeds by more than 100 kilometers the altitude of the highest cloud chamber photographs obtained before the January 22, 1948 V-2 flight. A highly ionizing particle traversing both lead plates is visible. Its scattering, ionization and penetrating power indicate that it is an alpha particle having an energy greater than 500 million electron volts. It is presumably a primary particle.

UPPER ATMOSPHERE RESEARCH

REPORT NO. V

INTRODUCTION

The Naval Research Laboratory conducted upper air studies in four of the six research V-2's which were fired by Army Ordnance at its White Sands Proving Ground between May 15, 1947, and January 22, 1948. On only one of these four flights did the V-2 deliver the research instrumentation into the upper atmosphere in operating condition while providing a reasonably stable platform from which to make measurements and observations. This was almost a complete reversal of the Laboratory's experience in its first five V-2 firings. Only one of these had resulted in a poor flight from the standpoint of the requirements of the upper atmosphere research program.

During this period a comprehensive analysis of the ultraviolet spectrum of the sun was completed. Solar spectrograms were obtained by the Laboratory on three occasions during the first two years of rocket-sonde research. These spectra, exposed on October 10, 1946, and March 7, and October 9, 1947, were all analyzed in great detail. The findings will be published in The Astrophysical Journal.¹ This paper is reproduced here in Chapter II. An analysis of the geometry of cosmic ray counter telescopes was published in The Review of Scientific Instruments,² and is presented here in Chapter V. Special attention was given to the main problem of rocket instrumentation. In particular, means for accurate determination of aspect were investigated.

A fresh approach to the problem of studying the ionosphere was made on July 10, 1947, when two new experiments were attempted for the first time. They made use of a positive ion gage which was mounted at the nose of the missile and a generating voltmeter which was installed in the midsection. These experiments will be reported upon later. An account of the pressure measurements made on January 22, 1948, is given in Chapter VI. The pressure and temperature observations of the latter date were the first ever to be made at very high altitudes during midwinter.

The many problems which are associated with the use of a cloud chamber are further multiplied and complicated when this delicate instrument is operated in a rocket. The difficulties were overcome, to a large extent, in the V-2 flight of January 22, 1948. On that day were obtained the first cloud chamber photographs of cosmic ray events ever taken above the earth's atmosphere. One of these, exposed at an altitude of 145 kilometers, appears in the Frontispiece. Chapter IV contains a description of the cloud chamber, and discussions of the counter telescope studies which were made on May 15 and July 10, 1947.

¹E. Durand, J. J. Oberly and R. Tousey, Astrophys. J., (1948).

²Homer E. Newell, Jr., Rev. Sci. Instr. 19, 384, (1948).

CHAPTER I

THE FIFTH, SIXTH AND SEVENTH CYCLES OF V-2 FIRINGS

The fifth cycle of V-2 firings was to have begun with missile no. 25. Actually, the fifth cycle consisted of V-2 no. 26, launched on May 15, 1947, while missile no. 25 was not fired until the end of the seventh cycle, on April 2, 1948. In the months between, eight additional V-2's, including five upper atmosphere research rockets, were flown.

Five of the seven research missiles launched in these three cycles carried scientific equipment installed by the Naval Research Laboratory. This report deals with all but the last of these five flights. The essential details of the firings in the three cycles are given in Table I. The four flights treated in this report will be described in somewhat greater detail.

The single upper atmosphere research rocket of the fifth cycle was launched at 4:10 P.M., M.S.T. on May 15, 1947. Soon after take-off the missile began to turn toward the east. An explosion occurred in the rocket after sixty-four seconds of flight when the rocket had an altitude of thirty-three kilometers (twenty-one miles). The cause of this accident was not determined. The rocket reached a maximum altitude of 135 kilometers (84 miles) and landed near Alamogordo. The spectrograph, the cosmic ray recording camera, the two K-25 cameras mounted in the midsection, and the two gun cameras mounted in the tail were all recovered.

All available evidence points to the fact that no power was supplied to the research instrumentation after the explosion. No telemetering transmission was received after this time. The cameras were examined and it was found that their motors had stopped simultaneously when the mishap occurred.

The sixth cycle opened with the launching of V-2 missile no. 29¹ on July 10, 1947. Beginning with this firing more elaborate methods and apparatus for predicting the location of the impact area were employed. It became clear very early in the flight that the rocket would land outside the firing range if powered flight were allowed to continue until the fuel was spent. Accordingly, the NRL emergency cutoff system² was used to

¹This was actually the twenty-fifth White Sands V-2 launching, and the twenty-sixth missile expended, the first missile having been expended in a static firing test. Due to postponements, etc., missile numbers bear no direct relation to the firing order after the fourth cycle.

²Cf. Naval Research Laboratory Report No. R-2955, Chapter II, Section B.

TABLE I
SUMMARY OF THE FIFTH, SIXTH AND SEVENTH CYCLES OF V-2 FIRINGS
May 15, 1947 through April 2, 1948

Firing	Mis- file	Date	Research Agencies	Altitude		Range		Remarks
				Km.	Mi.	Km.	Mi.	
<u>The Fifth Cycle</u>								
25	26	May 15, 1947	Naval Research Laboratory	135	84	72	45	Internal explosion occurred 64 seconds after take-off. No research equipment operated after this time. Complete recovery was effected.
<u>The Sixth Cycle</u>								
26	29	July 10, 1947	Naval Research Laboratory	16	10	3	2	Emergency cutoff applied 32 seconds after take-off. Nothing of value recovered due to impact explosion.
27	30	July 29, 1947	Applied Physics Laboratory	161	100	5	3	Successful flight. Recovery very satisfactory.
28	27	Oct. 9, 1947	General Electric Company, Signal Corps, Naval Re- search Laboratory	156	97	51	32	Internal explosion occurred 84 seconds after take-off. The NRL spectrograph did not operate after this time; but, it was recovered in good condition.
29		Nov. 20, 1947	General Electric Company	22	14	3	2	Rocket power plant failed after 39 seconds of flight. American-made components functioned satisfactorily.
30	28	Dec. 8, 1947	Air Materiel Command	105	65	45	28	Exceptionally stable flight.
<u>The Seventh Cycle</u>								
31	34	Jan. 22, 1948	Naval Research Laboratory	159	99	77	48	Attempt to spin rocket was unsuccessful. Cosmic ray cloud chamber photographs were obtained for the first time on this flight.
32	36	Feb. 6, 1948	General Electric Company	111	69	5	3	Successful flight.
33	39	Mar. 19, 1948	General Electric Company	5	3	3	2	Low altitude attributed to failure of one of the rocket motor components.
34	25	Apr. 2 1948	Signal Corps, Naval Research Laboratory	145	90	77	48	Very successful flight. Control chamber blowoff resulted in excellent recovery.



Fig. 1. The explosion resulting from the impact of the V-2 fired on July 10, 1947. This view was taken from the blockhouse area, more than two and one-half kilometers away.

terminate the operation of the rocket motor thirty-two seconds after take-off. This V-2 reached a maximum altitude of only sixteen kilometers (ten miles) after seventy seconds of flight. The unusual nature of the flight made it impossible to blow off the warhead. As a result, the rocket landed intact, at a distance of less than 2,700 meters from the launching platform. More than four tons of propellant were in the tanks when the impact occurred. The explosion (cf. Fig. 1) which took place precluded the possibility of recovering anything of value.

V-2 missile no. 27, originally scheduled to be fired on June 13, 1947, was launched at 12:15 P.M., M.S.T. on October 9, 1947. This rocket developed a spin of fifty-seven rpm during the ten seconds before Brennschluss. An internal explosion occurred at an altitude of sixty-five kilometers (forty miles) after eighty-four seconds of flight. The spectrograph motor did not operate after this happened. The instrument was recovered, however, and in good condition.

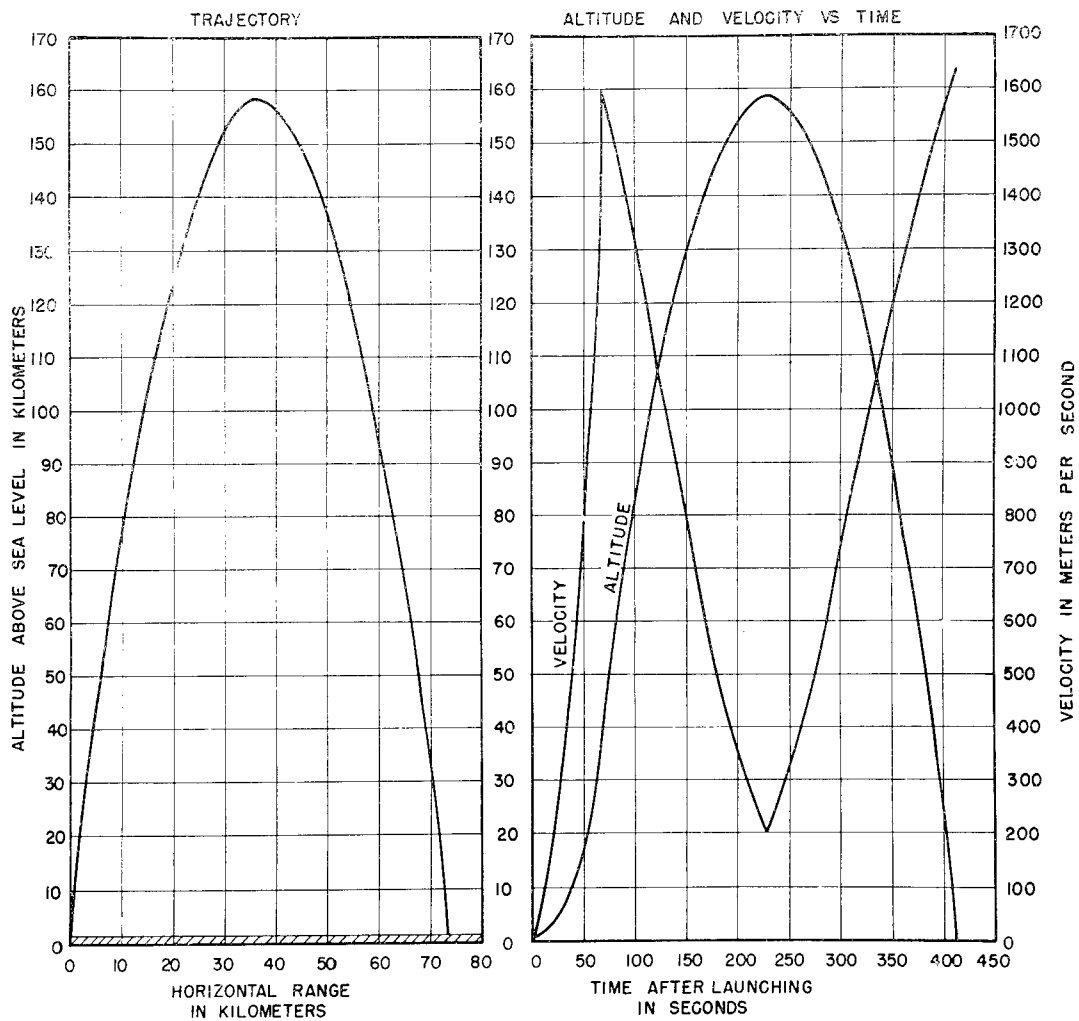


Fig. 2. Trajectory information for the V-2 flight of January 22, 1948 .

The first V-2 to be fired in 1948, the eighth Naval Research Laboratory rocket, was launched at 1:12 P.M., M.S.T. on January 22. An attempt was made to introduce a one rps spin into the rocket's motion by means of four jato units mounted in the midsection. These appear to have fired at the proper time shortly after Brennschluss. The telemetering record showed that the firing signals actually were given by the timer, and some observers reported that they had seen puffs of smoke issuing from the rocket at about this time. Telephotographs of the flight did not show the smoke puffs, however. The jato shells were recovered in a condition which indicated that the units had fired. Nevertheless, the rocket spun at the rate of only two rpm during the free fall period.

A maximum altitude of 159 kilometers (99 miles) was attained after 232 seconds of flight. The signal for warhead blowoff was given by radio at 310 seconds after take-off. It was also given fifteen seconds later by a timer in the rocket. The instrumentation and the telemetering continued to operate, however, until the rocket apparently exploded after 409 seconds of flight at an altitude of only 400 meters. Detailed trajectory information appears in Fig. 2. The cosmic ray cloud chamber film was recovered. The warhead impact crater can be seen in Fig. 3, and the cloud chamber film canister is shown in Fig. 37.

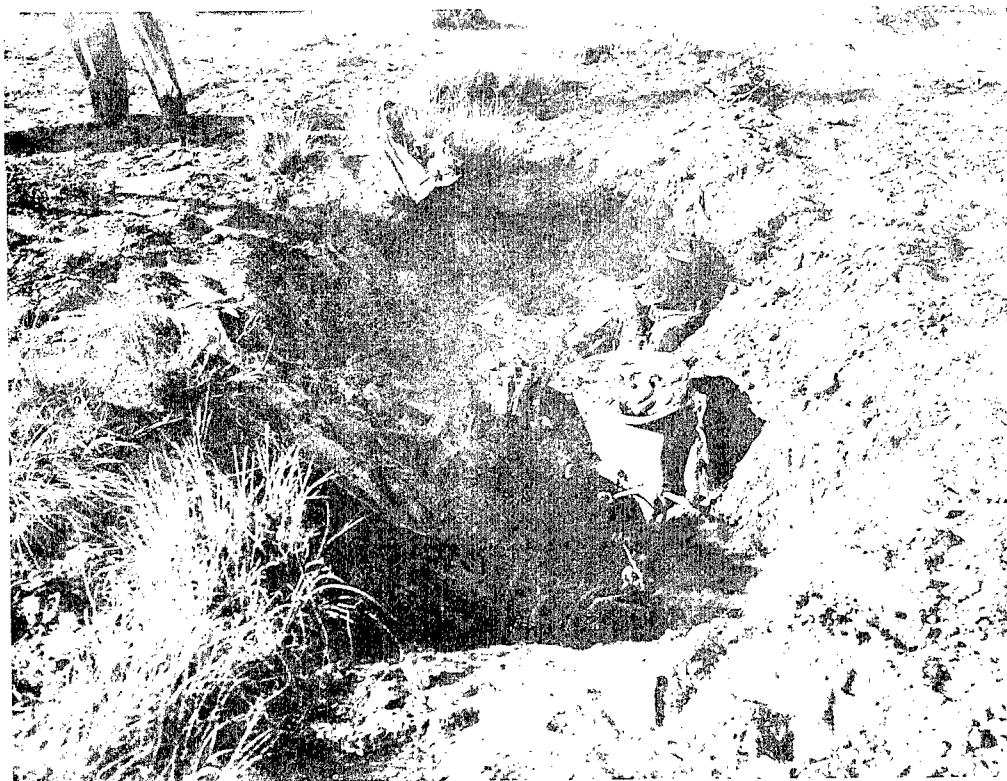


Fig. 3. The impact crater dug by the warhead of the V-2 fired on January 22, 1948 .

CHAPTER II

ANALYSIS OF THE FIRST ROCKET ULTRAVIOLET SPECTRA*

by

E. Durand, J. J. Oberly and R. Tousey¹

ABSTRACT

Solar spectra obtained from V-2 flights on October 10, 1946^{2,3} and March 7, 1947^{4,5,6} were analyzed. The spectrum in the hitherto unobserved region from 2900 Å to 2200 Å was found to be intensely complex and filled with unresolved blends. The low resolution (1.5 Å) made positive identification difficult in many instances. Tables showing the wave length, visual estimated intensities, character and identification of the lines observed are given. Reproduction of densitometer traces are given and part of the spectrum is shown replotted on an intensity scale.

Certain multiplets of Fe I, Fe II, Si I, and Mn II appeared in great strength. Four lines, Si I, 2882 Å, Mg I, 2852 Å, Mg II 2803 Å, and Mg II 2796 Å, were very broad, similar to H and K of Ca II. The Mg II pair showed a central core of emission of great strength. The structure between 2200 Å and 2300 Å could not be interpreted in terms of atomic lines, and may be caused by atmospheric bands of NO.

SECTION I - Introduction

The first successful attempt to photograph the sun's spectrum from above the ozone layer was made at White Sands, New Mexico, on October 10, 1946,^{2,3} using a vacuum grating spectrograph designed at the Naval Research Laboratory and installed in the tail fin of a German V-2 rocket. Radiation

* This article has been accepted for publication in the Astrophysical Journal.

¹Head of the Micron Waves Section of the Optics Division. This program was carried out jointly by the Micron Waves Section of the Optics Division, E. O. Hulburt, Superintendent; and the Rocket-Sonde Research Section, H. E. Newell, Jr., Head, of Radio Division I, J. M. Miller, Superintendent.

²W. A. Baum, F. S. Johnson, J. J. Oberly, C. C. Lockwood, C. V. Strain, and R. Tousey, Phys. Rev. 70, 781 (1946).

³Naval Research Laboratory Report No. A-3030, Chapter IV, Section A.

⁴E. Durand, J. J. Oberly, and R. Tousey, Phys. Rev. 71, 827 (1947).

⁵Naval Research Laboratory Report No. R-3120, Chapter II, Section A.

⁶Naval Research Laboratory Report No. R-3171, Chapter V.

was observed down to wave lengths as short as 2100 Å. A second flight on 7 March 1947^{4,5,6} gave spectra of considerably improved resolution. During April of that year the Applied Physics Laboratory of the Johns Hopkins University launched a rocket carrying a spectrograph equipped with a servo-controlled mirror designed to track the sun in one axis. An analysis of the excellent spectra they obtained has now been published.⁷ A third successful flight with a Naval Research Laboratory instrument was made on October 9, 1947. This report is an extension of the analysis already published⁴ of the spectra obtained on the flights sponsored by this laboratory.

SECTION II - The Spectrograph

The spectrograph was designed at the Naval Research Laboratory and built by Baird Associates in Cambridge, Massachusetts. It is shown in Figs. 4 and 5. It has previously been described in detail^{3,8} but since these reports are not generally available a brief description will be given here.

The rocket is vertical when launched and remains so during the accelerating period of about one minute. For the balance of the flight it is uncontrolled and its orientation with respect to the sun may vary greatly, depending on its chance residual angular momentum at fuel burnout. For mid-day flights, the spectrograph is mounted with its cone axis vertical in either the east or the west tail fin. It is provided with two optical entrance axes, one aimed north, the other south, pointing to the sun. Both axes are 45° down from the zenith. Either axis may be used to obtain spectra, the former serving, if by chance the rocket rolls 180° about its axis.

To increase further the acceptance angle of the spectrograph, 2 mm spheres of lithium fluoride are used to collect radiation in place of the usual condenser and slit or the ground quartz diffusion plate and slit that has been used on other rocket spectrographs.⁷ A solar image - about 0.013 mm in diameter - is formed behind the spheres and acts effectively as a narrow slit.

This arrangement permits useable spectra to be obtained with the sun as much as 70° in any direction away from either axis. It suffers from the drawback, however, that there is some defocussing for large angles, and that changes in solar position during an exposure produce a displacement of the solar image and a blurring of the spectrum, especially for displacements parallel to the dispersion. The advantage in speed over the diffusing system, however, is tremendous.

⁷John J. Hopfield and Harold E. Clearman, Jr., Phys. Rev. 73, 877 (1948).

⁸Naval Research Laboratory Report No. 2955, Chapter III, Section H.

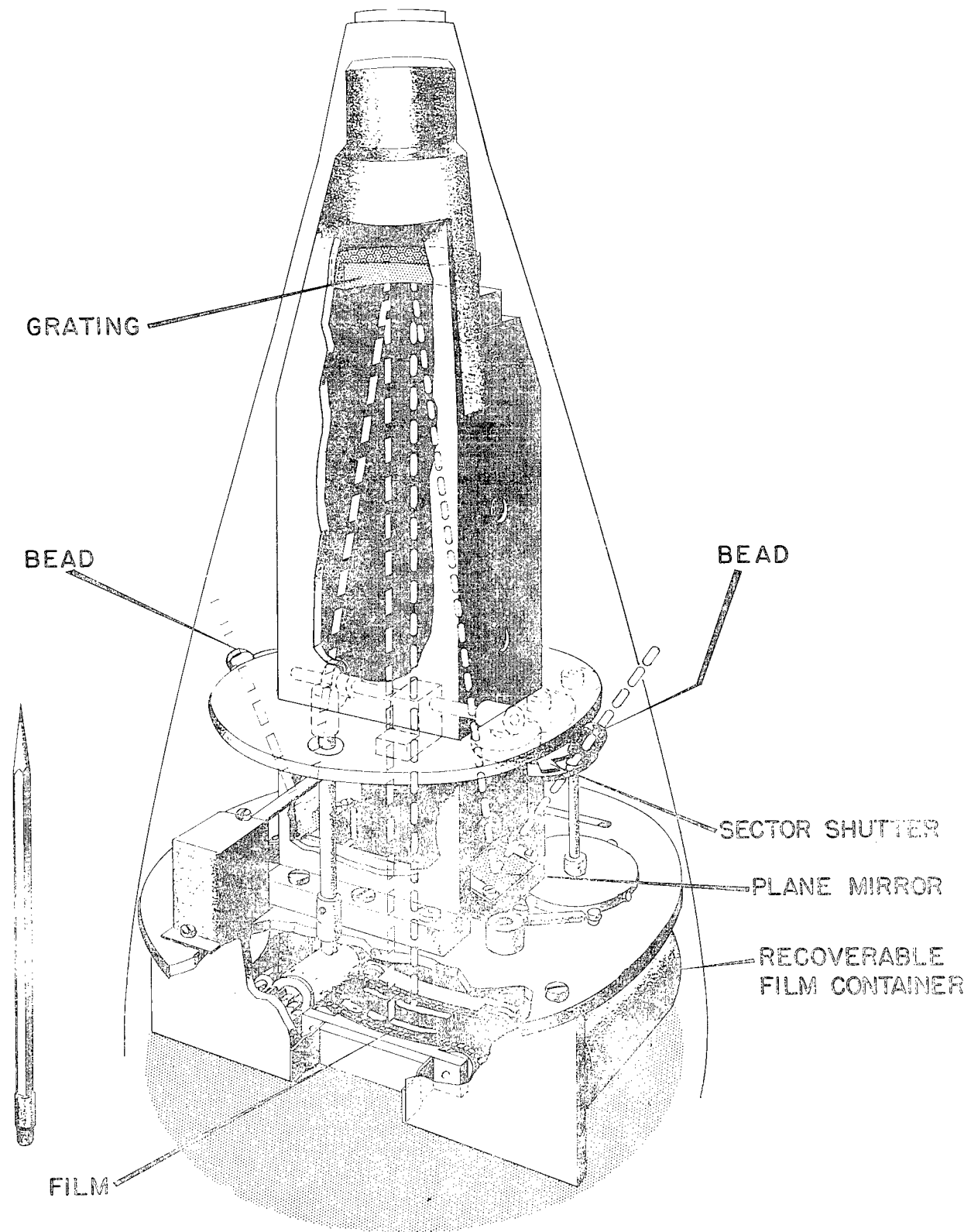


Fig. 5. Schematic diagram of rocket spectrograph.

After leaving the bead, the radiation falls on a small mirror and is reflected back to a concave grating at the apex of the cone. The grating, whose radius of curvature is 40 cm, is ruled with 15,000 lines per inch on aluminized glass. It focuses the spectrum on the 35 mm film which lies on the Rowland circle at the base of the instrument.

The spectra from the two beads are displaced to either side of the median plane by a slight tilting of the small mirrors. If plane mirrors are used, the spectrum lines will be about 1 mm high because of the astigmatism characteristic of this mounting. If cylindrical mirrors are used, the astigmatism may be entirely eliminated at one wavelength and greatly reduced at other wavelengths. The resulting reduction in height of the spectrum increases the photographic density obtained for a given exposure and usually reduces the blurring action referred to above. On the other hand, densitometry of the spectra becomes most difficult because of the changing height of the spectral lines at different wavelengths. There is also some loss of effective resolution because of the graininess of the photographic film.

In spectrum No. 43 taken at 75 km on March 7, 1947 the roll of the rocket during the exposure was such that the spectrum moved perpendicular to the plane of dispersion. This fortunate chance gave a resolution nearly as good as the best obtained in the laboratory, and most of the analysis presented in this report was based on this particular spectrum. It is reproduced in Fig. 6.

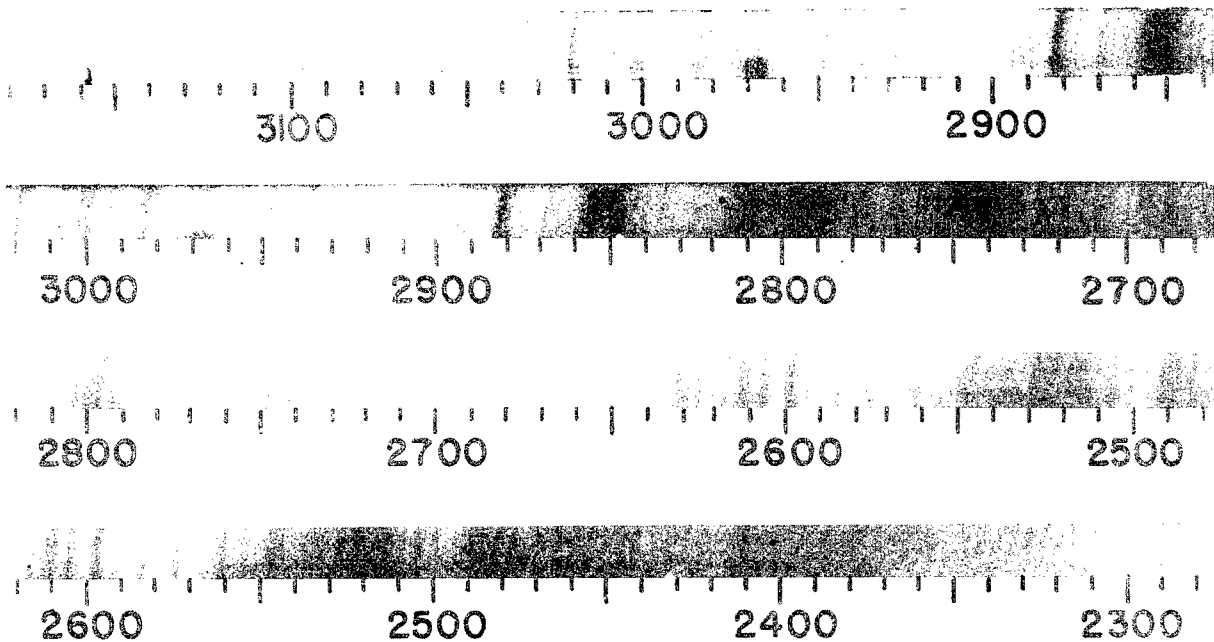


Fig. 6. Solar ultraviolet spectrum from 3180 Å to 2350 Å. Note the Mg II emission lines at 2796 Å and 2803 Å (line 3 of the spectrum).

The instrument was equipped with a motor driven shutter and film transport mechanism which automatically provided exposures of 0.1, 0.6, and 3.0 seconds. This exposure cycle was repeated over and over until the rocket was well past the top of the flight, after which the remaining film, if any, was wound up into an armor steel cassette. Eastman ultraviolet sensitized type 103-0 film was used.

SECTION III - The Spectra

Because of the changes in rocket orientation referred to above, many of the spectra were either blurred or of low density. Densitometer traces of three of the best spectra are reproduced in Fig. 7.

Fig. 7A is the trace of the high-resolution spectrum of Fig. 6.

Fig. 7B is the trace of a spectrum taken at 35 km on October 10. It was not used in the analysis, but is of interest since it shows the shortest solar wavelengths observed - 2100 Å or less - and also shows the often-predicted "window" in this region between the absorption bands of O₂ and O₃. The radiation between 2300 Å and 2630 Å is absorbed by the residual ozone above the spectrograph.⁹

Fig. 7C is the trace of another October 10 spectrum, taken at 55 km. At this altitude less than 1% of the total ozone remained between the instrument and the sun so that the entire spectral region obscured at 35 km may be seen.

SECTION IV - Wavelengths

Most of the wavelength determinations are based on visual comparator observations. A few unresolved and weak lines showing up on the tracings in the short wavelength regions were taken from the densitometer traces. These are denoted by a D following the observed wavelengths in Table II.

Several determinations were made by independent observers. The constants for the wavelength equation were chosen to give the best overall fit for fourteen strong lines of Fe I and Fe II distributed through the spectrum. The probable wavelength error for other lines varies from 0.2 Å to 1.0 Å depending on sharpness and freedom from blending.

⁹This film together with others taken at different altitudes on the same flight were used to determine the vertical distribution of ozone in the earth's atmosphere.⁶

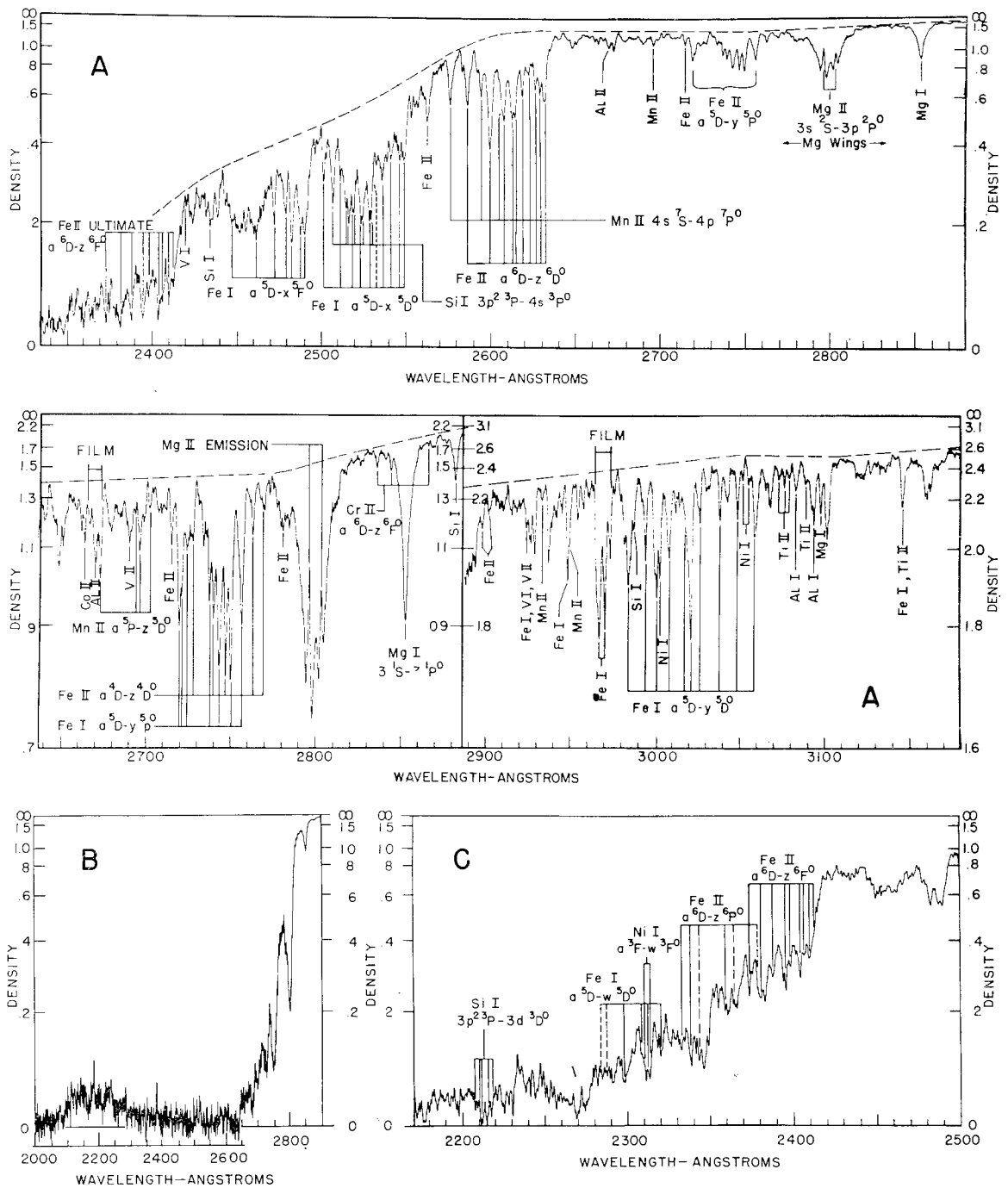


Fig. 7. Densitometer tracings of solar spectrum. (A) Spectrum No. 43 taken at 75 km on March 7, 1947. The blisters which may be seen on Fig. 6 at 2670 A and 2970 A are shown by the word FILM and a limit bracket. (B) Spectrum No. 23 taken at 35 km on October 10, 1946. Compressed wavelength scale used to emphasize the "hump" near 2200 A. (C) Spectrum No. 29 taken at 55 km on October 10, 1946. Below 2415 A the resolution of No. 43 is inferior to that of No. 29 because of its very low density.

SECTION V - Intensities

Most of the intensity estimates are visual. The scale is similar to that used in the revised Rowland table,¹⁰ which means that it is an approximate measure of the central core intensity and width of the lines. A comparative study of the rocket spectra, the Rowland Table, and a table of solar lines prepared by Babcock and Moore from Mt. Wilson plates¹¹ showed that the weakest observable lines in the rocket spectra corresponded roughly to a Rowland intensity 3 while the strongest line had a Rowland intensity of about 1000. Between 2650 Å and 2388 Å the numerical estimates were dropped because of low density. For this region the notations in Section VII are used. Below 2388 Å it was considered that the resolution of the spectrum of Fig. 7C was superior to that of Fig. 7A, since the high density gave a greater freedom from graininess. For this region the former spectrum was used and the numerical estimates were resumed.

The spectrum in the rocket ultraviolet region is more complex than that in the previously known region. There are several regions (e.g., 2500-2550 Å, Fig. 7A) in which the overlapping of many strong lines produces a large general depression of the spectrum, such that the location of the background continuous spectrum can only be surmised. Certain anomalies in the visual estimates in such regions resulted. Typical examples of this effect are cited in Section VIII.

SECTION VI - Identifications

The features to be identified are listed in Table II. A Finding List containing about 1200 entries arranged according to wavelength was prepared. These entries represented the classified lines that might be expected to show up at the available resolution. Most of them were taken from unpublished multiplet lists which Dr. C. E. M. Sitterly of the National Bureau of Standards is using for the preparation of her new Violet Multiplet Table.

The finding list was compared with the list of observed features and the likely contributors to each observed line noted. In some cases the major contributor or contributors were easily identified but more often there were found to be several possible contributors.

A careful study of multiplet relations and laboratory intensities was made to determine the relative importance of the various contributors. In Col. 3 of the table probable major contributors are indicated by the symbol † preceding the element abbreviation. Absence of this symbol means either the line is minor (less than 20%) or that evidence of its importance is lacking. In cases of several possible contributors with little evidence as to relative importance the laboratory wavelengths and intensities are omitted.

¹⁰Revision of Rowland's Preliminary Table of Solar Spectrum Wavelengths. Carnegie Institution of Washington, 1928.

¹¹Astrophys. J. Mt. Wilson Contribution. In press.

SECTION VII - Symbols Used in Table II

Column I - Observed Wavelengths.

1. Lines seen by four or more observers are considered certain. Doubtful lines are indicated by ? following the wavelength. Doubtful lines showing clearly on densitometer traces are indicated by D following the wavelength.
2.) This symbol links two wavelengths which form the extremes
) of a broad absorption line or depressed feature. Wavelengths
) listed between the extremes indicate internal structure.

Column II - Observed Intensities.

1. Numerical values range from 3 for the weakest observable line up to 1000 for the strongest.
2. In certain low density regions the numerical scale was dropped. The notations used and their approximate numerical equivalents are as follows:

St (strong)	greater than 40
Md (medium)	20 to 40
Wk (weak)	less than 20

3. The following letters appearing after the intensity estimates indicate special characteristics:

n - wide line - probably a blend of contributing lines separated by 2 A or less.

N - wide line - more than 2 A. Usually used in conjunction with the parenthesis symbol in the wavelength column.

d? - may be double.

v - the line is an imperfectly resolved violet component in the wing of a stronger line.

r - the line is an imperfectly resolved red component in the wing of a stronger line.

Em - emission line.

no line - intensity minimum at the base of an emission line.

Column III - Spectrum

1. # denotes a major contributor.

Column IV - Laboratory Wavelength

1. * This symbol indicates the existence of another line of the same spectrum having the same laboratory wavelength.

Column V - Laboratory Intensities

1. Intensities were taken from Mrs. Sitterly's multiplet lists (See Section VI). A discussion of her general notation and the types of scale used may be found on page XV of her Revised Multiplet Table.¹²

Column VI - Multiplet Numbers

1. These are arbitrary numbers assigned to the multiplets for reference purposes. See Table III. These numbers are also used to identify certain multiplets in the text, e.g., Fe I 9 stands for multiplet #9 of the Fe I spectrum.

SECTION VIII - Multiplets of Interest

A number of important multiplets are shown in Fig. 7A. Many others may be picked out from Table II by reference to the multiplet numbers. Among the more important multiplets are Fe I 9 and Si I 1, which combine to produce the large depression in the spectrum between 2500 and 2550 Å. A careful examination of these two strong multiplets reveals some of the difficulties of visual observations of the original spectra. For example, the two weak lines listed at 2514.5 Å and 2516.2 Å are attributed to 2514.32 and 2516.11 of Si I 1. They should be very strong. Reference to the densitometer record of Fig. 7A shows that these lines combine with a broad line at 2518.7 Å to produce a large depression in the spectrum. The apparent weakness then comes from the close proximity of these lines to each other and to other strong lines. Also note that 2518.7 and 2523.0 are broad and flat bottomed. In contrast, other lines in this vicinity are quite sharp. This is clearly due to the fact that each of these lines is double, each receiving strong contributions from both Si I 1 and Fe I 9.

A second interesting pair of multiplets is Fe II 1 and Mn II 17, near 2600 Å. Each of the thirteen lines of the Fe II multiplet is resolved as well as two of the three Mn II lines. The third Mn line was seen by some observers as a shoulder to the violet side of the Fe line at 2607 Å while other observers saw the two as a single line. The densitometer trace shows that the shoulder is well defined and that both lines are definitely present.

SECTION IX - Energy Distribution

Intensity calibration marks were put on each film prior to the flight using a carbon arc as a source of radiation of known energy distribution.

¹²Charlotte E. Moore, "A Revised Multiplet Table of Astrophysical Interest", Princeton University Observatory, Contribution No. 20.

A curve of the solar energy distribution as a function of wavelength, deduced from the October 10 spectra, has already been published.⁵ Fig. 8 is a similar curve based on the March 7, 1947 spectra except that the absorption line structure is reproduced in more detail. Intensities are plotted as percentages of the intensity values for a 6000° K black body. The black body curve was adjusted so that its maximum coincided with the maximum of the solar intensity curve at about 4800 Å and the intensity at this point was taken to be 100 percent.

The March 7 spectrograph used a cylindrical mirror, so that the calibration spectra exhibited the change in width referred to in Section II. Densitometry of these spectra was so difficult that it was finally abandoned, and the H and D characteristic curves of the October 10 film were used instead.

Developing conditions were carefully controlled, and the two films were from the same emulsion lot. The uncertainty in film contrast (γ) value is therefore probably less than 10%. For the density range of 1.9 represented in Fig. 8, the maximum uncertainty would be 0.19 in density, 0.125 in log intensity, or 0.10 in intensity.

Of particular interest in Fig. 8 is the region surrounding the great Mg II pair at 2803 and 2796 Å. The wings of these two lines clearly extend out 25 Å or more to either side and may extend much farther still. Presumably, this magnesium absorption occurs deep in the reversing layer where pressure broadening effects are large.

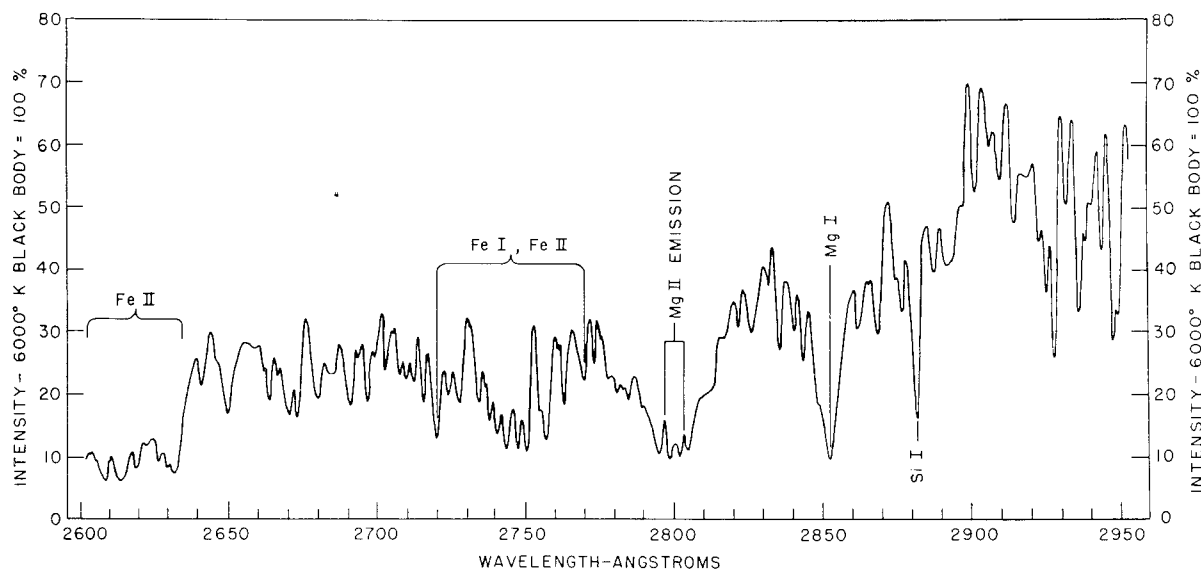


Fig. 8. Spectrum No. 43 replotted on a linear intensity scale relative to intensity of a black body at 6000° K.

In the "bottom" of the absorption valley three maxima may be noted. Two of these coincide within a fraction of an Angstrom with the known wavelengths of the magnesium lines and are undoubtedly due to the emission of these lines in a high temperature, low pressure region high in the sun's atmosphere. The third peak in the center is the result of the intersection of the rising slopes of the two broad absorption lines. It is interesting to note that in Fig. 7A, the emission peaks are pointed, corresponding to the characteristic response of the spectrograph for isolated lines, while the third peak is of a rounded nature. The intensity minima to either side of the emission lines are obviously not central cores of true absorption lines. They are listed in Table II with the notation "no line".

Dr. D. H. Menzel of Harvard predicted that these emission lines would be found in great strength. He also was the first to point them out in the rocket spectra. In the previously known regions of the solar spectrum, only H and K of Ca II show emission in the total sun, and they are weak in comparison with the Mg II pair.

The shape of the Mg emission lines is undoubtedly determined primarily by the response characteristic of the spectrograph. 2803 A shows up as would a very sharp line. There is some suggestion, however, that 2796 A may be slightly broadened, indicating a true line-width of the order of 1 A. The true intensities of these lines must be somewhat greater than is shown in Fig. 8, and they might be several times greater.

Section X - Bands

The concept of the band interpretation came about from the failure of an attempt to explain the structure between 2200 A and 2280 A in terms of atomic lines. A large number of lines of Fe I and Fe II exist in this region but no assumed values of multiplet strengths were able to account for the observed structure. For instance, although the region between 2255 A and 2279 A is clearly depressed below the regions to either side, one can find no corresponding increase in either the number or the strength of the Fe lines in this region. Other regions that may be caused by bands lie from 2440 A to 2470 A and from 2205 A to 2221 A, although part of the structure in the latter region may be caused by the multiplet Si I 2.

It is not the purpose of this paper to analyze the possible band spectra involved, but it might be noted that there does exist a strong band of nitric oxide centered at 2264 A. Leifson¹³ has shown that a layer of NO only 0.5 mm thick (NTP) produces appreciable absorption in this band. The spectrum of Fig. 7C was taken at 55 km, at which altitude the residual atmosphere above the spectrograph was equivalent to about 5 meters of air at NTP. Consequently, an average concentration of only 0.01% of NO in the outer atmosphere would be detectable.

¹³S. W. Leifson, Ap. J. 63, 73, (1926)

NOTES FOR TABLE II

Most of the following notes serve to call attention to features on the densitometer traces of Figure 7 that are not apparent in Table II. All references to structure apply to Figure 7.

2966.0	Wavelength discrepancy possibly due to blister on film.
2923.7 - 2917.7	Depressed region. Probably contains V II 13 and 14 and others.
2893.8 - 2886.5	Depressed region.
2878.5	Probable error in visual wavelength caused by neighboring Si I line.
2865.0 - 2840.0	Wings of Mg I 1, 2852.12 A. Several small inflections show in either wing. These are probably due to Na I 1, CR II 4 and several multiplets of Fe II.
2825.8	Unresolved line in violet wing, possibly Cu I. 2824.7 A.
2825.0 - 2775.0	Wings of Mg II 1, 2802.698 and 2795.523. Most of the numerous inflections which may be seen in the traces were excluded from the Table. Between 2812.7 A and 2810.3 A, the depression below the wing contour is pronounced. This is attributed to Co I 186 and 188, and V II 59, in addition to the lines tabulated.
2821.7	Four partially resolved lines fill the region between 2423.1 and 2421.0. These are identified as Fe I 49, 23.28, Cr II 15, 22.37, Co I 198, 21.74 plus the lines in the Table.
2711.7 - 2705.9	Broad uniform absorption apparently caused by numerous closely spaced lines. Six individual peaks are resolved on the trace.
2689.4 - 2687.0	Moderate absorption between 2691 A and 2687 A on which is superimposed the listed line.
2669.4	Unresolved line in violet wing, probably Cr II 7.
2661.5	Unresolved line in violet wing, probably Al I 1, 2660.39 A.
2650.7	Unresolved line in red wing, probably Al I 1, 2652.48.
2562.6	Ca I 14, 2564.07 and 2565.17, probably present in red wing.

- 2516.2 See Section VIII for discussion of true intensity of the lines in this region.
- 2498.5 - 2496.4 Weak general depression, probably caused by Fe I, Fe II, and Cr I, but the ultimate lines of B I 1, 2497.73 A and 2496.78 A may be present.
- 2498.0 - 2475.0 Large general depressed region apparently caused by many lines of Fe I and Fe II.
- 2475.0 - 2442.0 Large general depressed region. The many lines of Fe I and Fe II present here are apparently unable to account for this feature. May be caused by unidentified band.
- 2456.1 The As I 2456.53 line was considered at the suggestion of Dr. H. N. Russell. The high excitation potential, 6.37 volts, and inconclusive evidence for As in the sun make this identification doubtful without further evidence. Other lines of As I in the region photographed are badly masked.
- 2395.5 Possible unidentified strong line at 2394 A.
- 2292.0 - 2200.0 See Section X.

TABLE II

SOLAR SPECTRUM FROM 3000A to 2200A

3000A to 2488 from March 7, 1947; 2488 to 2200 from October 10, 1947. For explanation of symbols see page

OBSERVED			IDENTIFICATIONS				OBSERVED				IDENTIFICATIONS			
Solar λ	Est. I	Spectr.	Lab. λ	Lab. I	Mult.	Solar λ	Est. I	Mult.	Solar λ	Est. I	Mult.	Solar λ	Lab. I	Mult.
2999.4	10	#Fe I	99.512	30R	45	2944.4	8n		47.658		13	47.658		94
94.2	20	#Fe I	94.507	100R*	3				44.568		250	44.568		13
91.8	4	#Fe I	94.427	100R*	1	41.2	8n		44.399		13	44.399		94
87.7	7	Cr I 9; Cr II 14							41.485		100	41.485		13
		Fe I Uncl; Ni I 27							41.372		200	41.372		13
		#Si I	87.65	25	10				41.343		15r	41.343		2
		Fe I	87.292	10	45	38.8?	5		39.506		5	39.506		71
85.1D	5r	#Fe II	85.545	13	94				39.309		150	39.309		1
		#Fe II	84.831	15	94	36.8	18		36.904		60R	36.904		2
84.0	20	#Fe I	83.574	125R	1				36.496		(35)	36.496		2
81.5	9	Ni I	81.65	20R	28	33.0	5		33.057		100	33.057		1
		#Fe I	81.446	20r	3	28.8	20		29.008		25r	29.008		2
78.5	5	#Fe II	79.349	8	71				28.812		50	28.812		2
75.9	4	#V II 120-3 lines							28.625		(35)	28.625		2
		Fe I	76.126	5	139	26.4	8		26.584		12	26.584		71
		Fe II	75.938	5	71	23.7	6		24.017		300R	24.017		13
73.1	15	#Fe I	73.237	60R	2				23.851		7	23.851		177
		#Fe I	73.134	60R	2				23.627		70R	23.627		2
69.6	25	Fe II	70.510	10	71	17.9	4n		18.023		10	18.023		194
		#Fe I	*70.106	40R	2				17.465		4	17.465		72
		#Fe I	69.474	40R	3	14.8	10n		14.924		50R	14.924		2
		#Fe I	*70.106	10	45				14.62		50	14.62		1
66.0	20	#Fe I	66.901	125R	2	10.8?	N							
64.6?	10v	#Fe I	*65.255	20	2	07.8?								
		#Fe I	*65.255	20	174	05.6?								
		Fe II	64.629	9	94	02.2	8n							
		Fe II	64.131	7	357				03.068		100	03.068		14
60.1	10n	#Fe II	61.272	5	71	2898.1	10nd?		02.459		5	02.459		387
		#Fe II	59.601	7	359				98.539		12	98.539		20
57.0	7	V II	57.520	100	13	93.8	8n		97.264		8	97.264		359
		#Fe I	57.365	30R	2				94.776		7	94.776		333
53.7	12	#Fe I	53.940	50R	2									
		Fe II	53.774	11	71	81.1	80		81.595		200r	81.595		11
		Fe I	53.486	5	177	78.5	8		79.241		4	79.241		387
51.7D	3	V II	52.07	150	13	75.8	7		79.158		40	79.158		15
		Cr II	51.40	10	25				75.998		20	75.998		9
49.1?	15r	Mn II	49.209	200	1	73.2	9n		75.302		5	75.302		94
		Fe II	49.178	10	386									
47.8	30	#Fe I	47.877	60R	2	69.3	8							

TABLE II (Cont.)

OBSERVED			IDENTIFICATIONS				OBSERVED				IDENTIFICATIONS						
Solar λ	Est. I	Spectr.	Lab. λ	Lab. I	Mult.	Solar λ	Est. I	Spectr.	Lab. λ	Lab. I	Mult.	Solar λ	Est. I	Spectr.	Lab. λ	Lab. I	Mult.
2867.4	10d?		69.131	150	244	2781.5D		V II	81.48	100N	332			V II	81.48	100N	332
			68.874	5	72			Fe II	*81.418	10	18			Mg I		10	18
			67.655	12	4	79.7?	6	Cr II	79.832	12	18			Mg I		12	18
			66.711	15	4			Cr II	79.302	11	337			#Fe II		11	337
			65.112	25	4	78.4?	6	#Cr II	78.813	75	188			Co I		75	188
65.2?	6								*78.277	10	18			Mg I		10	18
61.2?	5n								78.221	20	49			Fe I		20	49
58.8?	7		58.92	25	4	76.0?	4	Cr II	*76.695	10	18			Mg I		10	18
			*58.340	11	285			#Fe II	76.180	4	290			Fe II		4	290
			*58.340	11	388			#Fe II	75.654	50	8			Mn II		50	8
51.6	200		52.120	300R	1			#Mg I	72.083	20	50			Fe II		20	50
48.1?	5v		48.046	8	286	72.0	10	Fe II	*70.507	5	288			Fe II		5	288
43.4	15		43.977	20r	49	70.2D	3	Fe I	69.915	50r	11			Cr I		50r	11
			43.631	10	48			Fe I	68.940	8	74			Cr I		8	74
			43.254	75	4	68.5	15n	#Cr II	67.523	20	51			Fe I		20	51
40.5	7		40.756	8	389			Fe II	*67.500	13	338			Fe II		13	338
			40.644	9	315			Fe II	66.542	30	5			Co I		30	5
			40.342	7	285	66.7	8	Fe II	64.364	25r	11			Cr I		25r	11
			40.022	30	15			Cr II	64.188	100r	65			Co I		100r	65
35.5	15		35.716	9	314	64.1D	3	Fe II	63.913	3	290			Fe II		3	290
			35.640	100	4			#Cr II	62.027	15	51			Fe I		15	51
34.1?	4		34.428	50	65			Co I	61.813	9	74			Fe I		9	74
			33.922	40	5	62.0	20	Co I	61.780	18	51			Fe I		18	51
31.9?	3		32.436	25r	49			#Fe I	60.710	60	224			Fe I		60	224
			31.562	11	315			Fe II	60.122	40	121			V II		40	121
30.8D	3		30.473	50	15	59.9?	8nd?	Cr II	59.814	4	52			V II		4	52
26.7D			26.797	50w	186			Co I	56.329	20	7			Fe I		20	7
25.7	5		25.557	20	50			#Fe I	55.733	15	73			Fe I		15	73
			25.151	75w	188	55.7	-60	Co I	53.687	3	51			Fe I		3	51
21.7	3		22.020	20	27			Cr II	53.289	12	338			#Fe II		12	338
			21.30	15	30	53.6?	10	Ni I	50.140	25r	7			#Fe I		25r	7
18.2	15N		18.592	30	5			Co I	49.482	14	74			Fe II		14	74
15.3			15.555	50r	65	49.6	60	Co I	49.324	12	73			Fe II		12	73
12.7	12		13.288	30R	49			Fe I	49.178	13	74			Fe II		13	74
			12.006	40	31			Cr II	*46.982	20	50			Fe I		20	50
03.7	no line				1	46.5	50	See Section IX	46.978	14	74			#Fe II		14	74
02.3	700 Em		02.698	40				#Mg II	46.487	14	73			Fe II		14	73
01.1	no line							See Section IX	44.068	10	7			Fe I		10	7
2796.8	no line		95.523	60	1	42.6	60n	See Section IX	43.196	14	73			Fe II		14	73
95.4	1000 Em							#Mg II	42.406	30r	7			Fe I		30r	7
94.1	no line							See Section IX	42.256	20	51			#Fe I		20	51
83.6?	5		83.690	12	337			#Fe II						Fe I			
			82.974	10	18			Mg I						Fe I			

TABLE II (Cont.)

OBSERVED			IDENTIFICATIONS				OBSERVED			IDENTIFICATIONS			
Solar λ	Est. I		Spectr.	Lab. λ	Lab. I	Mult.	Solar λ	Est. I		Spectr.	Lab. λ	Lab. I	Mult.
2739.5	40		#Fe II	39.545	15	74				#Mn II	72.588	20	14
37.1	40		#Fe I	37.310	20r	7				#V II	72.005	150r	3
35.4	4		#Fe II	36.968	12	74	2669.4	25		Cr II	71.818	25	7
33.5	15		#Fe I	35.475	8	51				#Al II	69.116	10	1
30.7	8n		#Fe I	33.581	15	51				Cr II	68.722	25	7
			Ti I	33.265	30	43	66.5	15		Mn II	67.033	12	15
			Cr I	31.914	40r	4				#Fe I	66.811	8	53
27.3	20n		#Fe II	30.735	11	73	63.6	18		#Cr II	66.026	35	7
			#Fe II	27.538	13	74				Co II	63.530	60	4
23.7	20n		Cr I	26.524	35r	4				Cr II	63.430	20	7
			Fe II	24.879	9	73				V II	63.25	250N	326
20.8	30		#Fe I	23.577	15	7	61.5	10		#V I	61.424	(70R)	4
19.2	45		#Fe I	20.902	40r	7	58.4?	6		Cr II	58.603	30	7
14.5	30		#Fe I	*19.027	60R	7	56.2?	4		#V I	56.224	(60R)	4
11.7	N		#Fe II	14.414	13	74				Mn II	55.925	10	15
			#V II	06.17	200r	1				#V II	55.68	200N	326
			#Mn II	05.561	10	14	53.6?	3		Cr II	53.594	25	7
05.9	20		Cr II 32; Fe I 52				50.7	12		V I	51.896	(50R)	4
01.4			Fe I 53; Fe II 292				48.4	35n		Co I	50.266	50w	68
			Fe II 316; Mn II 11							V II	49.37	150N	326
			Mn II	01.696	30	11				V I	47.710	(40R)	4
			#Mn II	01.171	12	13				Fe I	47.558	3	8
			#Mn II	01.035	10	14	46.5	45N		Fe I 57; Ti I 8			
			V II	00.944	300r	1				Ti II 26; V II 138			
2698.5	35nd?		Fe II	99.107	6	53	44.1			V II 326			
95.5	40nd?		Mn II	98.989	8	13	41.8?	55N		Mn II 15; Ti I 8			
			Co I	95.846	50w	68	39.4?			V II 138			
			Mn II	95.366	8	14	35.6?	15		#Fe I	35.808	8	57
92.9	8		Co II	94.679	25	4	31.3	60d?		#Fe II	31.321	13	1
			Mn II	93.191	15	14				#Fe II	*31.045	13	1
			Fe II	92.826	5	73				#Fe II 248 - 4 lines			
89.4	30nd?		Fe II	92.601	10	392	28.3	12		#Fe II	28.291	13	1
			#Fe I	89.212	8	53	25.4	30		#Fe II	25.664	13	1
85.9	20N		#V II 3 - 5 lines	83.09	100	3	23.5?	6		#Fe I	23.532	5	57
			#V II	82.875	100	3				#Fe II	21.669	10	1
82.8			Co I 68; Fe II 392				20.3?	4v		#Fe II	20.408	6	1
79.2	10		#V II 3 - 3 lines	79.062	10	52	17.7	45		#Fe II	17.618	12	1
			Fe I	77.20	35	7	13.6	50		#Fe II	13.820	13	1
77.3D	8v		#Cr II	77.12	25	7	11.4	50		#Fe II	11.873	13	1
			Cr II	72.838	20	7	07.2	40		Fe II	11.075	6	75
72.4	35		Cr II				05.2?	25v		#Fe II	07.086	13	1
										#Mn II	05.696	75	17

G. T. ...

TABLE II (Cont.)

OBSERVED		IDENTIFICATIONS				OBSERVED				IDENTIFICATIONS			
Solar λ	Est. I	Spectr.	Lab. λ	Lab. I	Mult.	Solar λ	Est. I	Mult.	Spectr.	Lab. λ	Lab. I	Mult.	
2598.9	80	#Fe II	99.395	14	1				#Fe I	35.604	8r	9	
		Mn II	98.910	15	18				#Fe II	35.480	7	254	
		#Fe II	98.369	14	1				Fe II	34.413	9	228	
93.6	35	#Mn II	93.731	90	17	2532.4?	Wk		Fe II	33.626	10	228	
		Fe II	93.722	7	75				Si I	32.38	20	14	
91.1	30n	Cr I	91.861	50r	17	28.2	Stn		#Fe II	*29.545	10	254	
		#Fe II	91.542	10	75				Fe I	29.134	10r	9	
88.3	20	Fe II	87.945	7	443				#Si I	28.513	175r	1	
85.8	50	#Fe II	85.876	13	1				#Fe I	27.433	15r	9	
		Fe I	84.536	8	57	26.2?	Wk		Fe II	25.386	10	228	
82.6	30	#Fe II	82.582	10	75	23.0	Stn		#Si I	24.112	125r	1	
75.7	60	Fe II	76.859	7	443				#Fe I	22.848	40R	9	
		#Mn II	76.113	100	17	18.7	Md		#Si I	19.206	100r	1	
		V II	74.520	60	64				Fe I	18.100	12r	9	
70.8?	6	Fe II	70.843	7	393	16.2?	Wk		#Si I	16.111	250r	1	
62.6	50d?	#Fe II	63.472	12	75	14.5	Wk		#Si I	14.320	100r	1	
		#Fe II	*62.535	13	75	10.9	20		Ni II	10.87	30	5	
		Fe II	62.094	6	320				#Fe I	10.833	15R	9	
60.2?	10nv	Cr I	60.69	30	17	06.7	50		#Si I	06.896	150r	1	
		Fe II	60.278	7	320	03.0?	8		Fe II 297; Fe II 298				
57.1	12	Cr I	*57.14	25	17				Fe II 394; V II 35				
		Co I	56.762	50w	73	01.3	35		#Fe I	01.130	20R	9	
55.1D		Fe II	55.447	5	254	2498.5?	6		Fe II	98.897	10	230	
		Fe II	55.066	5	254				Fe I	98.895	10	11	
		P I	54.93	30	4				Fe II	97.817	7	298	
53.1	20	V II	53.668	40	64	96.4	8		Cr I	96.30	35r	20	
		P I	53.28	40	4	90.4	St		#Fe I	91.155	20R	10	
		Co I	53.004	40r	74				#Fe I	90.642	30R	10	
49.4	Md	#Fe I	49.612	10r	9				Fe I	89.751	15r	10	
		Fe II	49.453	8	254	87.8	Md		#Fe I	88.143	40R	10	
		Fe II	49.399	8	254	83.0	St		#Fe I	83.270	60	10	
		Fe II	48.590	6	227	79.4	Md		#Fe I	79.775	20R	10	
45.9?	Wk	Fe II	46.667	8	254				V II	79.518	180	107	
		#Fe I	45.977	10r	9				V II	79.043	200	107	
		Fe II	45.215	7	228				Cr I	78.525	10	1	
41.0	Wk	Fe II	41.831	7	227	73.0	Md		#Fe I	72.910	12R	10	
		Fe II	41.096	7	254	63.0	MdN		#Fe I	62.645	10r	10	
		#Fe I	40.971	10R	9				Fe II	61.855	8	300	
		Fe II	*40.669	6	254	60.4			Fe II	61.282	8	300	
38.6?	Wk	#Fe II 227 - 4 lines							Co I	60.800	20	9	
35.5	Md	Fe II	*36.822	9d	228	56.1?	Wk		Fe II	58.782	8	300	
		P I	35.65	50	4				See notes				

TABLE II (Cont.)

OBSERVED			IDENTIFICATIONS				OBSERVED				IDENTIFICATIONS						
Solar λ	Est. I	Spectr.	Lab. λ	Lab. I	Mult.	Solar λ	Est. I	Spectr.	Lab. λ	Lab. I	Mult.	Solar λ	Est. I	Spectr.	Lab. λ	Lab. I	Mult.
2453.7?	MdN	V II	53.346	80	143	61.8	25N	#Fe II	60.287	8	43						
50.5?		Mn II	52.488	25	27	2358.3		#Fe II	*59.111	8	3						
47.4?	Wk	Fe II 410-2 lines				55.6	15n	Ni II	56.41	25	9						
		Fe I	47.708	4	10	50 D	N	#Fe II	48.300	8	3						
		Fe II 410-3 lines						#Fe II	48.118	8	43						
43.4	Wk	Fe II	39.301	8	300	44 D		#Fe II	44.278	8	3						
39.2	Md	Co I	39.038	20R	9	39 D	20n	#Fe II	43.495	8	3						
36.7	Wk	#Co I	36.657	50R	9			#Fe II	38.005	8	3						
		Mn II 27-3 lines				35 D	30N	Ni I	37.49	50	9						
35.3	Md	#Si I	35.160	100r	4	33 D		#Fe II	32.798	8	3						
32.3	Wk	#Co I	32.213	40R	9	31 D											
28.7	Wk	Fe II 410; Fe II 411; V I 10				29 D	n	Ni I	29.97	50	9						
26.0	StNd?	#Co I	24.932	250R	9	28 D	35N	#Fe II	27.391	7	3						
23.1	StNd?	Fe II 411-3 lines				25 D	60N	Ni I	25.80	50	10						
13.6		#Fe II	13.308	9	2	23 D		#Ni I	21.39	60	10						
		#Fe II	11.062	9	2			#Fe I	20.356	(40)	16						
		#Fe II	10.521	9	2	18 D	150N	#Ni I	20.03	100	10						
10.1	Md	Co I 10; Co I 14				15		Ni I	17.16	50	9						
07.3?		Co I	07.249	100	10			#Ni I	13.98	100	11						
		#Fe II	06.660	9	2			#Fe I	13.102	(40)	16						
		#Fe II	04.882	9	2			#Ni I	12.34	50	11						
04.7	Md	#Fe II	04.430	7	2	08		#Ni I	10.96	100	11						
		#Fe II	*99.237	9	2	04		#Fe I	08.997	(30)	16						
2398.8?	Md	Fe II	*99.237	9	43	2297	N	#Fe I 16-5 lines									
		Ca I	98.58	(2)	4	92?D	n	#Fe I 17-3 lines									
95.5	St	#Fe II	95.627	9	2	80 D	N	Fe I	92.523	(30)	17						
		#Fe II	95.416	7	2	36 D	N										
						32 D											
88.9	St	Fe I	89.971	(25)	13	07 D		Si I 2-6 lines									
		Co II	88.90	100	1												
		#Fe II	88.629	9	2												
85 D	100N	Fe II	83.060	4	2												
		#Fe II	82.034	9	2												
		#Fe II	80.757	7	3												
79 D		Fe II 43-3 lines															
73.9	30N	Fe II	75.180	10	43												
		#Fe II	73.733	8	2												
69.6	N	Fe II	68.593	7	43												
65.5		#Fe II	64.825	8	3												
		Cr I 8-3 lines															

TABLE III
MULTIPLETS AND EXCITATION POTENTIALS

Mult. No.	E. P. Low	Multiplet	Mult. No.	E. P. Low	Multiplet	Mult. No.	E. P. Low	Multiplet
Al I			Cr II (Continued)			Fe II		
1	0.00	3p ² P ⁰ -5s ² S	5	1.48	a ⁵ D-z ⁵ P ⁰	1	0.00	a ⁶ D-z ⁶ D ⁰
Al II			7	1.48	a ⁶ D-z ⁶ D ⁰	2	0.00	a ⁶ D-z ⁶ F ⁰
1	0.00	3 ¹ S-3 ³ P ⁰	9	2.41	a ⁴ D-z ⁴ D ⁰	3	0.00	a ⁶ D-z ⁶ P ⁰
3	7.39	3 ¹ P ⁰ -4 ¹ S	14	3.72	a ⁴ H-z ⁴ H ⁰	43	0.23	a ⁴ F-z ⁴ D ⁰
B I			15	3.72	a ⁴ H-z ⁴ I ⁰	71	0.98	a ⁴ D-z ⁴ F ⁰
1	0.00	2p ² P ⁰ -3s ² S	20	3.84	a ⁴ F-z ⁴ G ⁰	72	0.98	a ⁴ D-z ⁴ P ⁰
C I			25	4.13	b ⁴ G-y ⁴ F ⁰	73	0.98	a ⁴ D-z ⁴ F ⁰
1	2.67	2p ² ¹ S-3s ¹ P ⁰	27	4.13	b ⁴ G-y ⁴ H ⁰	74	0.98	a ⁴ D-z ⁴ D ⁰
Ca I			31	4.90	c ² G-x ² F ⁰	75	0.98	a ⁴ D-z ⁴ P ⁰
4	0.00	4 ¹ S-5 ¹ P ⁰	32	4.13	b ⁴ G-x ⁴ G ⁰	94	1.66	a ⁴ P-z ⁴ P ⁰
14	1.87	4 ³ P ⁰ -3d ⁴ d ³ P	Fe I			227	2.62	a ⁴ H-z ⁴ G ⁰
Co I			1	0.00	a ⁵ D-y ⁵ D ⁰	228	2.62	a ⁴ H-z ⁴ H ⁰
2	0.00	a ⁴ F-y ² G ⁰	2	0.00	a ⁵ D-y ⁵ F ⁰	230	2.62	a ⁴ H-z ⁴ I ⁰
5	0.00	a ⁴ F-y ² D ⁰	3	0.00	a ⁵ D-z ³ P ⁰	248	2.79	b ⁴ F-z ⁴ G ⁰
9	0.00	a ⁴ F-x ⁴ F ⁰	4	0.00	a ⁵ D-z ³ G ⁰	254	2.79	b ⁴ F-y ⁴ F ⁰
10	0.00	a ⁴ F-x ⁴ G ⁰	7	0.00	a ⁵ D-y ⁵ P ⁰	285	3.14	a ⁴ G-z ⁴ G ⁰
14	0.00	a ⁴ F-w ⁴ D ⁰	8	0.00	a ⁵ D-y ³ D ⁰	286	3.14	a ⁴ G-z ⁴ H ⁰
65	0.43	b ⁴ F-x ⁴ D ⁰	9	0.00	a ⁵ D-x ⁵ D ⁰	288	3.14	a ⁴ G-z ⁴ I ⁰
68	0.43	b ⁴ F-x ⁴ F ⁰	10	0.00	a ⁵ D-x ⁵ F ⁰	290	3.14	a ⁴ G-y ⁴ F ⁰
73	0.43	b ⁴ F-w ⁴ D ⁰	11	0.00	a ⁵ D-y ⁷ P ⁰	292	3.14	a ⁴ G-z ⁴ I ⁰
186	1.87	b ⁴ P-s ⁴ D ⁰	13	0.00	a ⁵ D-x ⁵ P ⁰	297	3.14	a ⁴ G-z ⁴ H ⁰
188	1.87	b ⁴ P-w ⁴ P ⁰	16	0.00	a ⁵ D-w ⁵ D ⁰	298	3.14	a ⁴ G-x ⁴ G ⁰
198	2.13	a ² G-t ² F ⁰	17	0.00	a ⁵ D-w ⁵ F ⁰	300	3.14	a ⁴ G-y ⁴ H ⁰
Co II			45	0.86	a ⁵ F-x ⁵ F ⁰	314	3.18	b ² P-z ² C ⁰
1	0.41	4s ⁵ F-4p ⁵ F ⁰	48	0.86	a ⁵ F-x ⁵ P ⁰	315	3.18	b ² P-z ² D ⁰
4	1.21	4s ³ F-4p ⁵ G ⁰	49	0.86	a ⁵ F-y ⁵ G ⁰	316	3.18	b ² P-y ⁴ D ⁰
13	5.99	4p ³ G ⁰ -5s ³ F	50	0.86	a ⁵ F-z ⁵ H ⁰	320	3.18	b ² P-z ² P ⁰
14	5.81	4p ⁵ G ⁰ -5s ⁵ F	51	0.86	a ⁵ F-w ⁵ D ⁰	333	3.23	b ² H-z ⁴ H ⁰
Cr I			52	0.86	a ⁵ F-w ⁵ F ⁰	337	3.23	b ² H-z ² G ⁰
4	0.94	a ⁵ S-w ⁵ P ⁰	53	0.86	a ⁵ F-v ⁵ D ⁰	338	3.23	b ² H-z ² I ⁰
8	0.00	a ⁷ S-x ⁷ P ⁰	57	0.86	a ⁵ F-x ⁵ G ⁰	357	3.37	a ² F-z ⁴ G ⁰
9	0.96	a ⁵ D-y ⁵ D ⁰	94	1.48	a ³ F-u ⁵ D ⁰	359	3.37	a ² F-z ² D ⁰
11	0.96	a ⁵ D-w ⁵ P ⁰	126	2.17	a ⁵ P-t ⁵ D ⁰	386	3.75	b ² G-z ² F ⁰
17	0.96	a ⁵ D-u ⁵ P ⁰	139	2.27	a ³ P-u ³ D ⁰	387	3.75	b ² G-y ² G ⁰
20	0.96	a ⁵ D-u ⁵ F ⁰	174	2.68	a ³ G-v ³ H ⁰	388	3.75	b ² G-z ² H ⁰
Cr II			175	2.68	a ³ G-x ³ H ⁰	389	3.75	b ² G-x ⁴ G ⁰
4	1.48	a ⁶ D-z ⁶ F ⁰	177	2.68	a ³ G-s ³ G ⁰	392	3.75	b ² G-y ² H ⁰
			194	3.22	b ³ H-t ³ H ⁰	393	3.75	b ² G-y ² F ⁰
						394	3.75	b ² G-x ² G ⁰
						410	3.87	b ⁴ D-w ⁴ F ⁰

TABLE III (Cont.)

Mult. No.	E. P. Low	Multiplet	Mult. No.	E. P. Low	Multiplet	Mult. No.	E. P. Low	Multiplet
Fe II (Continued)			Ni I			Ti II		
411	3.87	$b^4D-w^4D^0$	9	0.00	$a^3F-w^3D^0$	13	1.22	$a^2P-x^2D^0$
443	4.13	$c^2G-x^2H^0$	10	0.00	$a^3F-y^3G^0$	16	1.22	$b^4P-y^4P^0$
Mg I			11	0.00	$a^3F-w^3F^0$	V I		
1	0.00	$3^1S-3^1P^0$	27	0.03	$a^3D-y^3F^0$	2	0.00	$a^4F-v^4D^0$
18	2.70	$3^3P^0-3p^2^3P^0$	28	0.03	$a^3D-y^3D^0$	4	0.00	$a^4F-t^4D^0$
Ni II			30	0.03	$a^3D-y^1F^0$	10	0.00	$a^4F-t^4F^0$
1	0.00	$3s^2S-3p^2P^0$	Ni II			V II		
2	4.40	$3p^2P^0-4s^2S$	5	1.85	$a^2F-z^4G^0$	1	0.00	$a^5D-z^5F^0$
Mn I			9	1.85	$a^2F-z^2D^0$	3	0.00	$a^5D-z^5D^0$
1	2.27	$z^6P^0-s^8D$	P I			13	0.32	$a^5F-z^5F^0$
Mn II			4	2.31	$3p^3^2P^0-4s^2P$	14	0.32	$a^5F-z^3D^0$
1	1.17	$a^5S-Z^5P^0$	Si I			15	0.32	$a^5F-z^5D^0$
11	3.40	$a^5G-z^5G^0$	1	0.00	$3p^2^3P-4s^3P^0$	35	1.07	$a^3F-y^3G^0$
13	3.69	$a^5P-z^5S^0$	2	0.00	$3p^2^3P-3d^3D^0$	59	1.39	$a^3P-y^5D^0$
14	3.69	$a^5P-z^5D^0$	4	0.78	$3p^2^1D-3d^1D^0$	64	1.39	$a^3P-y^3P^0$
15	4.05	$b^5D-y^5F^0$	10	0.78	$3p^2^1D-4s^3P^0$	107	1.67	$b^3F-w^3D^0$
17	0.00	$a^7S-z^7P^0$	11	0.78	$3p^2^1D-4s^1P^0$	120	1.67	$a^5P-y^5D^0$
18	3.69	$a^5P-y^5P^0$	14	1.90	$3p^2^1S-5s^1P^0$	121	1.67	$a^5P-z^5S^0$
27	4.74	$z^7P^0-e^7D$	Ti I			138	1.79	$a^3G-x^3F^0$
Na I			8	0.00	$a^3F-u^3D^0$	143	1.79	$a^3G-x^3G^0$
1	0.00	$3^2S-5^2P^0$	43	1.04	$a^3P-t^3P^0$	224	2.37	$a^1I-z^1I^0$
						244	2.50	$b^3H-x^3G^0$
						326	4.27	$z^5G^0-e^5H$
						332	4.59	$z^5F^0-e^5F$

ACKNOWLEDGEMENTS

The authors are grateful to the many persons who have assisted both in the experimental work of obtaining the spectra and in the analysis which is reported here. Particular thanks are due Mr. F. S. Johnson of the Micron Waves Section, Optics Division, for his work in preparing spectrographs for flight and supervising their installation and launching. Thanks are also due Mr. J. D. Purcell for his work with Mr. Johnson and also for his assistance in the densitometry of the film and the preparation of Fig. 8, to Mrs. Sitterly who generously supplied a veritable gold mine of material and who gave much needed help and advice based on her long experience in spectral analysis, and to Dr. E. H. Krause* and the other members of the Rocket-Sonde Research Section of Radio Division I for assistance in the experimental phases of the work.

*Dr. Krause is now a member of the Nucleonics Division, NRL.

CHAPTER III

THE V-2 AS A RESEARCH VEHICLE

Introduction

Further progress was made toward improving the usefulness of the V-2 as a research vehicle. The warhead was modified in several ways, larger pressurized housings were constructed for use in the control chamber, and experiments were conducted in the midsection. The details are given in Section A. Determination of rocket attitude during flight is discussed in Section B.

A. Instrumentation Techniques Employed in the V-2 Rockets Fired on May 15, and July 10, 1947 and January 22, 1948

by

T. A. Bergstrahl and C. P. Smith

1. The May 15, 1947 V-2

The instrumentation of V-2 rocket no. 26, fired on May 15, 1947, followed the pattern used in the rockets of the third cycle.¹ The heavy steel forward section was replaced by a cone constructed of 1.6 mm (0.062 in.) steel. This cone housed the gages for ram pressure measurement at the nose tip, two ionization gages and two Pirani gages for pressure measurement, and two elements for determining the skin temperature. A cosmic ray Geiger counter telescope was mounted in the forward section of the warhead proper. In order to reduce the mass of material in the solid angle viewed by telescope the upper access door was made of 1.6 mm (0.062 in.) steel, and a 30.5 cm x 30.5 cm (1 ft x 1 ft) section between the lower access doors was removed and replaced by 1.6 mm (0.062 in.) steel. The ionosphere transmitter was mounted on track members between the lower access doors. The method was the same as that employed in missile no. 21, fired on March 7, 1947.¹ A roll gyroscope was mounted on the gyroscope plate in the control chamber. Two K-25 aircraft cameras were mounted in the midsection. This installation was identical to that used in missile no. 21.²

¹Naval Research Laboratory Report No. R-3171, Chapter III.

²Naval Research Laboratory Report No. R-3171, Chapter IX.

2. The July 10, 1947 V-2

The warhead of this rocket was altered considerably in order to permit the installation of a very large cosmic ray telescope. Fig. 9 is a photograph of this warhead. The shell was cut at the level of the bottom edge of the lower access doors, 40.6 cm (16 in.) forward of the base. The upper portion consisted of a conical aluminum section 1.52 m (62.2 in.) in length. The lower 76.2 cm (30 in.) of this cone was constructed of 2.5 mm (0.102 in.) aluminum. The next 81.8 cm (32.2 in.) was made of 1.6 mm (0.064 in.) aluminum. A positive ion gage was mounted at the tip of the cone.

Since the entire warhead section was occupied by the cosmic ray telescope and its electronics, the balance of the experimental equipment had to be located elsewhere in the rocket. That portion of the remaining electronic equipment which used high voltages was enclosed in a pressurized housing. The assembly is seen in Fig. 10. It was mounted in quadrant IV of the control chamber, as shown in Fig. 11. The primary power batteries also were placed in a pressurized container which was located in the control chamber. Equipments which did not require high voltages, e. g. the program timer, the telemetering sub-commutator etc., were not pressurized. Three attitude gyroscopes were mounted in the control chamber on the main gyroscope plate. The

Fig. 9. The July 10, 1947 warhead.

instrumentation in the afterbody of this missile consisted of a generating voltmeter installed in the midsection between the fuel tanks, and a cosmic ray camera recorder mounted in the tail section. The recorder installation was identical to the one used in missile no. 21.3

A diagram showing all of the wiring for the experimental equipment installed in the missile by the Naval Research Laboratory is given in Figs. 12 and 13.

³Naval Research Laboratory Report No. R-3171, Chapter IV, Section D.

Fig. 10. Electronic equipment mounted in a pressurized housing.

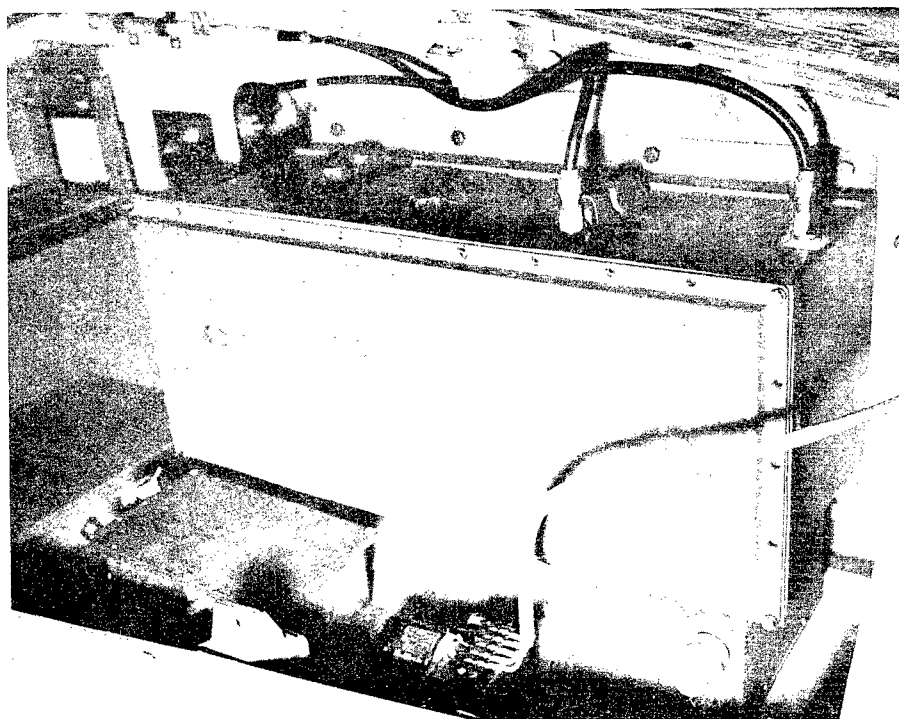
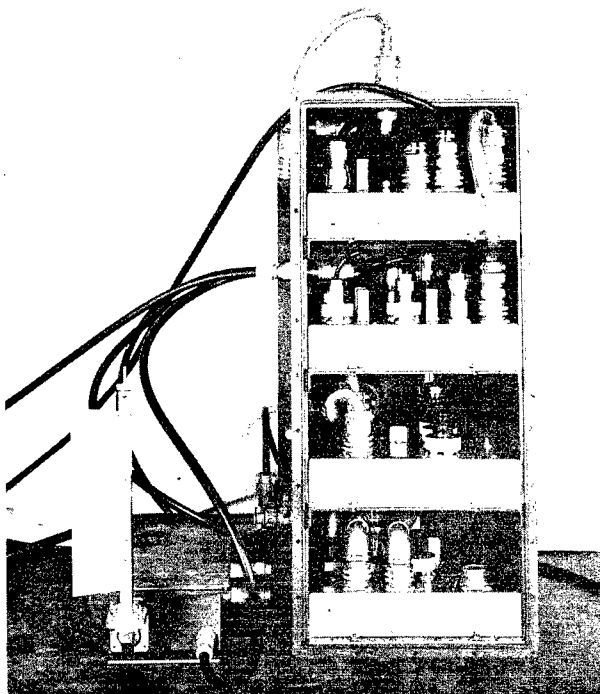


Fig. 11. The pressurized housing mounted in the control chamber of the July 10, 1947 V-2.

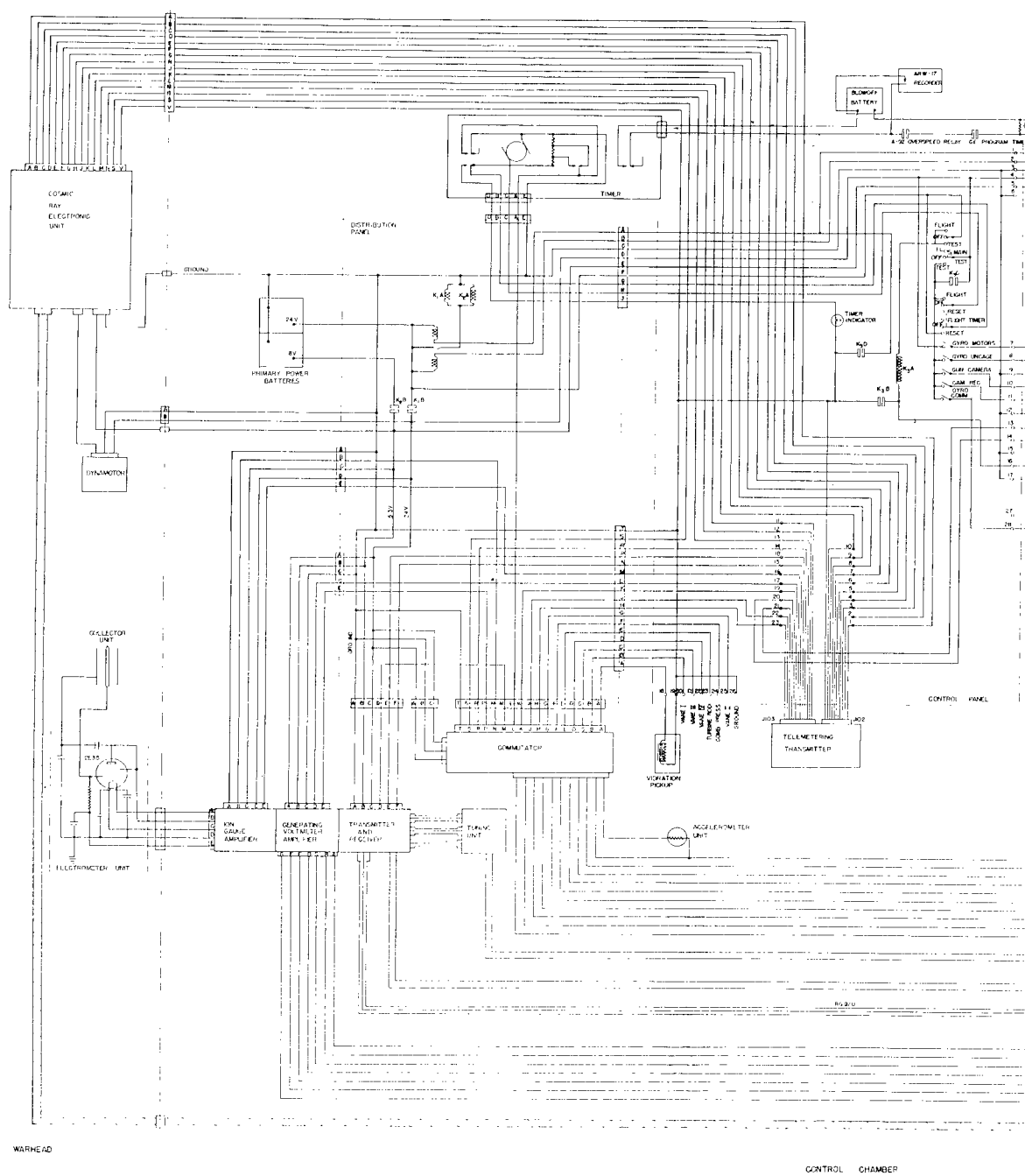


Fig. 12. Wiring diagram for the experimental equipment installed in the July 10, 1947 missile, part I.

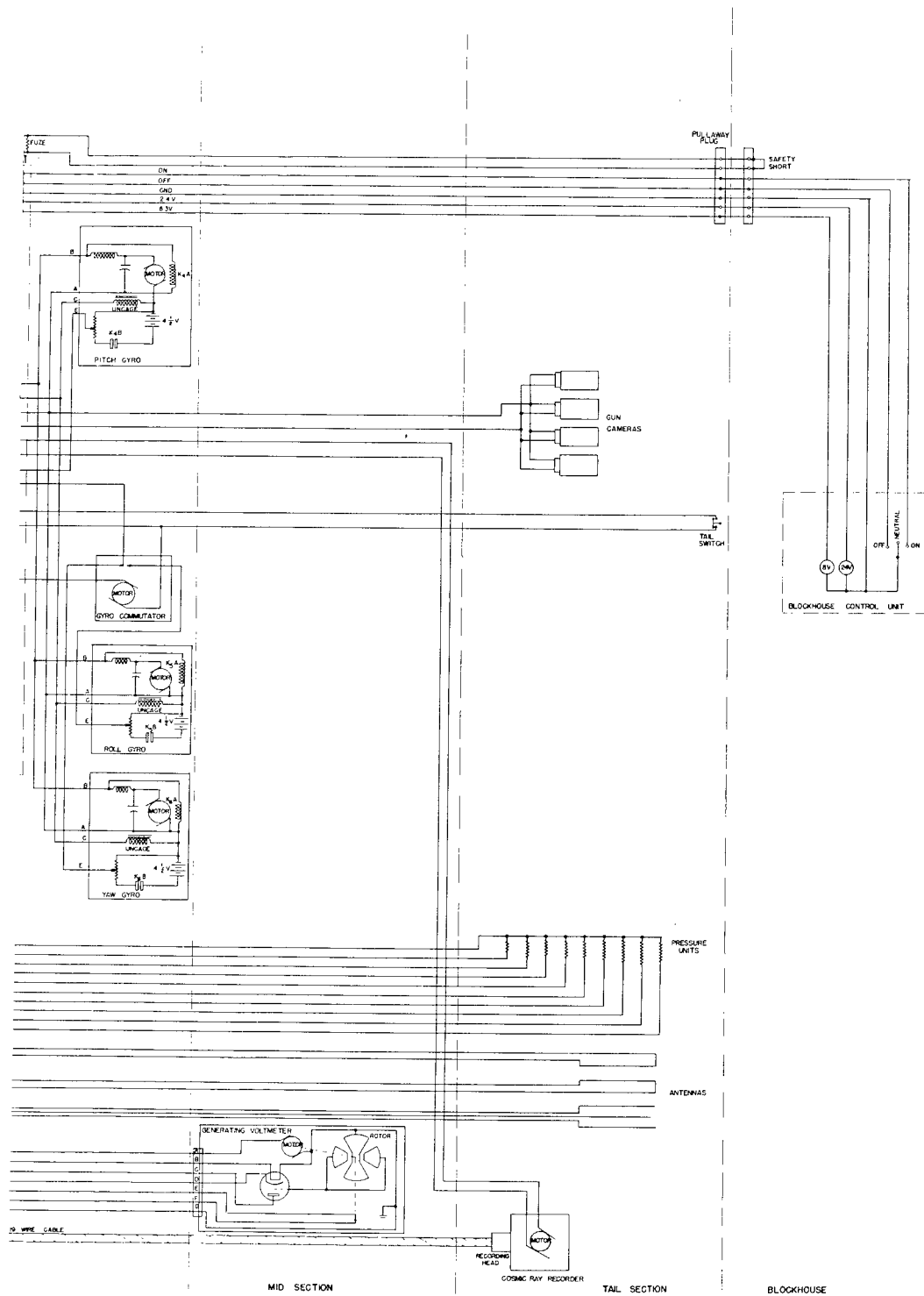


Fig. 13. Wiring diagram for the experimental equipment installed in the July 10, 1947 missile, part II.

3. The January 22, 1948 V-2

The warhead used on this rocket was similar to the one employed on March 7, 1947.⁴ The only difference lay in the fact that the forward nose cone of the January warhead was constructed entirely of aluminum. The warhead is shown in Fig. 14. The nose tip was occupied by a positive ion gage which was somewhat larger than, but otherwise similar to, the type used on July 10, 1947. The gage may be seen in Figs. 14 and 15. The center conductor contained an aperture which made it possible to make ram pressure measurements.

The nose cone section of the warhead was used to house the ionosphere transmitter and electronic units for the positive ion gage and the generating voltmeter. These are shown in Fig. 16. An electronic unit associated with the cosmic ray cloud chamber was suspended from the bulkhead separating the two warhead sections. It is visible in Fig. 17. The remaining space between the warhead access doors was occupied by the primary power batteries. These are also seen in Fig. 17. Two ionization gages and two Philips gages were mounted at 90° intervals on a circumference 12.7 cm (5 in.) forward of the warhead base. Two Pirani gages were mounted adjacent to the Philips gages. All of these instruments were exposed to the atmosphere through apertures in the warhead as shown in Fig. 14. The remaining equipments in the warhead, including the telemetering subcommutator, the program timer, the Philips gage battery, and the ionization gage control unit, were mounted



Fig. 14. The January 22, 1948 warhead.

⁴Naval Research Laboratory Report No. R-3171, Chapter III, Section B.

on a rack which was installed as a complete unit in the base of the warhead. The assembly appears in Fig. 18. The warhead was counterweighted by a 7.6 centimeter (3 inch) layer of lead attached to the base.

The cosmic ray cloud chamber assembly, including the pressure system, camera, and batteries, was installed in quadrant I of the control chamber. It is shown in Fig. 34. The telemetering transmitter and the control panel for the research equipment were relocated to quadrant IV. This change was necessitated by the fact that quadrant I was almost wholly occupied by the cloud chamber equipment. Three attitude gyroscopes were installed on the main gyroscope plate in the control chamber.

The midsection installation included a generating voltmeter similar to those used in May 15, and July 10, 1947. The midsection also included equipment for spinning the rocket. Seven Pirani gages were mounted in the tail section 15 centimeters forward of the leading edge of the fins. Four of the gages were located at fin I, the remaining three were located at fin III.

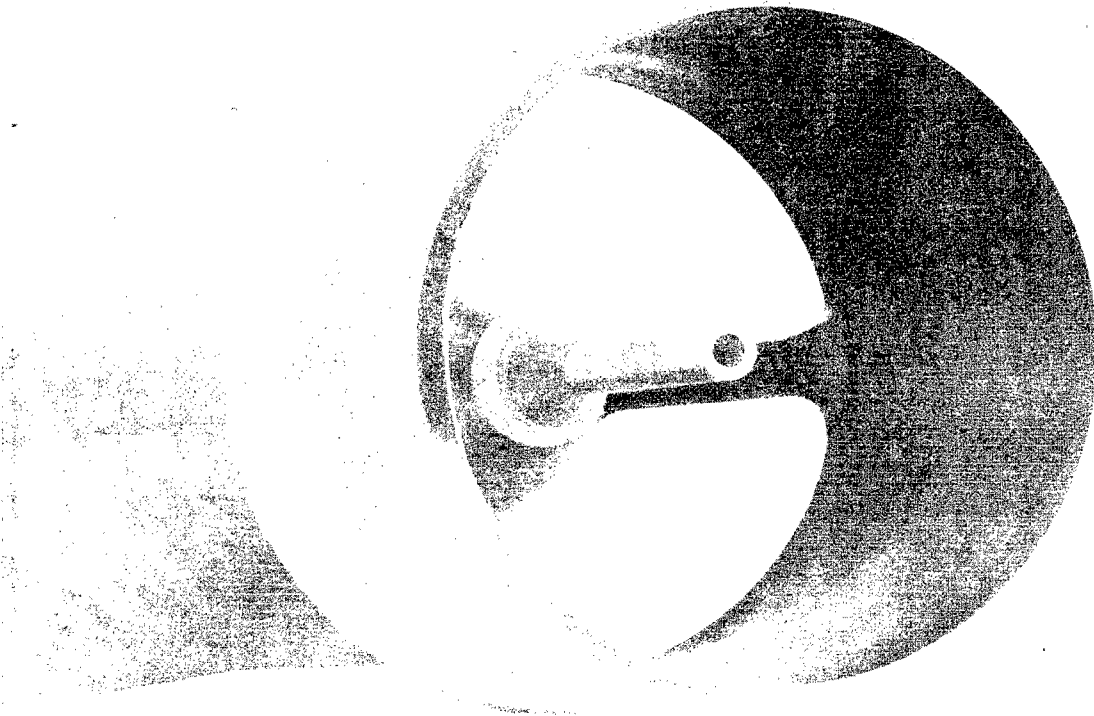


Fig. 15. The positive ion gage employed on January 22, 1948.

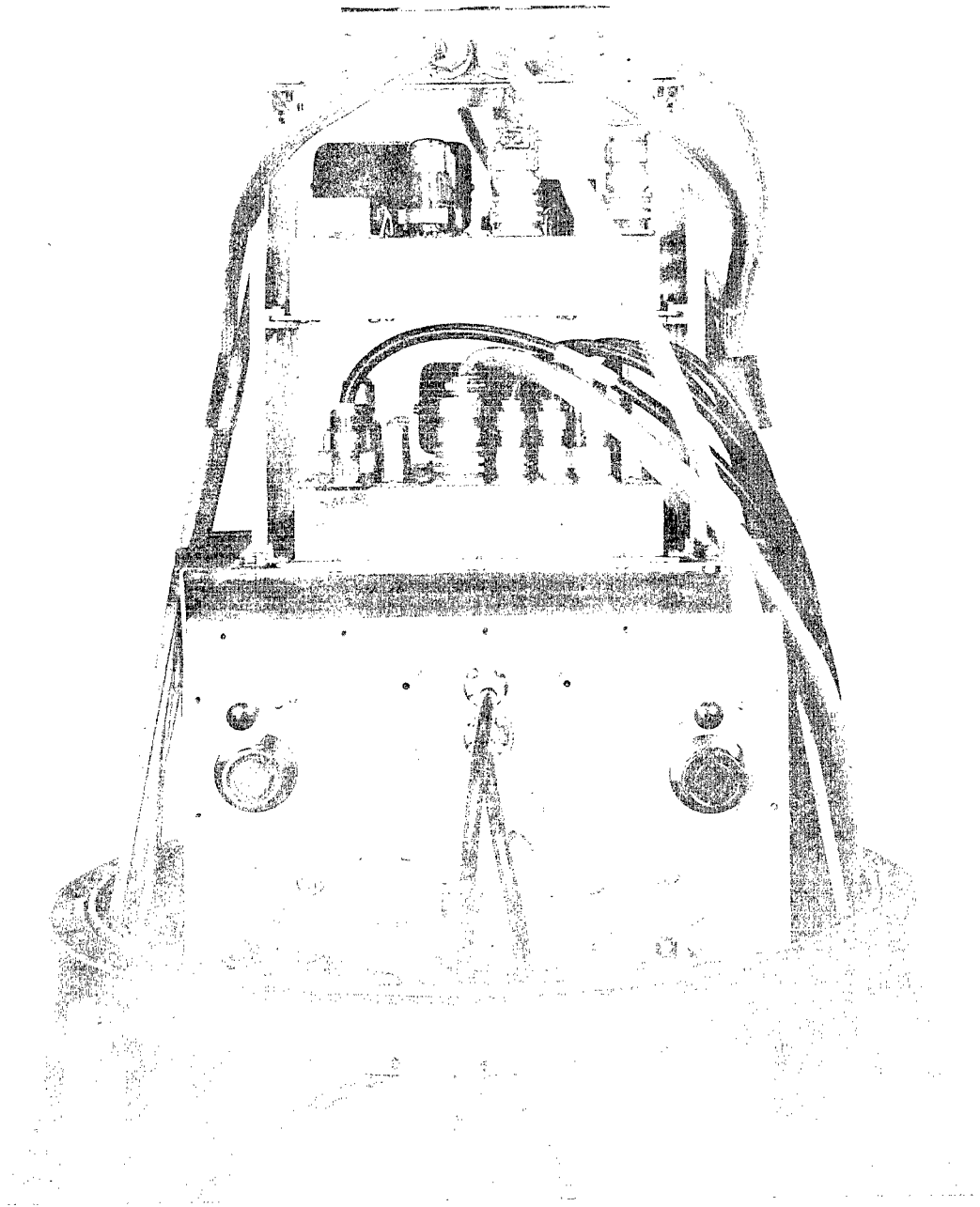


Fig. 16. The ionosphere transmitter, the generating voltmeter electronics, and the positive ion gage electronics mounted in the nose cone section of the warhead.

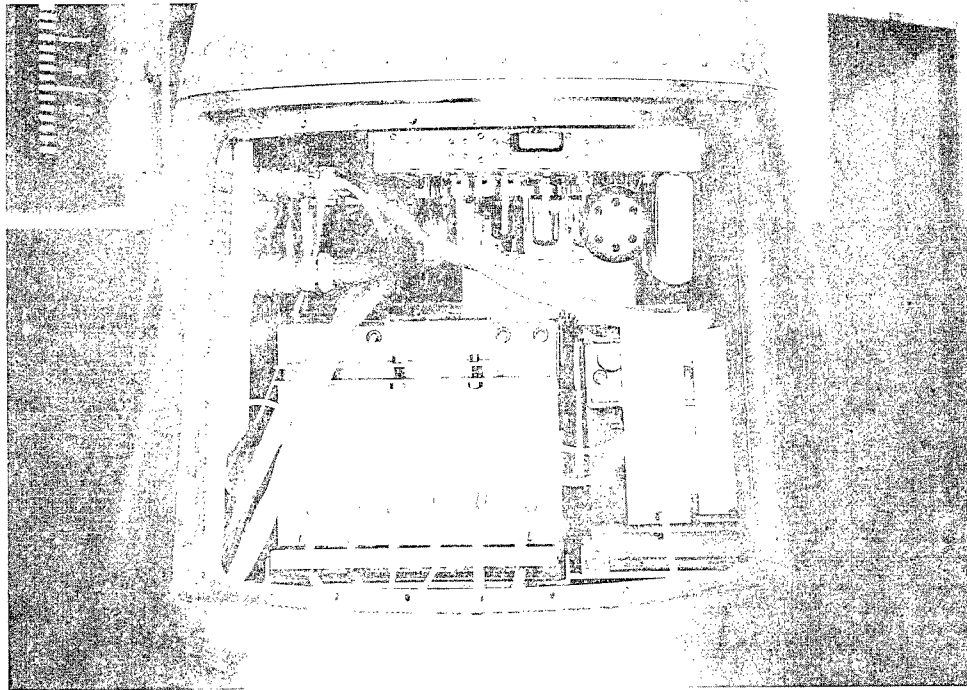


Fig. 17. Cloud Chamber electronics and primary power batteries installed in the main body of the warhead.

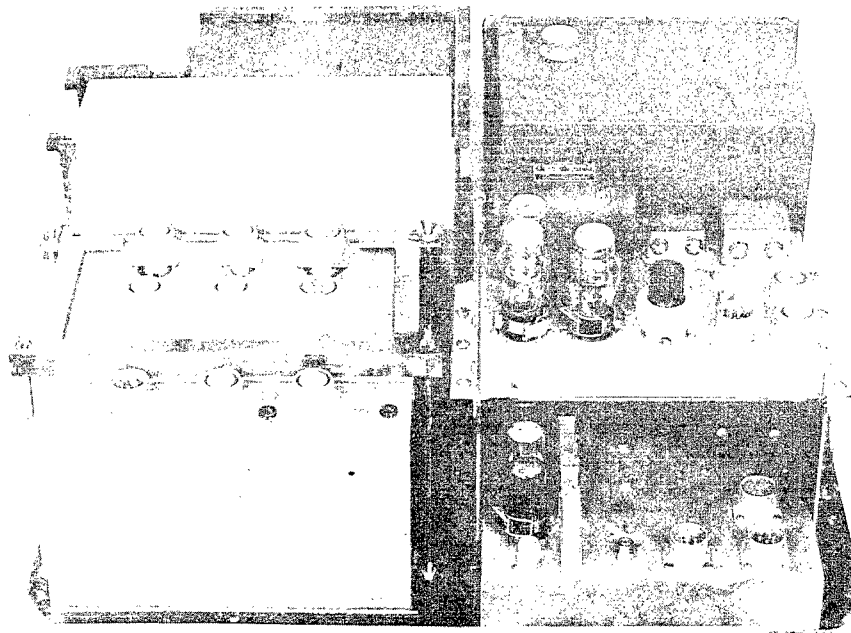


Fig. 18. Research equipment mounted on a single rack preparatory to installation in the warhead.

CHAPTER III

THE V-2 AS A RESEARCH VEHICLE

B. Rocket Attitude Determination by Means of Gyroscopes

by

H. Spitz

An exact knowledge of the attitude and aspect of the V-2 at all times during flight is essential to proper interpretation of the data obtained in many of the rocket experiments. These data may depend upon the missile's angle of attack, upon the angle between some axis fixed in the equipment and a line to the sun, or upon angles measured with respect to other instantaneously fixed axes. In such cases, the key relations are those associated with the Eulerian angles (cf. Fig. 19) between a set of orthogonal axes fixed in the rocket and a similar set, on the same origin, whose directions are fixed in space. These angles completely specify the attitude of the rocket. Hence any other angular information desired may be determined from them.

Gyroscopes are potentially capable of furnishing aspect information with a high degree of precision. Furthermore, this information is presented in a form which is suitable for telemetering. It is not possible in general, however, to read either yaw and pitch or the Eulerian angles directly with standard mounting arrangements.

The purpose of the present discussion is to derive analytical expressions relating the Eulerian angles to the angles actually read from three gyroscopes mounted in a rocket in a particular fashion.

Each of the gyroscopes used in this application consists of a gyrowheel mounted in two gimbals. The gyrowheel axis is perpendicular to the inner gimbal axis, which in turn is perpendicular to the outer gimbal axis. These three axes are oriented so as to be mutually perpendicular at take-off. The outer gimbal axis is fixed in the rocket. The angle through which this gimbal rotates with respect to the missile is converted to a voltage and telemetered to earth. The voltage is reconverted to an angle through the use of suitable calibration procedures.

Three gyroscopes are mounted in the rocket as shown in Fig. 20. The outer gimbal axis of one of these (cf. Fig. 20(c)) is parallel to the principal axis of the missile. This gyroscope measures the amount of roll directly.

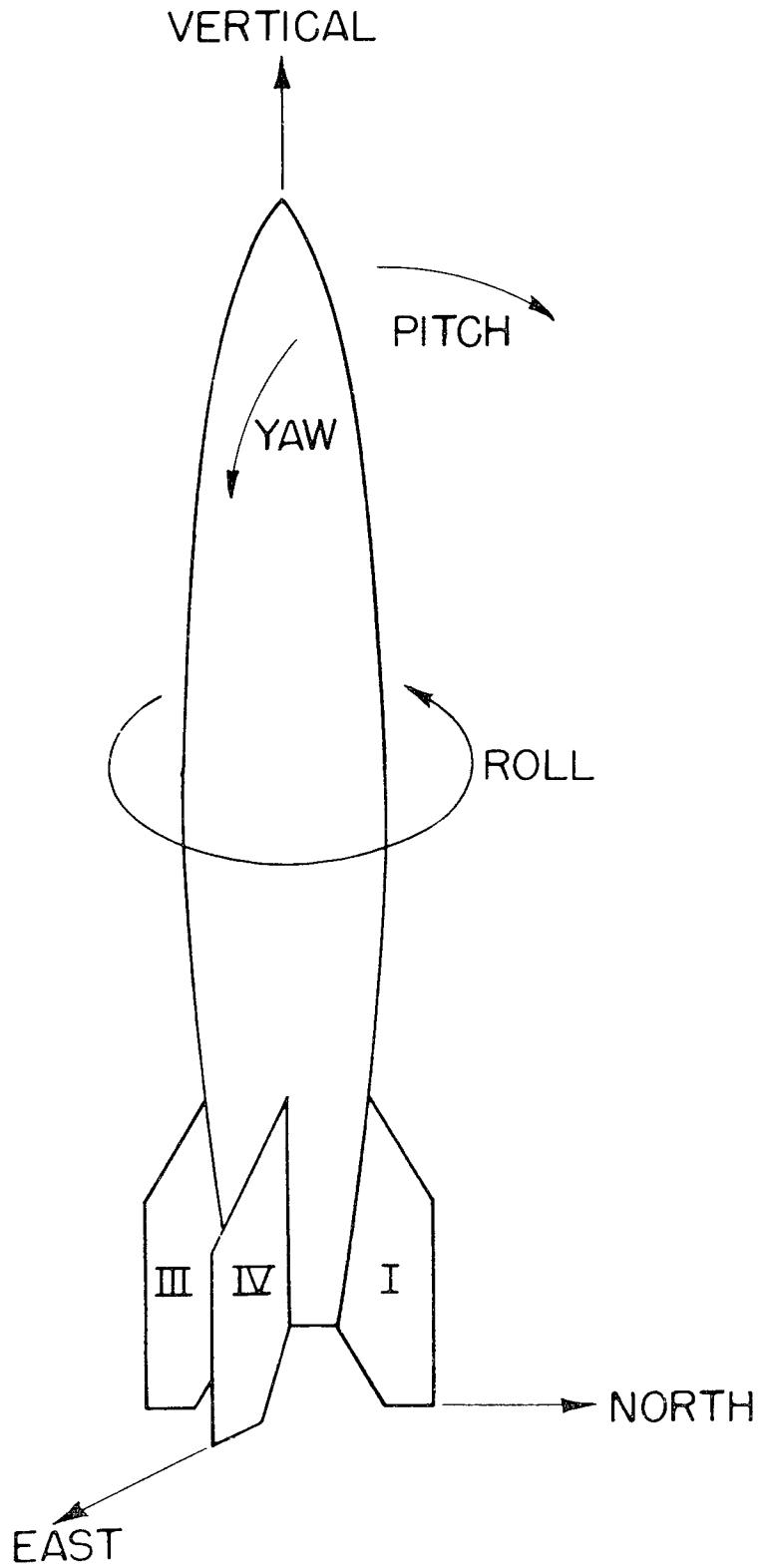
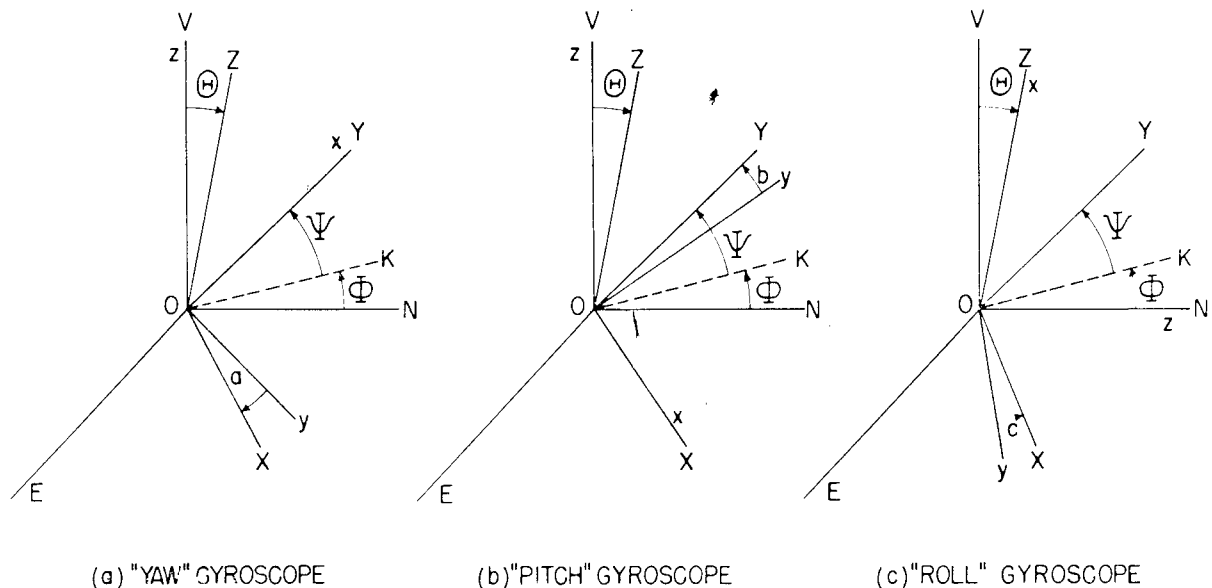


Fig. 21. V-2 Rocket in launching position.

The V-2 is axially symmetric. The fact that the course of a normal flight is toward the north, however, makes it possible to distinguish yaw from pitch in a manner which is consistent with the usual convention. Pitch is defined as a rotation of the rocket's principal axis (or its projection) in the meridian plane. Yaw is defined similarly with respect to the east-west vertical plane. This is illustrated in Fig. 21. The "pitch" gyroscope is therefore mounted in such a way that its outer gimbal axis is normal to the meridian plane at take-off. When so mounted, this instrument will read pitch directly in the special case where no yaw or roll has taken place. In the general case, however, the situation is more complicated. Similar remarks apply to the "yaw" gyroscope.

The general case may be analyzed as follows. The geometrical quantities which enter the discussion are all indicated in Fig. 22. Three sets of axes are employed. E, N and V are fixed in space, X, Y and Z are fixed in the rocket, and x, y and z are fixed in the gyroscope. In each case x is the outer gimbal axis, y is the inner gimbal axis and z is the gyrowheel axis. z is fixed in space and, as noted previously, x is fixed in the rocket and perpendicular to y, while y is perpendicular to z. E, N, V and X, Y, Z coincide at take-off. θ , ϕ and ψ are the Eulerian angles between these two sets of axes, OK being the intersection of the planes EON and XOY. a, b and c are the angles actually measured, i.e. the angles through which the outer gimbals have rotated with respect to the rocket.



AXES FIXED IN SPACE: E, N, V
 AXES FIXED IN ROCKET: X, Y, Z
 GYROSCOPE AXES: x, y, z
 EULERIAN ANGLES: θ , ϕ , ψ
 GYROSCOPE READINGS: a, b, c

Fig. 22. Rocket and gyroscope orientations in the general case.

In the case of the yaw gyroscope, y must always lie in the XOZ plane (cf. Fig. 22a). It is evident that a unit vector in the y direction is given by

$$y_1 = \cos a \ X_1 + \sin a \ Z_1 , \quad (1)$$

where the subscript "1" denotes a unit vector in the given direction. The scalar product $y_1 \cdot z_1$ must vanish, owing to the orthogonality of y and z , i.e.,

$$y_1 \cdot z_1 = y_1 \cdot V_1 = \cos a \ X_1 \cdot V_1 + \sin a \ Z_1 \cdot V_1 = 0 \quad (2)$$

The well-known relations⁵ between unit vectors in the directions of the two sets of axes E, N, V, and X, Y, Z are:

$$X_1 = (\cos \phi \cos \theta \cos \psi - \sin \phi \sin \psi) E_1 + (\sin \phi \cos \theta \cos \psi + \cos \phi \sin \psi) N_1 - \sin \theta \cos \psi V_1 , \quad (3)$$

$$Y_1 = (-\cos \phi \cos \theta \sin \psi - \sin \phi \cos \psi) E_1 + (-\sin \phi \cos \theta \sin \psi + \cos \phi \cos \psi) N_1 + \sin \theta \sin \psi V_1 , \quad (4)$$

$$Z_1 = \cos \phi \sin \theta E_1 + \sin \phi \sin \theta N_1 + \cos \theta V_1 . \quad (5)$$

Substitution of (3) and (5) in (2) yields

$$\cos a (-\sin \theta \cos \psi) + \sin a \cos \theta = 0 ,$$

which may be written as

$$\tan a = \tan \theta \cos \psi . \quad (6)$$

Similarly in Fig. 22b,

$$y_1 = \cos b \ Y_1 - \sin b \ Z_1 ,$$

and

$$y_1 \cdot z_1 = y_1 \cdot V_1 = \cos b \ Y_1 \cdot V_1 - \sin b \ Z_1 \cdot V_1 = 0 .$$

Using relations (4) and (5) we arrive at

$$\tan b = \tan \theta \sin \psi . \quad (7)$$

⁵Cf. Whittaker, E. T., Analytical Dynamics, Fourth Edition, Dover Publications, New York, 1944, p. 10.

For the roll gyroscope

$$y_1 = \cos c X_1 - \sin c Y_1 ,$$

and

$$y_1 \cdot z_1 = y_1 \cdot N_1 = 0 ,$$

which upon substitution of (3) and (4) gives

$$\tan c = \frac{\tan \psi + \tan \phi \cos \theta}{1 - \tan \psi \tan \phi \cos \theta} . \quad (8)$$

Solving equations (6) and (7) simultaneously for θ and ψ we obtain

$$\tan \theta = \sqrt{\tan^2 a + \tan^2 b} , \quad (9)$$

and

$$\tan \psi = \frac{\tan b}{\tan a} . \quad (10)$$

Equation (8) yields a relation for ϕ :

$$\tan \phi = \frac{\tan c - \tan \psi}{\cos \theta (1 + \tan \psi \tan c)} .$$

or

$$\tan \phi = \frac{\tan (c - \psi)}{\cos \theta} . \quad (11)$$

Thus, from the readings a , b and c obtained from the gyroscopes, the Eulerian angles characterizing the rocket's orientation may be determined by means of equations 9, 10 and 11.

CHAPTER IV

THE COSMIC RAY EXPERIMENTS

Introduction

The counter telescope experiments which were attempted in the V-2 firings on May 15 and July 10, 1947 were direct outgrowths of the section's previous rocket research. The May experiment singled out the non-primary cosmic-ray electrons for further investigation. This component had been observed during two previous V-2 flights, on January 10, and March 7, 1947¹. The July experiment came from the results of measurements made in the March missile. The May 15 and July 10 counter telescope experiments are treated in Sections A and B, respectively. The new developments which were incorporated in the electronic equipment designed for these experiments are detailed in Section C.

The first attempt to obtain cloud chamber photographs of cosmic ray events above the earth's atmosphere was made in the V-2 fired on January 22, 1948. Twelve pictures were taken at altitudes ranging up to the peak of the trajectory, which occurred at 157.9 kilometers above sea level. Five of the photographs were obtained above the 140 kilometer level. One of these appears in the Frontispiece. The first four in the series had good clarity, but a cumulative increase in background tended to limit the value of the later pictures. A detailed analysis of the photographs is now being carried out and will be reported upon when completed. A description of the cloud chamber is given in Section D. The electronics which were used to control it, both remotely during pre-flight calibrations and automatically during flight, are discussed in Section E.

¹Naval Research Laboratory Report No. R-3171, Chapter IV, Sections A and B.

CONFIDENTIAL

CHAPTER IV
THE COSMIC RAY EXPERIMENTS

A. The Counter Telescope Experiment of May 15, 1947

by

B. Howland, G. J. Perlow and J. D. Shipman, Jr.

This experiment was designed to furnish further evidence concerning the nature of the non-primary cosmic ray electron component previously observed in the rocket experiments. Data obtained in two earlier flights, on January 10 and March 7, 1947, indicated the presence above the earth's atmosphere of ionizing particles capable of being absorbed in a few centimeters of lead. On the basis of a hypothesis put forward by J. A. Wheeler, these particles were tentatively assumed to be electrons arising from the decay of low energy cosmic-ray mesons. Decay electrons having an initial upward direction would describe helical paths about the earth's magnetic field lines, and re-enter the atmosphere within small conjugate regions having geomagnetic latitudes opposite to those of the points of their origin. This conception of the phenomenon implies the existence of an observable upward intensity of soft electrons.

The May 15 experiment put the circulating electron hypothesis to a more definitive test. To this end, a double counter telescope was designed and constructed. Three views of the instrument are given in Figs. 23 and 24 and in Fig. 26. One of the telescopes, inclined at an angle of 45° to the rocket's principal axis, registered the conventional downward soft intensity. The other looked in the opposite direction; i.e. it had a zenith angle of 135° relative to the rocket. A portion of the latter telescope as it was installed in the V-2 warhead is visible in Fig. 31. The geometrical details of the twin telescopes are indicated in Fig. 25. This arrangement permitted the measurement of the relative magnitudes of the soft components of the upward and downward fluxes. The presence of comparable magnitudes would constitute strong experimental support for the circulating electron hypothesis.

Counters 1, 2 and 3, in coincidence with each other and in anticoincidence with counters X, served to define a downward beam. This beam was incident upon the first absorber which consisted of a 2.5 cm thickness of lead. Particles penetrating this absorber were detected by the next bank of counters, labelled 4, which completely covered the incident solid angle. Penetration of the next 2 cm thickness of absorber was similarly determined by the bank of counters labelled 4'. The counter in each of these banks were electronically paralleled in groups of three. Hence, in each bank, a shower was capable of being detected by any one of the three-fold coincidences designated by the subscripts a, b and c. As can be seen from the figure the lower telescope which studied the upward beam was identical with the

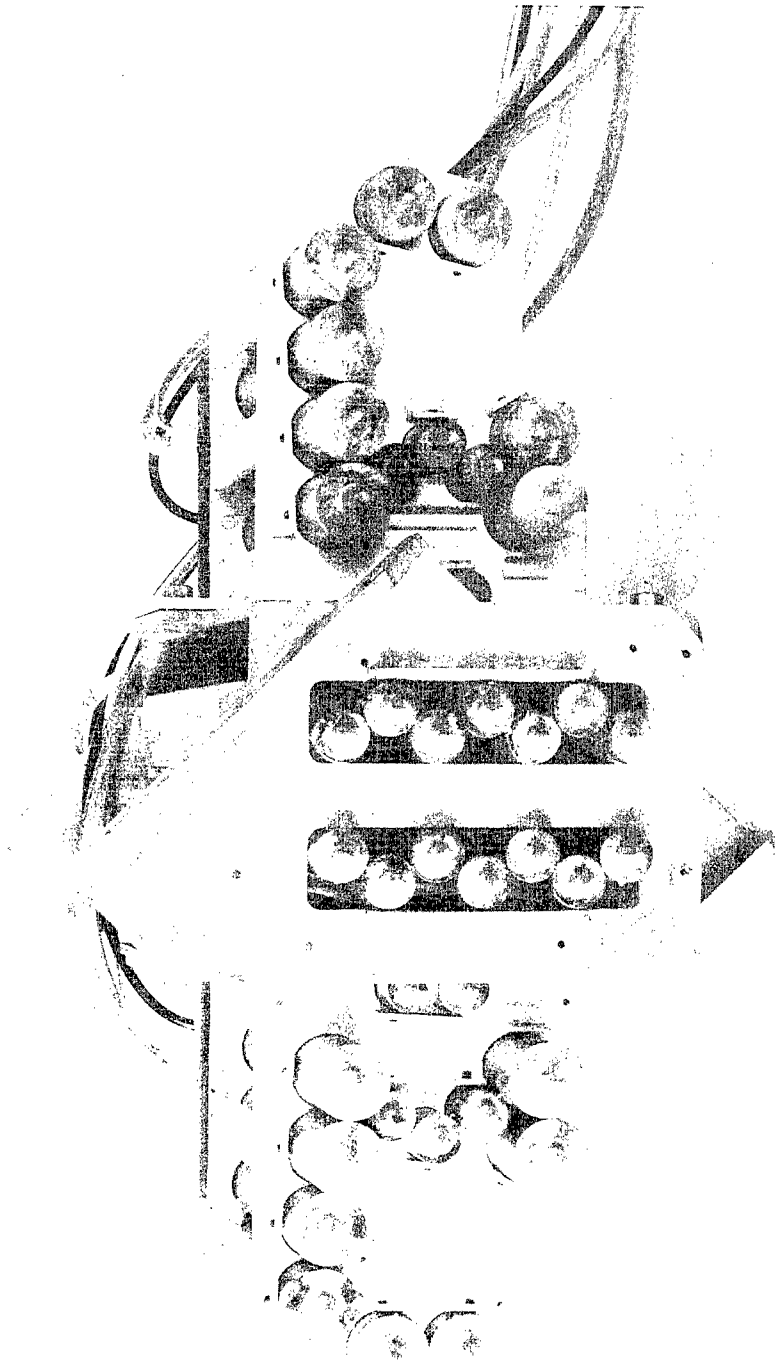


Fig. 23. Side view of the counter telescope employed on May 15, 1947.

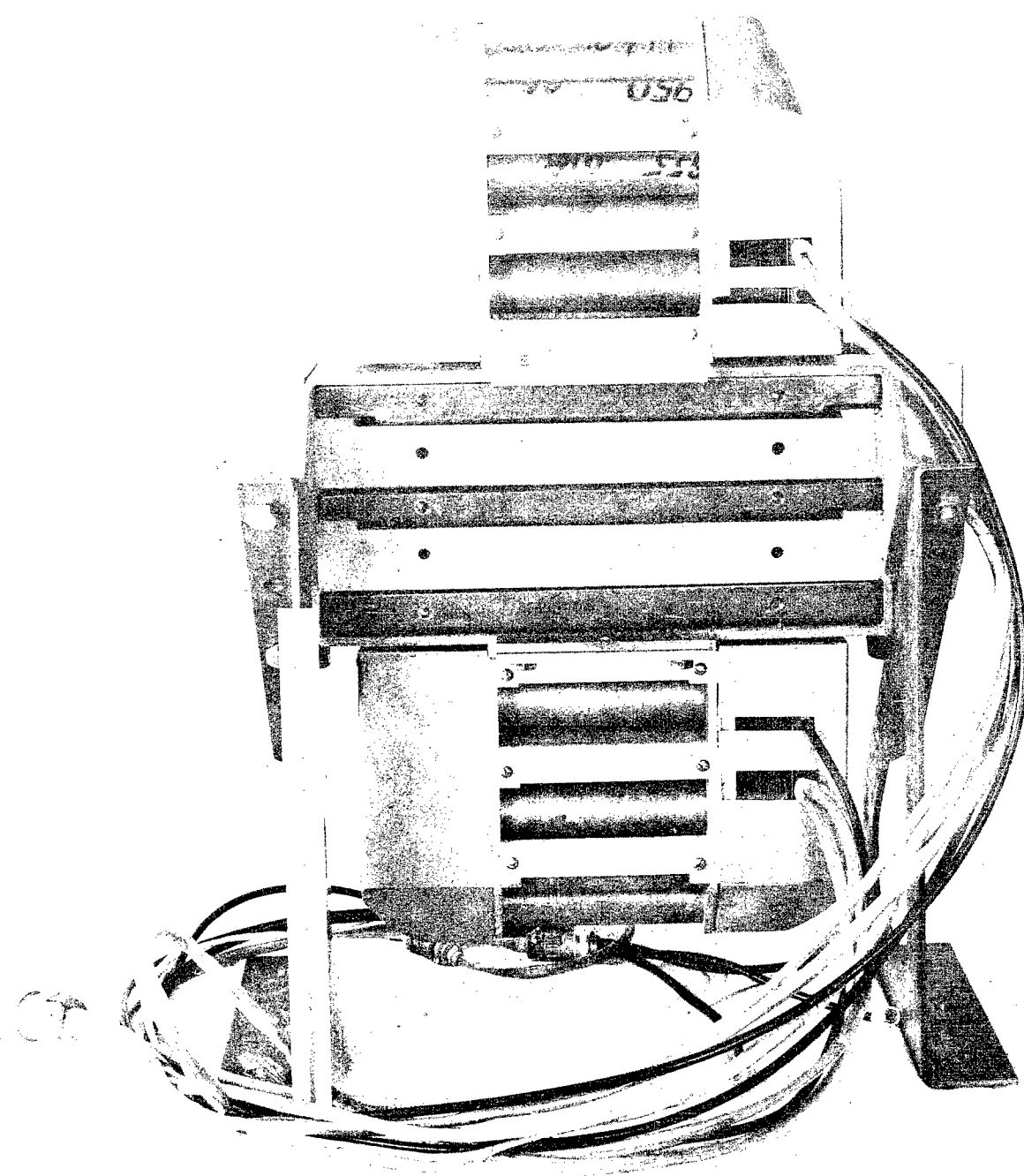


Fig. 24. View of the May 15, 1947 counter telescope showing the lead absorbers in place.

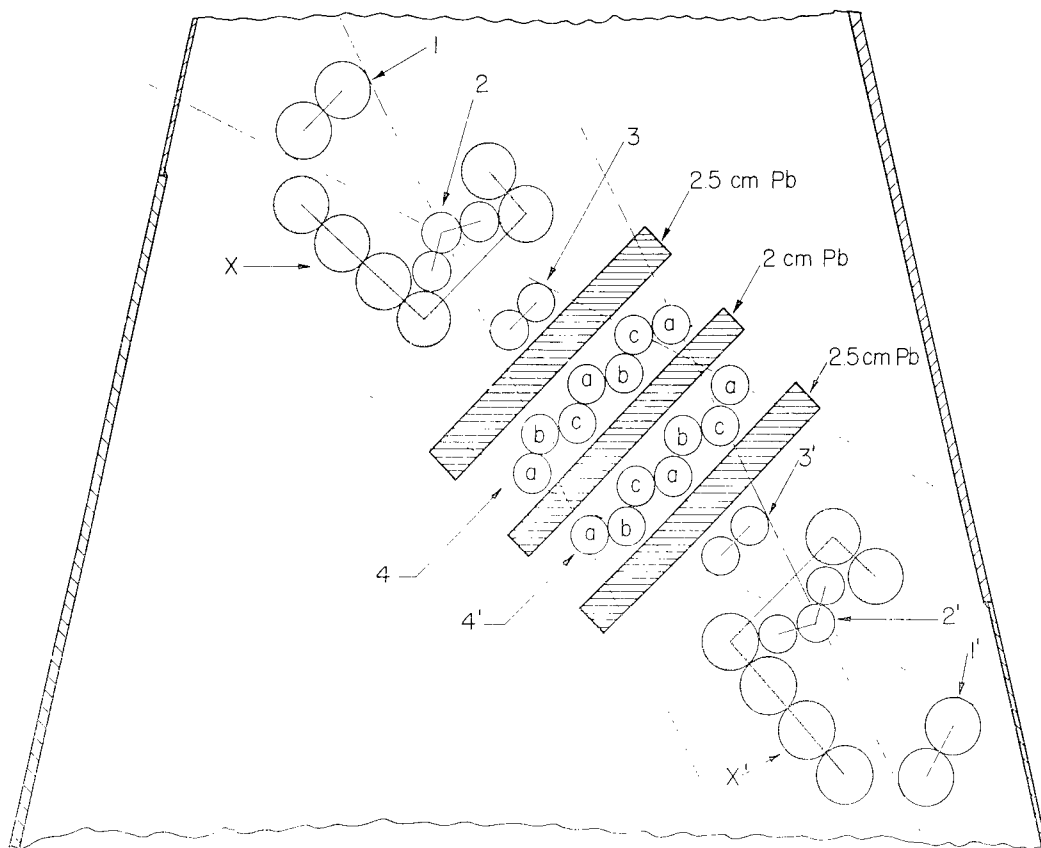


Fig. 25. Schematic drawing of the May 15, 1947 counter telescope.

upper one. The direction of a penetrating particle traversing both telescopes is not identified. Such a particle, having penetrated seven centimeters of lead, would be identified as being lead, however, and would not belong to the class of particles under study in this experiment.

The top-most detector served a double function: first, as has already been indicated, to identify soft particles incident from above, and secondly, to identify a number of high particles between gamma rays or neutral particles incident from above, and soft particles incident from below. For example, a fast gamma ray incident upon the top detector would be converted into an electron pair. If one of these electrons had sufficient energy, it would register in counter 1, 2, 3, and the lower telescope 1', 2', 3'. Such a particle would, in general, be indistinguishable from a hard particle coming from above, but it could not be confused with a soft particle coming from below.

This rocket exploded approximately 34 seconds after take-off. As a result, only meagre statistics were obtained. These are presented in Table IV. They indicate that prior to the explosion the number of particles incident from below was comparable to the number incident from above. This result is interpreted as being in agreement with the circulating electron hypothesis.

TABLE IV

The Relative Intensities of the Soft Components of the
Upward and Downward Cosmic Ray Flux Observed on May 15, 1947

Time Interval in seconds after take-off	Altitude in km at Mean Time in Each Interval	Pressure in cm Hg at the Mean Time	No. of Downwardly Incident Particles Absorbed in -		No. of Upwardly Incident Particles Absorbed in -	
			2.5 cm Pb	4.5 cm Pb but not in 2.5 cm Pb	2.5 cm Pb	4.5 cm Pb but not in 2.5 cm Pb
0-5	.02	65.5	0	0	0	0
5-10	.25	64.0	0	0	0	0
10-15	.75	60	0	0	0	0
15-20	1.60	54	0	0	0	0
20-25	2.85	46.3	0	0	0	0
25-30	4.50	36.5	1	0	0	0
30-35	6.60	27.2	2	0	1	0
35-40	9.05	19.1	4	2	1	0
40-45	12.05	12.2	3	4	2	0
45-50	15.65	7.0	10	3	2	1
50-55	19.05	3.5	3	6	0	1
55-60	25.15	1.6	3	4	2	1
60-64.2	30.75	0.68	0	0	2	0

CHAPTER IV

THE COSMIC RAY EXPERIMENTS

B. The Counter Telescope Experiment of July 10, 1947

by

S. E. Golian and E. H. Krause

The objectives of this experiment were suggested by certain facts revealed in the V-2 cosmic-ray experiment of March 7, 1947². The large number of penetrating showers registered in that experiment were apparently due to the increased amount of material of high atomic number in the immediate vicinity of the counter telescope. This material, heavy lead shielding, had been installed to absorb the showers which were thought to have been due chiefly to electrons. The March 7 experiment demonstrated, however, that the showers were considerably more penetrating than those usually generated by electrons.

The July 10 experiment had as its purpose the investigation of this primary shower process. The design adopted permitted the observation of three important characteristics of the showers, their points of origin, their extent, and their penetrating power. Two steps were taken to diminish the presence of unidentified electron showers in the data. First, almost all of the lead shielding was removed, and the warhead was constructed of material having the minimum thickness and atomic number consistent with safety. Secondly, shower protection was furnished by extensive banks of anticoincidence counters. These were grouped in such a way as to shed light on the question of where the showers originated. The associated circuitry had provisions for the identification of showers of many particles. The penetration of the showers was tested by three 6 cm lead absorbers. These were of somewhat greater thickness than those employed in the March 7 design.

The data were recorded both by the telemetering system and by means of a camera recorder. Fifteen types of information were telemetered over thirteen channels by duplexing two of the channels. These data and a time scale were also recorded by a twenty-channel camera recorder. The neon bulbs were mounted in a single line rather than staggered. Otherwise, the instrument was similar to the one employed in the earlier flights.³

The July 10 flight was terminated prematurely and as a result only a small quantity of data was obtained. The results were, accordingly, inconclusive. During the period of measurement, however, the incidence of rocket showers was significantly less than in the March 7 experiment.

²Naval Research Laboratory Research Report No. R-3171, Chapter IV, Section B.

³Naval Research Laboratory Report No. R-3030, Chapter IV, Section D.

CHAPTER IV

THE COSMIC RAY EXPERIMENTS

C. Electronics for the Counter Telescope Experiments

by

B. Howland, C. A. Schroeder,
and J. D. Shipman, Jr.

The electronic techniques employed in the May 15 and July 10, 1947 rocket experiments were, for the most part, similar to those used in the earlier work. They were amply described in previous articles.⁴ An innovation was, however, incorporated in the first of these two experiments.

The electronics chassis is often mounted at some distance from the Geiger counters comprising the cosmic ray telescope. In the May 15 rocket, for the first time, cathode followers were mounted directly on the counter telescope frame as shown in Fig. 26. 6K4 triodes were used in this application (cf. Fig. 27). The new arrangement obviated the need for double shielding the long leads connecting the counters with their electronics. Instead, ordinary single-shielded leads were used for this purpose. The main electronics chassis may be seen in Figs. 28 through 30. Its location in the V-2 warhead is shown in Fig. 31.

The modification also resulted in a somewhat larger counter pulse and in greater sensitivity. The crosstalk difficulties were unfortunately increased correspondingly. Their effect was minimized by taking advantage of the difference in amplitude between the true and the spurious pulses. A special circuit was designed for the grids of the input amplifiers. Each of these grids was returned to B^+ through a 27,000 ohm resistor and a 470,000 ohm resistor in series. The input connections were made in each case at the junction point of these two resistors, as shown in Fig. 27. The quiescent value at each of the grids was approximately +0.2 volts, and the quiescent value at each of the inputs was approximately +13 volts. This grid circuit attenuated the crosstalk to a much greater degree than it attenuated the counter pulses. The 13 volt differential proved to be optimum for the purpose of distinguishing between the counter pulses and crosstalk.

As in previous flights, the number of telemetering channels available was less than required. Hence, in the May 15 design, four of the eight channels carried two types of information alternately. Parallel jumpers, mounted externally, were used to duplex the output. Coding was accomplished by doubling the pulse length of one of the outputs in each pair. The cosmic ray events were also recorded on a ten-channel camera recorder.

⁴Naval Research Laboratory Report No. R-3171, Chapter IV, Sections C and D.

The circuit diagram of the cosmic ray electronics employed on July 10 is given in Figs. 32 and 33. Four of the events were duplexed on two of the telemetering channels. The large number of events involving the coincidence 1, 2, 3 made it desirable to develop this triple in three independent circuits in order to minimize crosstalk. The camera recorder employed in this missile had twenty channels, giving it twice the capacity of previous models. Thus it was possible to record each of the fifteen types of events on a separate channel.



Fig. 26. View of the May 15, 1947 counter telescope showing the cathode followers mounted on the frame.



Fig. 28. Top view of the May 15, 1947 cosmic ray electronics chassis.

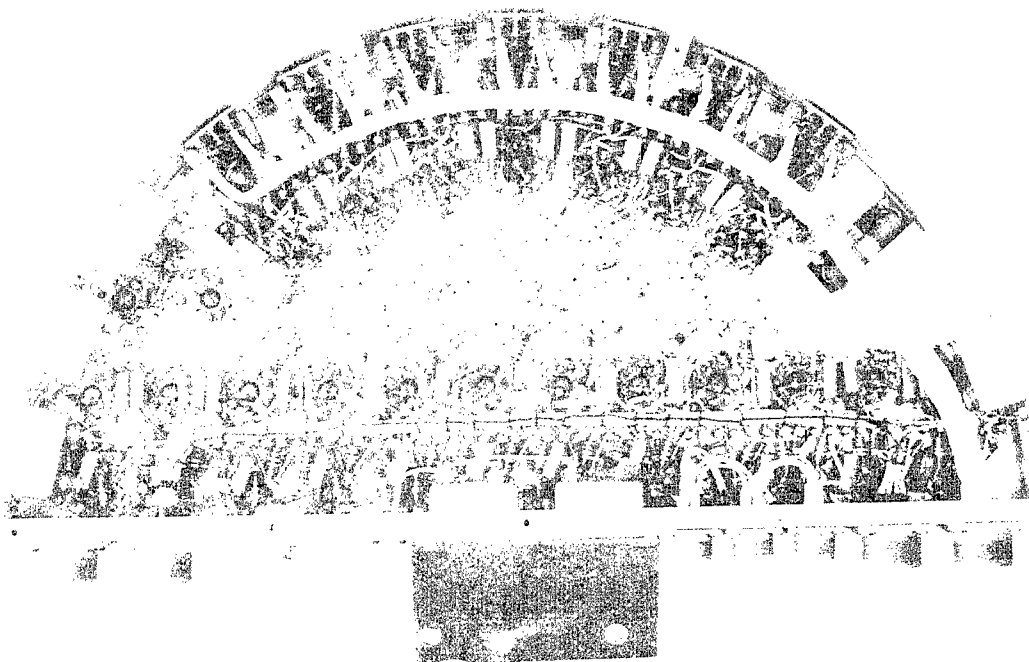


Fig. 29. Bottom view of the May 15, 1947 cosmic ray electronics chassis.

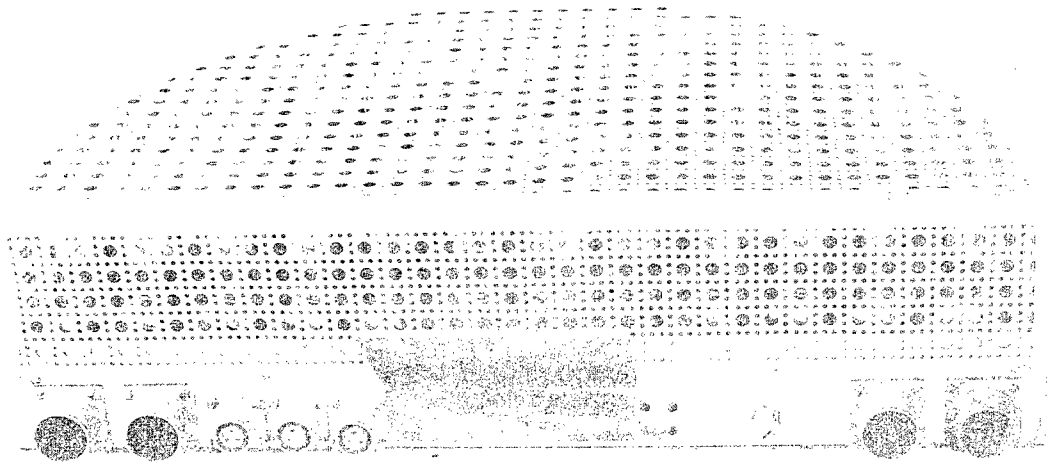


Fig. 30. Top view of the May 15, 1947 cosmic ray electronics chassis showing guard grille.

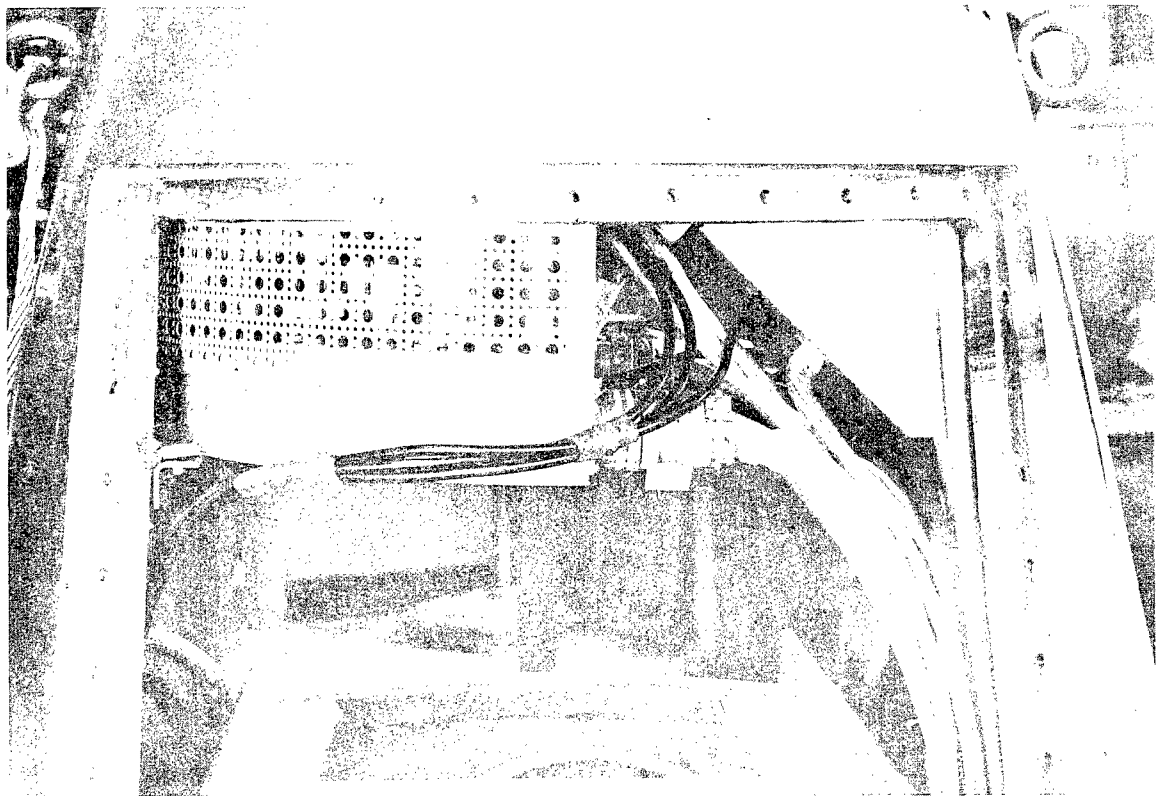


Fig. 31. The May 15, 1947 cosmic ray electronics chassis installed in the V-2 warhead.

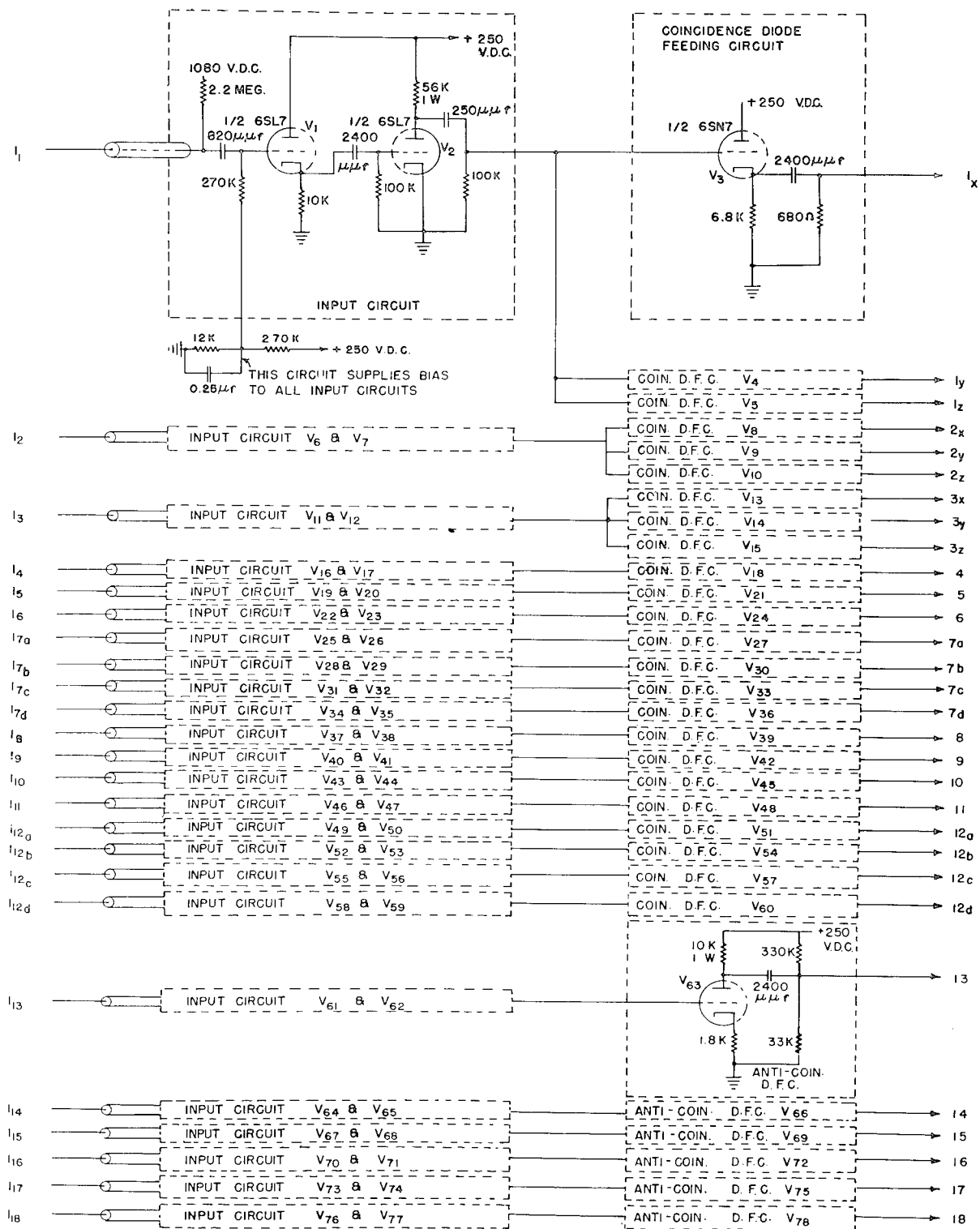


Fig. 32. Circuit diagram of the July 10, 1947 cosmic ray electronics, Part I.

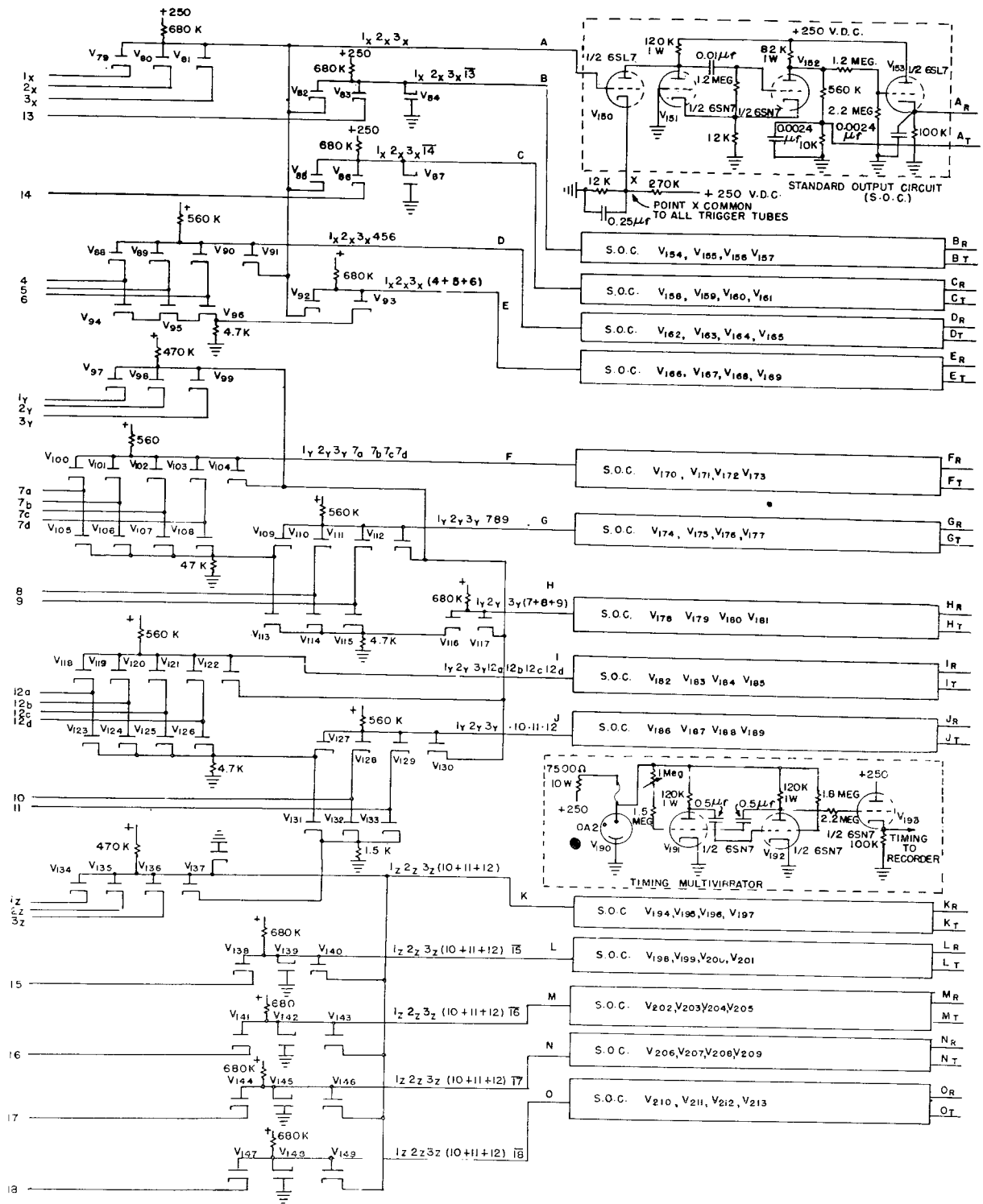


Fig. 33. Circuit diagram of the July 10, 1947 cosmic ray electronics, Part II.

CHAPTER IV

THE COSMIC RAY EXPERIMENTS

D. The Cloud Chamber

by

S. E. Golian, C. Y. Johnson, E. H. Krause
and M. L. Kuder

Cloud chambers, one of which the Naval Research Laboratory flew in a V-2 on January 22, 1948, are often used to investigate the characteristics of elementary particles occurring singly or in relatively small groups. The general principles of operation are as follows. A charged particle having sufficient energy ionizes atoms and molecules in the neighborhood of its path. These newly-ionized particles are potential condensation nuclei. The cloud chamber takes advantage of their presence within it by creating a supersaturated gas (through expansion cooling), portions of which condense upon the ions to form droplets. The characteristics of the droplet track are in general known functions of the incident particle's character, charge, mass, and speed. To facilitate analysis, the tracks are usually photographed stereoscopically.

Cloud chambers as normally used also enjoy the advantages which are derivable from the gravitational field. The clearing of droplets formed on uncharged nuclei is due to gravity. Since the V-2 is essentially a freely falling body after Brennschluss, gravitational effects are not present in the usual way. The V-2 cloud chamber used by NRL was mounted at some distance from the rocket's axis, and the rocket was given a spin.⁵ The centrifugal force associated with the rocket's spin thus afforded an alternative method for accelerating the droplets relatively to the cloud chamber.

The cloud chamber may be expanded randomly, i.e., without reference to knowledge of the passage of a particle, or it may be controlled by counters to expand only when a particular type of event has occurred within it. In the January 22 V-2 flight, random expansions were made; first, because this was simpler; and, secondly, because estimates of the flux indicated that there would be many tracks in each expansion.

The chamber which was flown in the January 22 V-2 was of the pneumatic type, 6 in. in diameter and 3 in. in depth. The assembly associated with it is partially visible in Fig. 34, and is diagrammed in Fig. 35. The chamber proper consisted of a glass cylinder closed by a plate glass top

⁵The attempt to spin the V-2 was not completely successful; a period of 29 seconds was obtained.

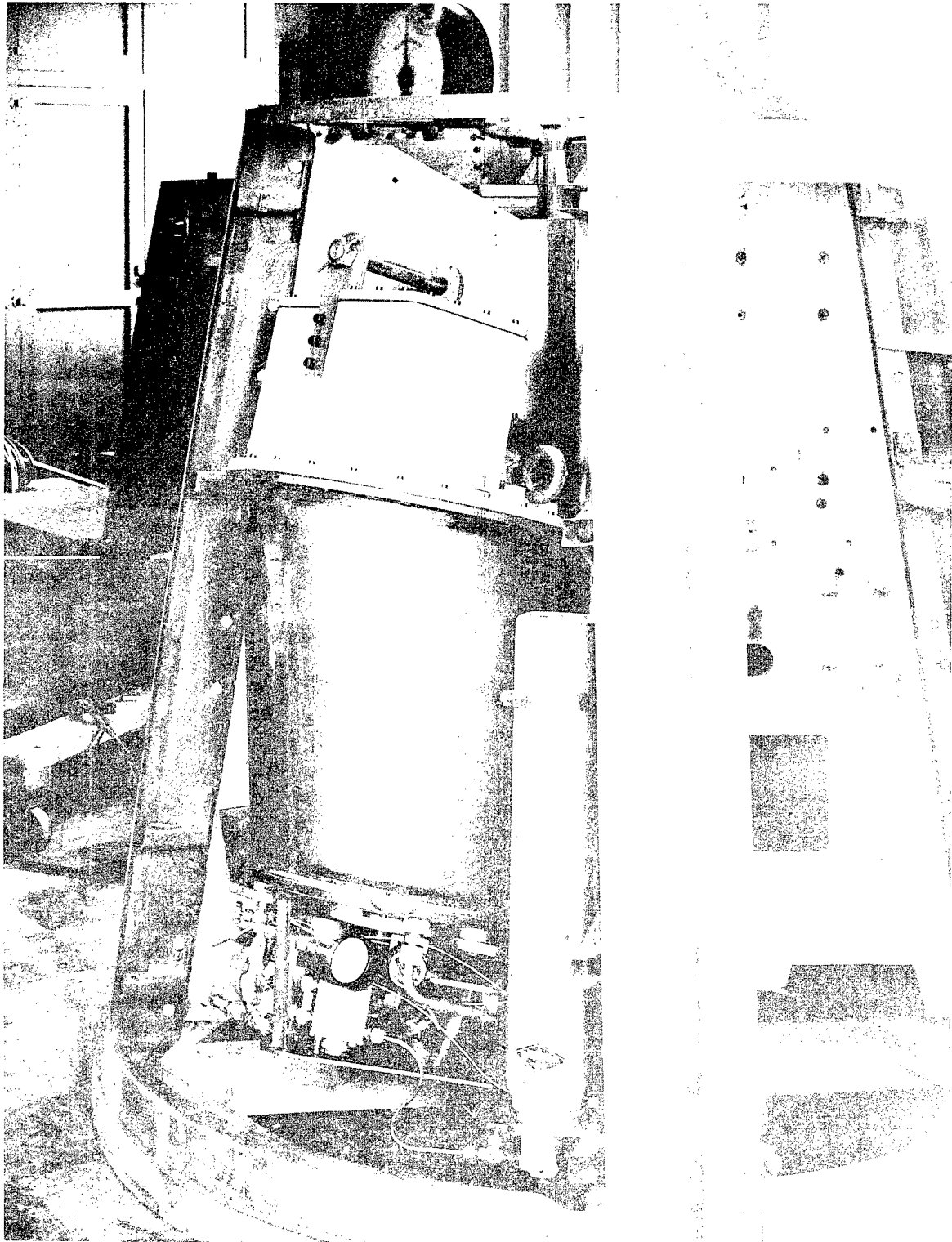


Fig. 34. The cosmic ray cloud chamber assembly mounted in the control chamber of the V-2.

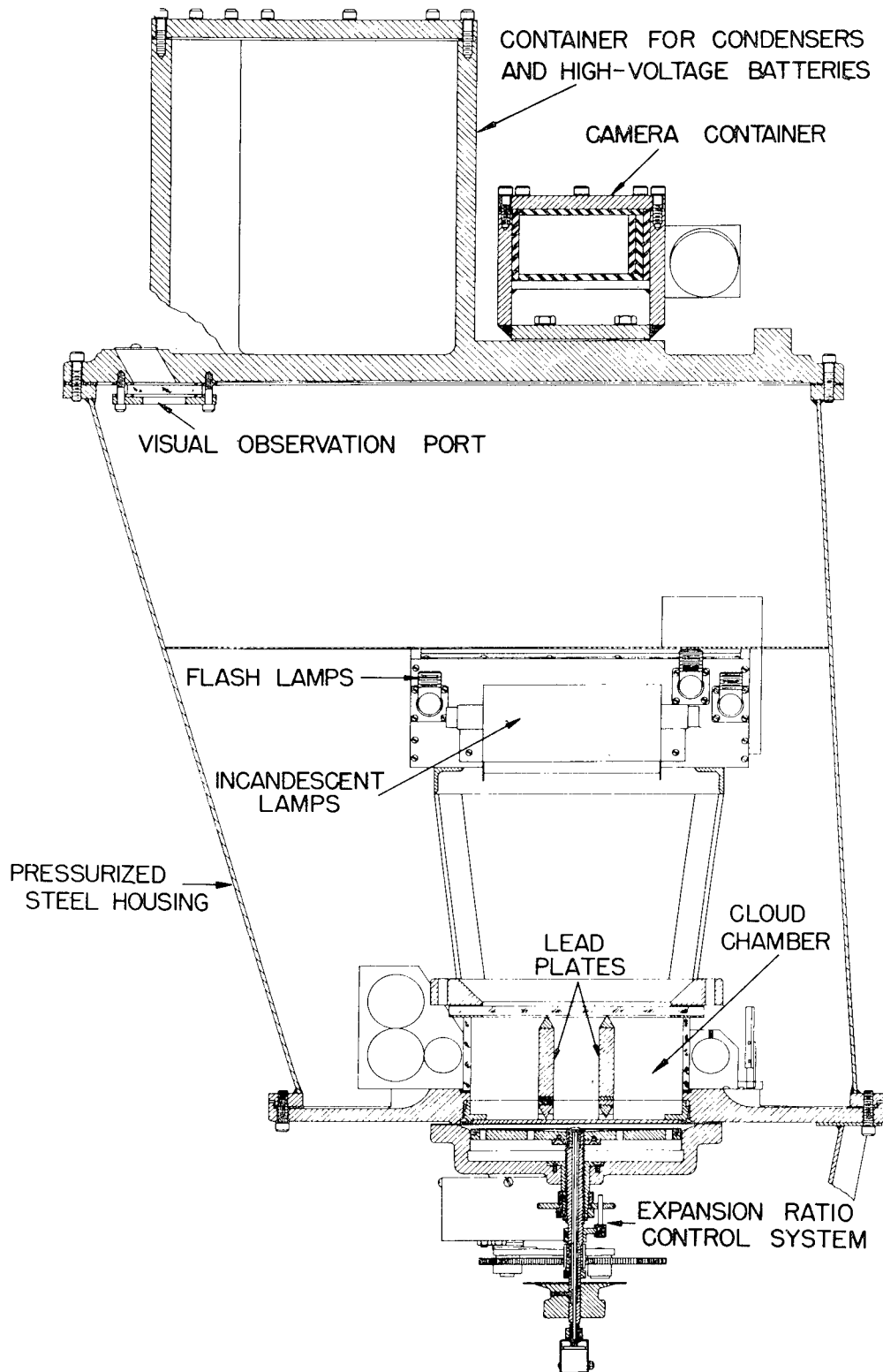


Fig. 35. Diagram of the cosmic ray cloud chamber.

and a rubber diaphragm base. An aluminum plate was cemented to this diaphragm, and the plate in turn was covered with black velvet to improve the photographic resolution. A pair of one-centimeter parallel lead plates were mounted in the interior, dividing it into three chambers of equal characteristic length.⁶ The lead plates permit one to distinguish between different types of particles by observing absorption, shower production, scattering and reduction in ionization after a traversal. The plates also served as electrodes for the clearing field.

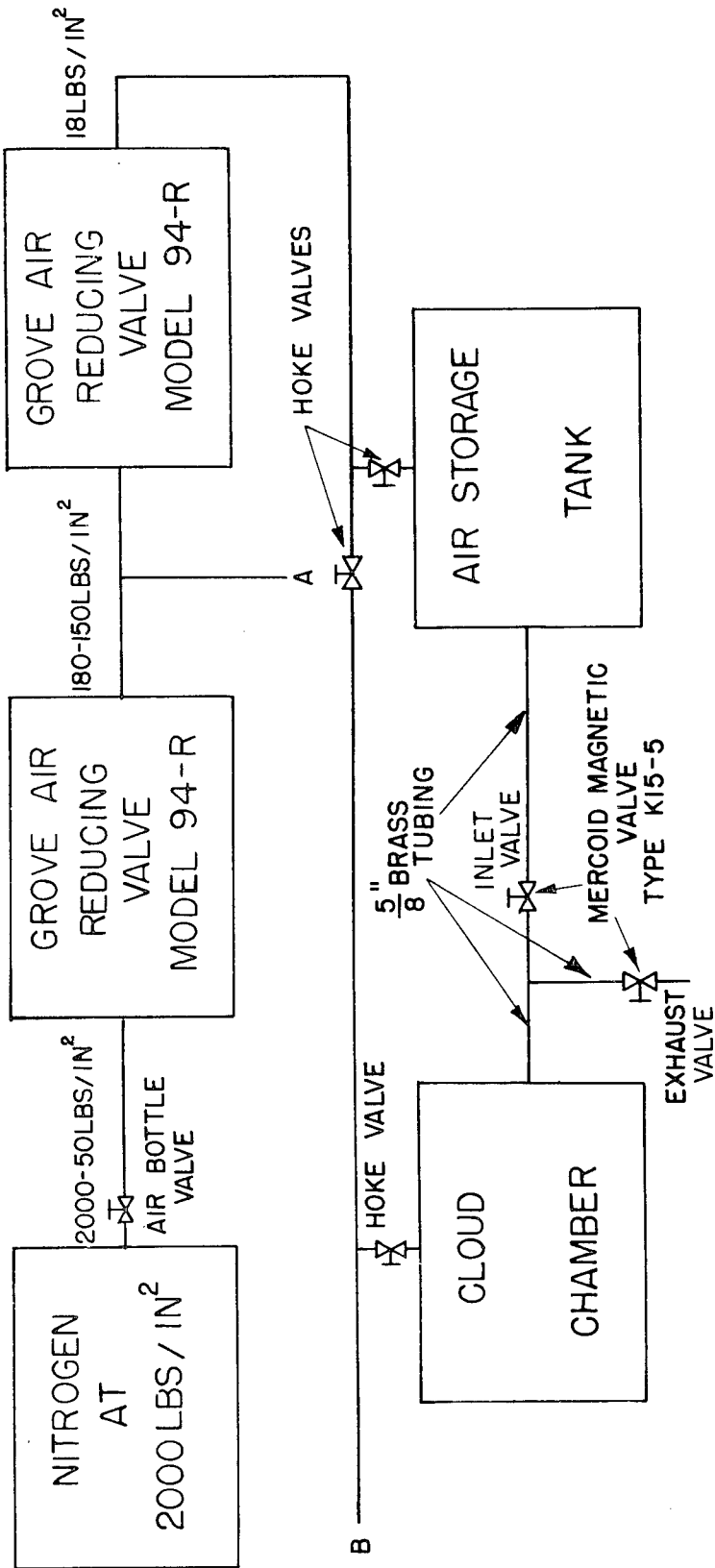
A steel housing was bolted to the base of the chamber. This housing, which can be seen in Fig. 34, served to make the unit light-tight and also to provide an intermediate-pressure reservoir of compressed air for the operation of the chamber. The mirrors and flash lamps were mounted inside this housing. The camera and the batteries and condensers used to operate the lamps were mounted in separate containers at the top of the main housing. The servo system associated with the expansion ratio control was also mounted externally to the main housing, immediately below the cloud chamber. All of these units, as well as a compressed air storage flask and a wiring distribution unit, were mounted in quadrant I of the control compartment in the manner shown in Fig. 34.

The plane of the chamber made an angle of twenty degrees with a transverse plane of the rocket.

The chamber was filled with a mixture of argon saturated by the vapor of 0.9 cm³ of ethyl alcohol and 0.6 cm³ of water. This mixture was maintained at a pressure of two atmospheres.

Expansion was accomplished through moving the aluminum plate by compressed air. The plate's excursion was determined by one fixed and one adjustable stop. An expansion ratio of about 1.07 was used. A schematic diagram of the pneumatic system is given in Fig. 36. Power for the expansion was obtained from a nitrogen flask, charged initially at 2,000 psi with a quantity of gas equivalent to seven cubic feet at ntp. The pressure was reduced to that actually used in operating the chamber by two Grove regulator valves in series. The housing itself served as the lower-pressure reservoir. Two Sylvania Fl. 333 flash lamps in series provided the light source for the photographs. They were flashed by three 32 μ f condensers which were charged by a 2,400 volt battery. The flash time was estimated at one millisecond. Light from the flash lamps was collimated by a polished reflector and a doubly-convex plastic lens. This arrangement gave two beams, each one inch wide, which were redirected into the chamber by aluminum front surface mirrors. Four fifty-candlepower lamps were used for visual observation.

⁶The characteristic length is the ratio of the enclosed volume to the enclosing surface. The rate at which a chamber's atmosphere cools is a function of this ratio.



AIR LINES ARE QUARTER-INCH BRASS TUBING UNLESS OTHERWISE INDICATED.
 ARGON OR LOW PRESSURE AIR CAN BE INTRODUCED, AND INTERMEDIATE PRESSURE
 AIR CAN BE MEASURED AT POINT A.
 ALCOHOL-WATER MIXTURE CAN BE INTRODUCED, AND CLOUD CHAMBER PRESSURE CAN BE
 MEASURED AT POINT B.

Fig. 36. Schematic diagram of the pneumatic power system employed to operate the cloud chamber.

A 35 mm Argus model A-2 camera was modified for the purposes of the experiment. It mounted a two-inch f/4.5 Wollensak enlarging lens. The camera was used without a shutter. Eastman Linograph ortho film and an f/5.6 setting were used. An aluminum mirror, appropriately mounted, was used to provide the second image for the stereoscopy.

The chamber was cycled once every twenty-five seconds by the control electronics mounted in the warhead. This equipment, designed and constructed especially for the purpose, is described in detail in the next section. A complete cycle of operation was as follows. The cycle began with the removal of the clearing field. Approximately 0.05 seconds later the expansion was initiated. A mechanical linkage caused the resulting motion of the chamber diaphragm to actuate a microswitch which controlled the flash lamp circuit. The lamps flashed 0.15 seconds after the expansion, exposing the film. Recompression of the chamber began shortly afterward. Simultaneously with this, the clearing field was reapplied and the film drive motor was started. This motor was stopped, five to seven seconds later, when the advancing of the film counter momentarily opened the circuit. The remainder of the cycle was set aside for the clearing of the chamber.

The rocket motor is usually found more or less intact in the impact wreckage. Accordingly, a length of half-inch steel elevator cable was threaded through the midsection and anchored to the motor. The other end of the cable was attached to an eyebolt on the camera case, and to a one-inch steel bar supported by extensions of the battery case. These latter anchoring points are visible in Fig. 34.

The rocket came apart much later than usual in this flight. When it did, shortly before impact, the warhead and control chamber broke away from the rest of the rocket in spite of the cables. These were severed. The warhead and control chamber entered the earth nose first at about twenty degrees from the vertical. They dug a clean crater about eight feet in diameter and six feet deep. The cloud chamber was totally destroyed, the camera's container was broken open and the camera itself was smashed. The film cartridge was found after two feet of earth were excavated in the region of the control compartment which had been occupied by the cloud chamber. The crater appears in Fig. 3 of Chapter I, and the remains of the camera container and parts of the cables are shown in Fig. 37. Several breaks in the cables may be seen.

The film was successfully developed and a number of acceptable photographs were obtained. The analysis of these is now in progress.



Fig. 37. The cloud chamber film canister as it was recovered after the flight.

CHAPTER IV

THE COSMIC RAY EXPERIMENTS

E. Equipment for the Automatic and Remote Control of the Cloud Chamber

by

C. Y. Johnson, M. L. Kuder
and C. A. Schroeder

1. The Automatic Control Equipment

The proper operation of the cloud chamber required the occurrence of a number of events according to a predetermined sequence. This sequence, or cycle, of events was detailed in Section D. It was controlled automatically by means of electronic equipment which was specially designed and constructed for the purpose. The equipment included circuits for both counter-controlled cycling and periodic random cycling. Only the latter circuits were used during this experiment. The equipment also had provisions for checking the operation of the chamber during flight by means of voltages recorded on the telemetering record.

The self-cycling control circuit which was used in this experiment is shown in Fig. 38. It was a modified cathode-coupled, blocked multivibrator, consisting of the tubes labelled V-1 through V-4, and V-7. V-3 and V-4 were normally conducting; V-2 was normally non-conducting. V-7 supplied a fixed 75 volt bias to V-1, the trigger tube. Relay 1 was used to select either counter-controlled or periodic cycling. In the January 22 experiment it was operated energized, allowing the circuit to act as a freely-running multivibrator with a period of approximately 25 seconds. The period could be varied by adjusting the value of the resistance in the discharge path of the grid circuit of V-1. Provision was made to do this remotely by means of relay 3.

The typical sequence described in Section D was controlled by the electronics as follows. V-1 conducted, reversing the multivibrator and energizing relay 4 in the common plate circuit of the V-5 and V-6. This removed the clearing field and de-energized relay 5. The latter was a delay relay which opened about 0.05 seconds later, energizing relay 6. This action opened the expansion valve, closed the compression valve and, in turn, energized relay 7. When the diaphragm reached the proper point in the expansion, it mechanically closed a microswitch which, in turn, closed relay 9. The latter action connected the grid of V-8 to B+ through an r-c circuit. The cathode of V-8 was biased at +90 volts. Its grid reached approximately this level 0.15 seconds later and the tube conducted. The energy stored in the flash lamp condensers was thereby released, flashing the lamps. A second contact on relay 9 broke the B+ lead to prevent the circuit from oscillating.

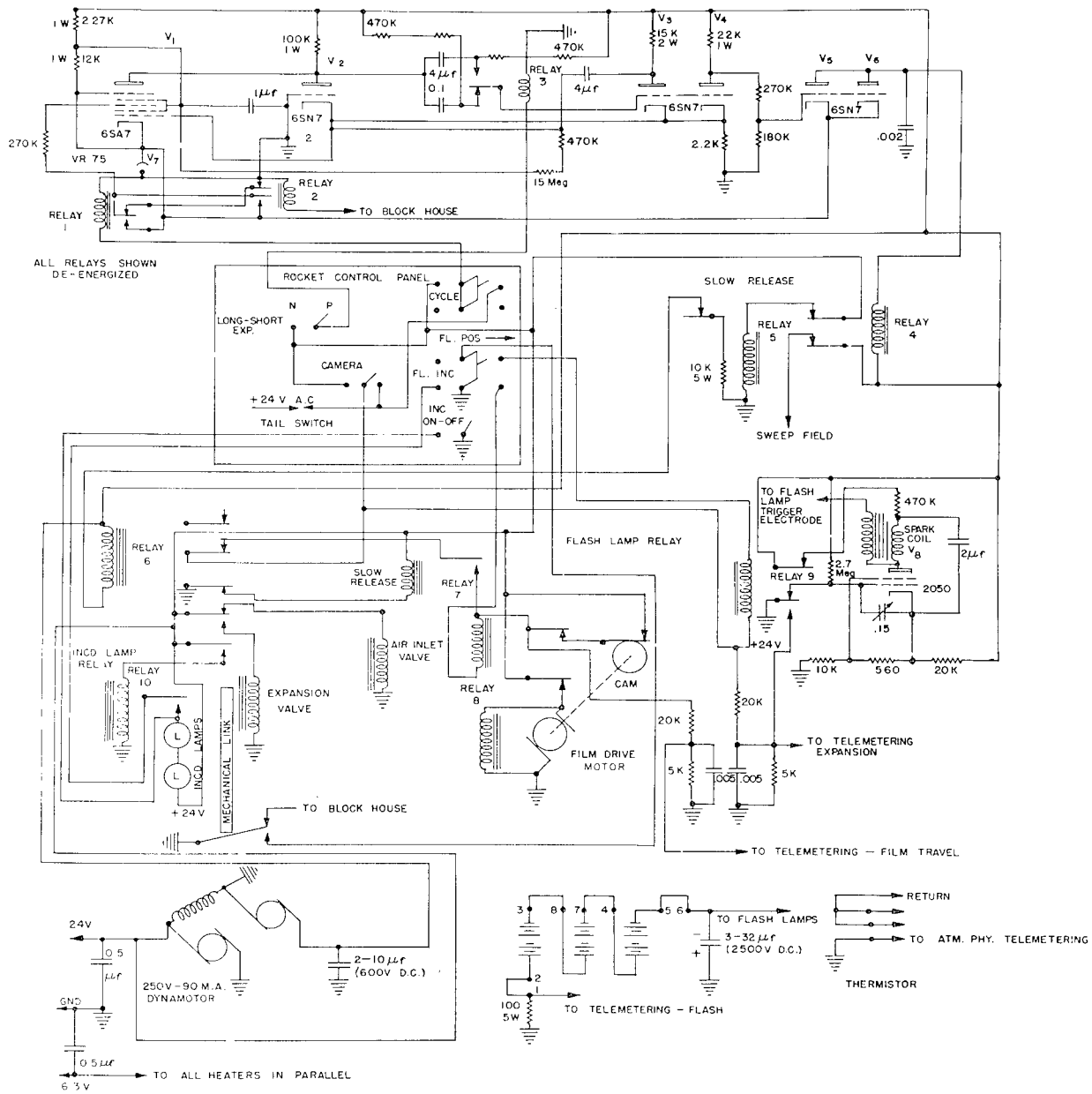


Fig. 38. Circuit diagram of the cosmic ray cloud chamber control electronics.

The control multivibrator returned to the normal state after a short period. Thereupon the cycle of events reversed. Relay 6 opened, closing the expansion valve and opening the compression valve. Relay 7 was a slow release relay, hence the opening of relay 6 also energized self-locking relay 8. This started the film winding motor. A switch at the camera broke the holding connection on relay 8 and stopped the motor at the proper time. The grid of V-1 then continued to rise toward +70 volts during the remainder of the cycle.

Indications that the chamber expanded, the lamps flashed and the film advanced in each cycle were telemetered to the ground station. A 100 ohm resistor in the grid return of the flash lamp batteries was used to furnish a positive voltage to telemetering during the charging of the flash storage condensers. Suitable dividers placed across relays 8 and 9 gave step-function indications while the film was advancing and the chamber was expanded, respectively.

The circuits permitted the manual operation of the cloud chamber during the testing periods before flight. Provisions were included for a longer expansion time, for disconnecting the camera motor, and for the use of continuous illumination (by means of ordinary incandescent lamps).

2. The Remote Control Equipment

The cloud chamber was more sensitive in its operation than most of the instruments used in the rocket studies. It was, therefore, particularly important that it be possible to assess its performance and make certain critical adjustments in the crucial period immediately before the firing. The nature of the rocket operations was such that these evaluations and adjustments had to be made remotely, for the most part. Accordingly, remote control equipment was built and installed to permit the study, operation and regulation of the cloud chamber from the blockhouse.

The apparatus consisted of a unit installed in the blockhouse, circuits in the rocket and a fourteen-conductor cable connecting them. The equipment is illustrated in Fig. 39. The cable entered the V-2 at a pull-away plug in the tail. A schematic diagram of the unit appears in Fig. 40.

Two switches on the console panel were connected to relay 2, making it possible to cycle the cloud chamber either once or continuously. The most important part of the remote equipment was the expansion control unit. This made it possible both to determine what the expansion ratio actually was, and to change its value. The mechanism controlling the expansion ratio also determined the setting of a potentiometer in the rocket. An identical potentiometer was mounted in the blockhouse remote control unit, and the two were fed from a common voltage supply. The two potentiometer arms were connected through sensitive directional relay 18, two opposite contacts of which were, in turn, connected to pilot lamps. When the two potentiometer arms had different settings, either one or the other of the pilot lamps would be lit; when they had identical settings, neither lamp would be lit. Thus the balance (or unbalance) of the potentiometer bridge circuit was

SECRET

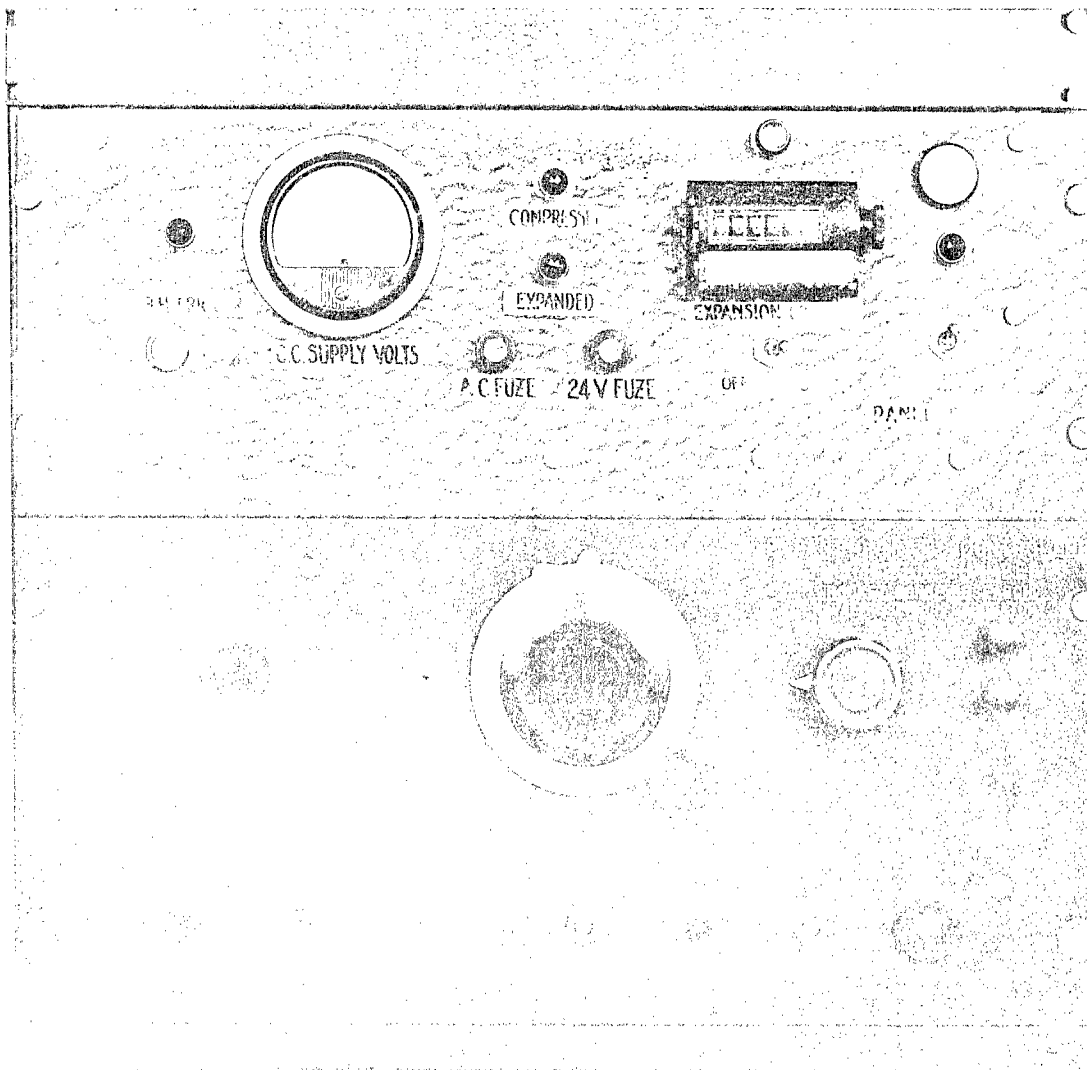


Fig. 39. The blockhouse unit of the cosmic ray cloud chamber remote control electronics.

reflected in the balance (or unbalance) of the relay and the pilot lamp indicating circuit. By moving the potentiometer arm in the blockhouse and observing the balance point as registered by the pilot lamps, it was possible to know, in the blockhouse, the expansion ratio setting in the V-2.

Remote adjustment of the expansion ratio was accomplished by means of the same circuit. The arms of relays 16 and 17 were also connected to a reversible d-c motor which drove the expansion ratio screw and indicating potentiometer through a gear train. When the relay was unbalanced, the motor could be started by a switch at the blockhouse station. The direction of rotation was determined by the relay and was always such as to decrease the difference between the settings of the two potentiometers of the bridge.

When the balance was re-established, the bridge relay assumed its neutral position. This opened the power circuit of the motor, stopping it automatically. Thus, it was possible for an operator in the blockhouse to cause either of the two bridge potentiometers to duplicate the setting of the other.

The remote control equipment also indicated, by means of relay-operated pilot lamps, whether the chamber was in the expanded or compressed state, and when it changed from one to the other. The unit included a counter which could be switched into the circuit to record the total number of expansions occurring after any given time. Provision was made for reading the temperatures at two points on the cloud chamber. Thermistors, embedded in the upper and lower rings of the chamber, were connected to the blockhouse where their resistances and the corresponding temperatures could be ascertained. The meter shown in Fig. 39 indicated the value of the voltage supplied to the equipment in the rocket.

Several error preventing provisions were incorporated in the remote control equipment. For example, the changing of the expansion ratio while the chamber was expanded might damage the gearing. Hence, power for the rocket expansion ratio control motor was supplied through relay 11, which was closed only when the chamber was in the compressed state.

The remote control equipment made it possible to make all the necessary adjustments to the cloud chamber from the blockhouse during the critical period immediately before the firing. The electronic control equipment installed in the rocket operated the cloud chamber automatically throughout the flight, and furnished indications via the telemeter of the satisfactory performance of the various key components.

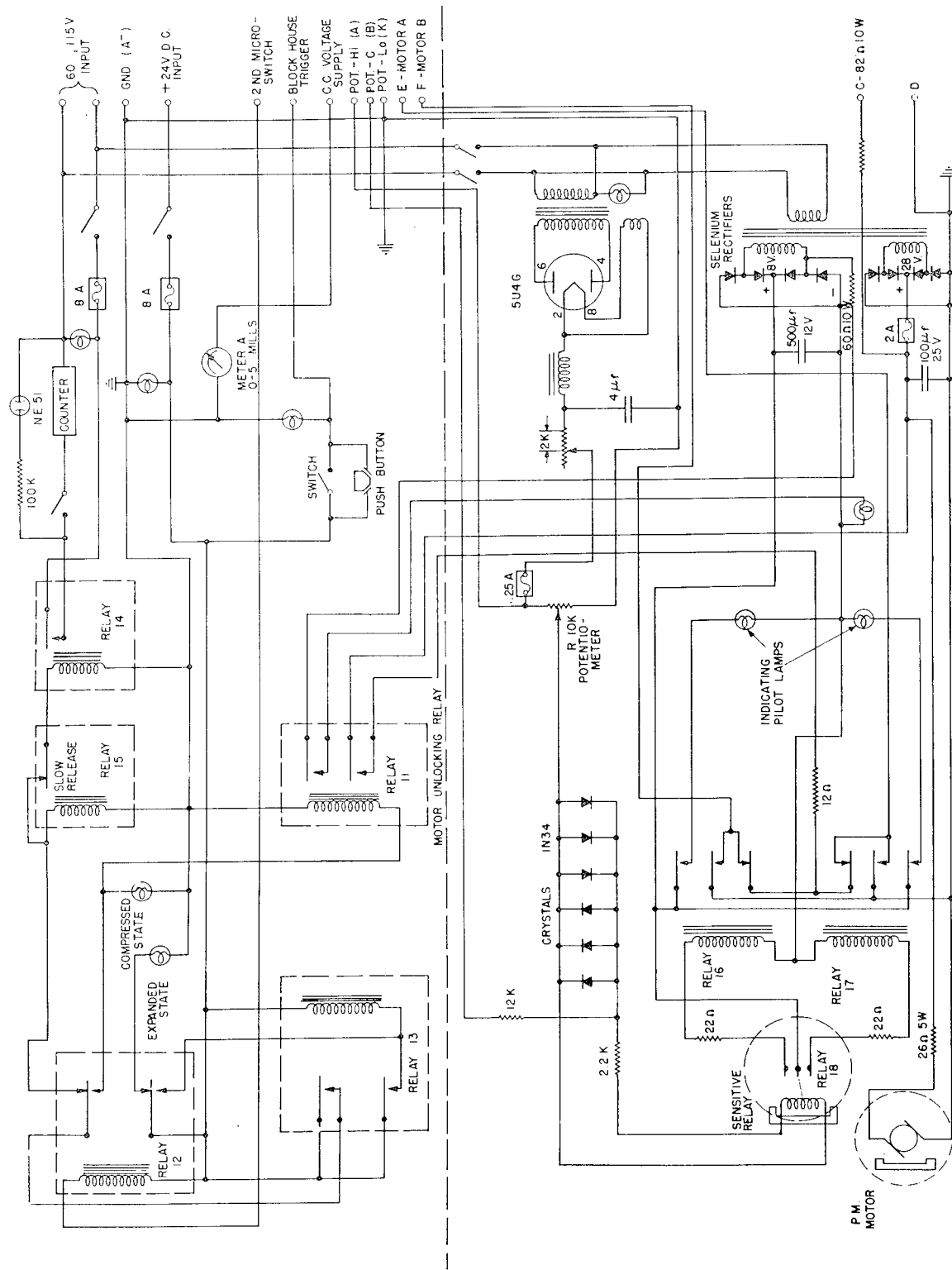


Fig. 40. Circuit diagram of the cosmic ray cloud chamber remote control electronics.

CHAPTER V

GEOMETRIC FACTORS UNDERLYING COINCIDENCE COUNTING WITH GEIGER COUNTERS*

by

Homer E. Newell, Jr.

The coincidence rate of a perfectly efficient two counter telescope embedded in an isotropic field of radiation is obtained in terms of the radiation intensity and the effective dimensions and separation of the counters comprising the telescope. By means of the formulas the counting rate may be located between an upper and a lower bound which in most practical cases differ by only a few percent. The information embodied in the formulas is also presented graphically in a form convenient for ready calculation of the ratio of coincidence rate to radiation intensity once the effective dimensions and separation of the two counters are known.

1. Introduction

The coincidence rate of a counter telescope depends not only upon the intensity of radiation in the surrounding space, but also upon the effective dimensions and efficiencies of the counters and upon their positions relative to each other. Formulas are obtained below which give the coincidence rate of a two counter telescope in terms of the various quantities listed above. It is assumed that the counters are identical right circular cylinders, the effective dimensions of which in practice are to be determined by appropriate calibration, and that the cylinders are placed parallel to each other with the line joining their geometric centers normal to the axes. By means of the formulas the counting rate may be located between an upper and a lower bound which in most practical cases differ by only a few percent. Curves are provided, by means of which the calculations may be effected graphically.

The formula for the counting rate N_2 may be put in the form

$$N_2 = GI,$$

where G is a factor depending upon the geometry of the telescope and upon the character of the radiation in which the telescope is embedded. In the case of an isotropic distribution of radiation, I is the intensity of the

*This was published in The Review of Scientific Instruments, Vol. 19, p. 384 (1948). Shortly after publication, however, an error was discovered in Figs. 5a and 5b. Corrected figures are given here.

radiation. If the radiation intensity varies with zenith angle ξ in accordance with a cosine squared law, then $I \cos^2 \xi$ is the radiation intensity. Only the former case is considered in the present paper. The latter case will be treated in a later paper.

2. Preliminary discussion

The drawing of Fig. 41 shows two orthogonal projections of a two counter telescope. As indicated, the counters are equal right circular cylinders. The projections on the left and right of Fig. 41 are made respectively onto planes parallel and normal to the axes of the counters. The axes $H_A' H_A'$ and $H_A'' H_A''$ are parallel to each other and normal to the line $C' C''$ joining the geometric centers of the cylinders. It is convenient to think of $C' C''$, or VV , as vertical, in which case $H' H'$, $H'' H''$ and the counter axes are all horizontal.

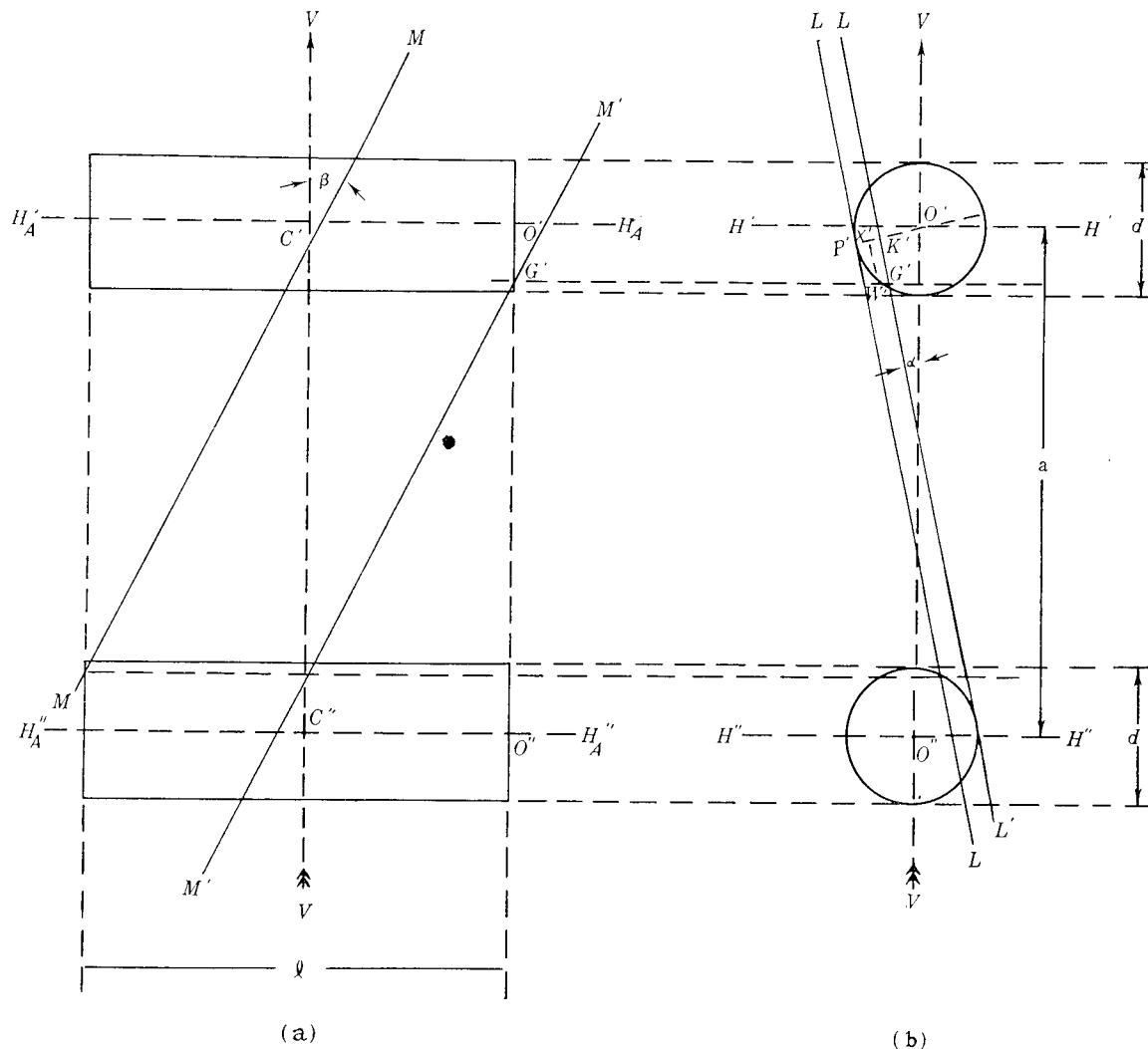


Fig. 41.

The four planes LL, L'L', MM and M'M' form the boundary of a prismatic tube as shown in Fig. 42, in which the labelling of Fig. 41 is retained. The parallelogram DEFG is a right section of the tube. On DEFG the two counters have a common projected area σ , labelled JEPG in the drawing.

Angles α and β uniquely specify the direction of the edges of the prismatic tube. Hence they likewise serve to fix the direction of rays which travel parallel to the edges of the tube. Assuming counter efficiencies of 100 percent, such rays give rise to coincidences if they travel within the tube and cross the area σ . By summing for a unit time all such rays corresponding to the different values of α and β between suitable limits, and correcting for inefficiency of the telescope, the coincidence rate of the telescope can be determined.

3. A formula for the coincidence rate

The number $e dN_2$ of registered coincidences per second caused by rays coming from a small solid angle $d\Sigma$ about the direction $[\alpha, \beta]$ is given by the relation

$$3.1) \quad e dN_2 = e I(\alpha, \beta) \sigma(\alpha, \beta) d\Sigma(\alpha, \beta),$$

where I is the radiation intensity, and where σ has the meaning assigned to it in the preceding section. The quantity $e dN_2$ is composed of the number dN_2 of rays traversing both counters multiplied by the efficiency e of the telescope. It is assumed that the telescope is adequately shielded against lateral irradiation, so that the number of registered coincidences is directly proportional to dN_2 .

Integration of dN_2 over a suitable range of values for α and β yields the number N_2 per second of rays which traverse both counters and come from a specified solid angle Σ . Generally, the last three factors on the right of 3.1) are functions of α and β , so that the expression for N_2 takes the form

$$N_2 = \int_{\Sigma} \int I \sigma d\Sigma.$$

When the radiation is isotropic, however, I is constant and may be removed from under the sign of integration. In such a case,

$$N_2 = I \int_{\Sigma} \int \sigma d\Sigma.$$

The integration in the above formula is carried out below to obtain the total coincidence rate of a perfectly efficient two counter telescope in a region of isotropic radiation. For this case the solid angle Σ includes all directions. The actual integration does not always extend over the complete sphere, however, since σ vanishes for all directions $[\alpha, \beta]$ for which no rectilinear path can traverse both counters of the telescope.

Moreover, the symmetry involved is such that the integration can be carried out over a single octant. Thus, finally, the expression for N_2 is

$$3.2) \quad N_2 = 8I \int_0^{\alpha_0} \int_0^{\beta_0} \sigma \, d\Sigma ,$$

where both α_0 and β_0 lie between zero and $\frac{\pi}{2}$.

4. The solid angle $d\Sigma$ in terms of α and β

To carry out the integration of 3.2) it is necessary first to express σ and $d\Sigma$ in terms of α and β . The latter may be so expressed simply by employing a suitable transformation from familiar spherical polar coordinates θ and ϕ , in terms of which

$$d\Sigma = \sin \theta \, d\theta \, d\phi .$$

Both sets of coordinates are shown as arcs on the sphere drawn in Fig. 42, from which it may be seen that

$$\theta = \operatorname{arccotn} (\cos \alpha \tan \beta)$$

$$\phi = \frac{\pi}{2} - \alpha .$$

It follows directly that

$$\frac{\partial (\theta, \phi)}{\partial (\alpha, \beta)} = - \frac{\cos \alpha}{1 - \sin^2 \alpha \sin^2 \beta} ,$$

and that

$$4.1) \quad \sin \theta = \frac{\cos \beta}{\sqrt{1 - \sin^2 \alpha \sin^2 \beta}} .$$

Finally, combining these, the expression for $d\Sigma$ is obtained:

$$4.2) \quad d\Sigma = \frac{\cos \alpha \cos \beta}{\left[1 - \sin^2 \alpha \sin^2 \beta \right]^{\frac{3}{2}}} \, d\alpha \, d\beta .$$

5. The area σ in terms of α and β

Fig. 43 combines the material depicted in Figs. 41 and 42 into a single three dimensional drawing. The labelling in Fig. 43 coincides with that of Figs. 41 and 42 wherever common elements appear. For example, in all three figures MM represents the same line. Similarly M'M', LL, L'L', H_A'H_A', H_A''H_A'', H'H', ... , are each permanently associated with a definite geometric entity.

The prismatic tube of Fig. 42 appears again in Fig. 43. In the latter case, however, both counters of the telescope are shown in the relationship they bear to the tube. As in Fig. 42 the right section of the tube is labelled DEFG. The "shadow" cast by the upper counter onto DEFG is DEFGD. It is obtained by orthogonal projection of D'E'P'G'K' onto DEFG. Similarly the shadow cast by the lower counter is FGJEF. The intersection of the two projections is JEPG, the area of which is the quantity σ of 3.2). For the discussion below it is convenient to express this area in the form

$$\sigma = \text{area (JQPK)} + 2 \times \text{area (PGK)}.$$

The quadrilateral JQPK is a rectangle the width PK of which is equal to P'K'. By reference to Fig. 41 it is readily verified that

$$P'K' = a (\delta - \sin \alpha), \quad \delta = \frac{d}{a}.$$

The length QP of the rectangle is given by

$$\begin{aligned} QP &= QT - PT \\ &= l \cos (\text{angle between } H_A''H_A'' \text{ and } QT) \\ &\quad - (\text{projection } PP'R''T \text{ onto } PT). \end{aligned}$$

With the aid of Fig. 42 it may be shown that the angle between H_A''H_A'' and QT is $\frac{\pi}{2} - \theta$. Also, PP' and R''T are both perpendicular to PT. Hence

$$QP = l \sin \theta - (\text{projection of } P'R'' \text{ onto } PT).$$

The angle between P'R'' and PT is θ , and P'R'' = a cos α . Using 4.1) it follows that

$$QP = l \sin \theta - a \cos \alpha \cos \theta,$$

$$5.1) \quad QP = a \frac{\Delta \cos \beta - \cos^2 \alpha \sin \beta}{\sqrt{1 - \sin^2 \alpha \sin^2 \beta}}, \quad \Delta = \frac{l}{a}.$$

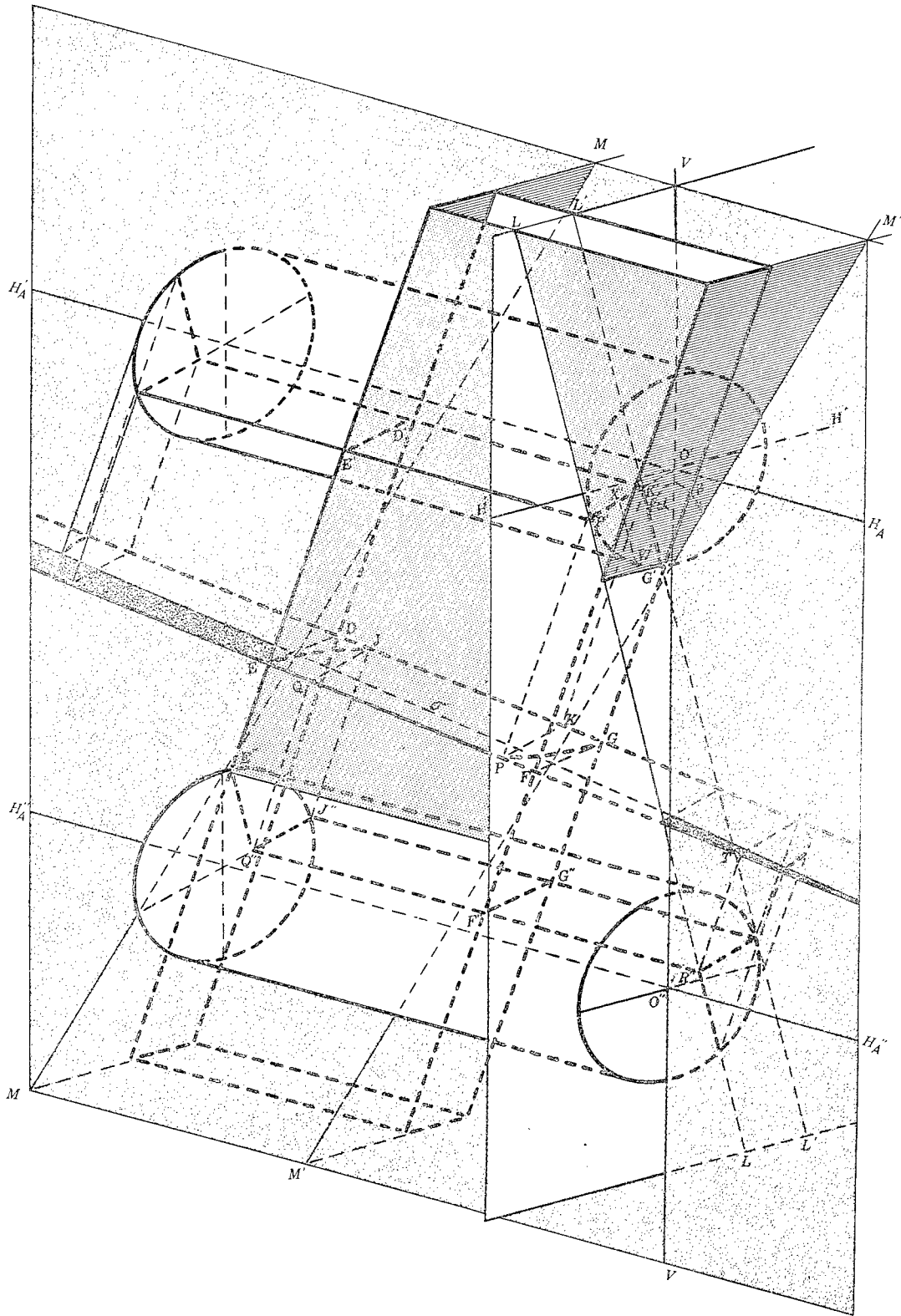


Fig. 43.

Thus

$$\text{area (JQPK)} = a^2 \frac{(\delta - \sin \alpha) (\Delta \cos \beta - \cos^2 \alpha \sin \beta)}{\sqrt{1 - \sin^2 \alpha \sin^2 \beta}}.$$

Twice the area (PGK) is the projection of twice the area (P'G'K') onto the plane of σ Hence

$$2 \times \text{area (PGK)} = 2 \times \text{area (P'G'K')} \cos \theta,$$

since the angle between $H_A'H_A'$ and the edge of the prismatic tube is θ , and since these are normal respectively to P'G'K' and PGK. Twice P'G'K' is simply a segment of height $d - a \sin \alpha$ cut from a circle of diameter d . The area of such a segment is easily obtained, and as a result

$$2 \times \text{area (PGK)} = a^2 \left[\frac{\delta^2}{4} \arccos \frac{2 \sin \alpha - \delta}{\delta} + \frac{1}{2} (\delta - 2 \sin \alpha) \sqrt{\delta \sin \alpha - \sin^2 \alpha} \right] \frac{\cos \alpha \sin \beta}{\sqrt{1 - \sin^2 \alpha \sin^2 \beta}}.$$

Finally

$$5.2) \quad \sigma = \frac{a^2}{\sqrt{1 - \sin^2 \alpha \sin^2 \beta}} \left\{ (\delta - \sin \alpha) (\Delta \cos \beta - \cos^2 \alpha \sin \beta) + \left[\frac{\delta^2}{4} \arccos \left(\frac{2 \sin \alpha - \delta}{\delta} \right) + \frac{1}{2} (\delta - 2 \sin \alpha) \sqrt{\delta \sin \alpha - \sin^2 \alpha} \right] \cos \alpha \sin \beta \right\}.$$

6. The limits of integration α_0 and β_0

The expression 5.2) for σ is not valid over the whole range of values for α and β . If α be fixed and β be made to increase from zero, the area σ changes as shown schematically in Figs. 44a - 44f. Starting as a rectangle, σ passes first into the form of 44a, then into that of 44b in which the rectangle QPKJ has collapsed into a line. As β continues to increase, line PK passes over QJ and the rectangle begins to increase in area again as shown in 44c. For the case depicted in Fig. 44c, σ is given by

$$6.1) \quad \sigma = \text{area (EQJ)} + \text{area (PGK)} - \text{area (QPKJ)}.$$

Note that the expression 5.1) for QP actually gives the length of QP with a negative sign in the cases depicted by Fig. 44c. As a consequence, 5.2) automatically passes over into 6.1) as PK crosses QJ.

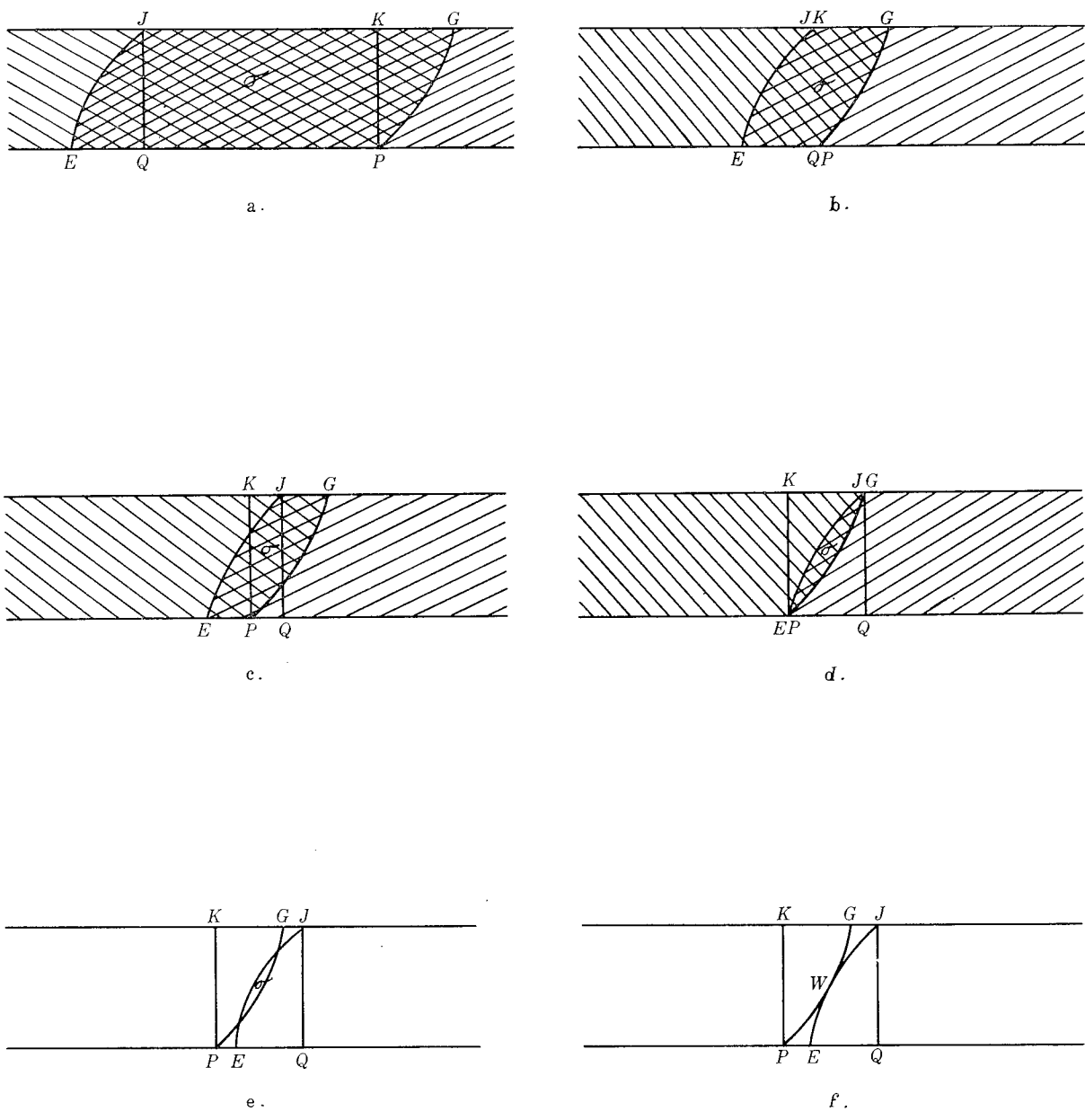


Fig. 44.

Formula 5.2) continues to be valid for σ until β has increased to such a magnitude β_1 , that P coincides with E, and J with G. For all β greater than β_1 , 5.2) no longer represents σ . As β increases beyond β_1 , P passes over E to its left, and σ takes the form shown in Fig. 44e, bounded by portions of the arcs \widehat{EJ} and \widehat{PG} . When \widehat{EJ} and \widehat{PG} have completely crossed over each other to become tangent as in Fig. 44f, σ vanishes and the corresponding value β_0 of β is the upper limit of integration in 3.2).

The integration limit α_0 is given by

$$6.2) \quad \alpha_0 = \arcsin \delta, \quad \delta = \frac{d}{a}$$

To obtain β_1 , simply set $QP + KG$ equal to zero and solve for β . It is to be remembered that QP is negative, whereas KG is positive. Thus

$$a \frac{\Delta \cos \beta_1 - \cos^2 \alpha \sin \beta_1}{\sqrt{1 - \sin^2 \alpha \sin^2 \beta_1}} + K'G' \cos \theta = 0.$$

Replacing $K'G'$ by

$$a \sqrt{\delta \sin \alpha - \sin^2 \alpha},$$

making use of 4.1), and solving:

$$6.3) \quad \beta_1(\alpha) = \text{arcctn} \left\{ \frac{\cos \alpha}{\Delta} \left[\cos \alpha - \sqrt{\delta \sin \alpha - \sin^2 \alpha} \right] \right\}, \quad \Delta = \frac{0}{a}.$$

Finally, β_0 can be determined with the aid of Fig. 44f. From symmetry considerations it is plain that W , the point of tangency of \widehat{EJ} and \widehat{PG} , is the geometric center of the rectangle $PQJK$. The length of PQ is, therefore, twice the length of $X'W'$ projected onto the right section of the prismatic tube, where X' is the midpoint of $P'K'$, $X'W'$ is parallel to $K'G'$, and W' lies on the arc $P'G'$. Thus

$$a \frac{\cos^2 \alpha \sin \beta_0 - \Delta \cos \beta_0}{\sqrt{1 - \sin^2 \alpha \sin^2 \beta_0}} = a \frac{\cos \alpha \sin \beta_0 \sqrt{\delta^2 - \sin^2 \alpha}}{\sqrt{1 - \sin^2 \alpha \sin^2 \beta_0}},$$

$$6.4) \quad \beta_0(\alpha) = \text{arcctn} \left\{ \frac{\cos \alpha}{\Delta} \left[\cos \alpha - \sqrt{\delta^2 - \sin^2 \alpha} \right] \right\}.$$

7. The coincidence rate of the two counter telescope

Rewrite 3.2) as follows:

$$N_2 = 8I \left\{ \int_0^{\alpha_0} \int_0^{\beta_1} \sigma \, d\Sigma + \int_0^{\alpha_0} \int_{\beta_1}^{\beta_0} \sigma \, d\Sigma \right\}$$

Let N_{2m} and N_{2M} be given by

$$7.1) \quad N_{2m} = 8I \int_0^{\alpha_0} \int_0^{\beta_1} \sigma(\alpha, \beta) \, d\Sigma$$

and

$$7.2) \quad N_{2M} = N_{2m} + 8I \int_0^{\alpha_0} \int_{\beta_1}^{\beta_0} \sigma(\alpha, \beta_1(\alpha)) \, d\Sigma,$$

where $\sigma(\alpha, \beta)$ is given by 5.2).

The information collected in the foregoing sections makes it possible to write N_{2m}/a^2I and N_{2M}/a^2I as functions of δ and Δ , where $\delta = \frac{d}{a}$ and $\Delta = \frac{l}{a}$. This may be seen by reference to 4.2), 5.2), and 6.2)-7.2).

The integration of 7.2) has been carried through numerically for the various values of δ and Δ . Fig. 45 presents the results graphically in the form of a plot of N_{2M}/a^2I versus δ for a number of values of Δ .

The quantity N_{2M} exceeds the actual coincidence rate N_2 , but by a relative error no greater than

$$E = \frac{N_{2M} - N_{2m}}{N_{2m}}.$$

A plot of $100E$ versus δ appears in Fig. 46.

8. Acknowledgement

The author wishes to express his thanks to Miss Eleanor Pressly for performing the numerical integrations of the present paper.

UNIVERSITY MICROFILMS

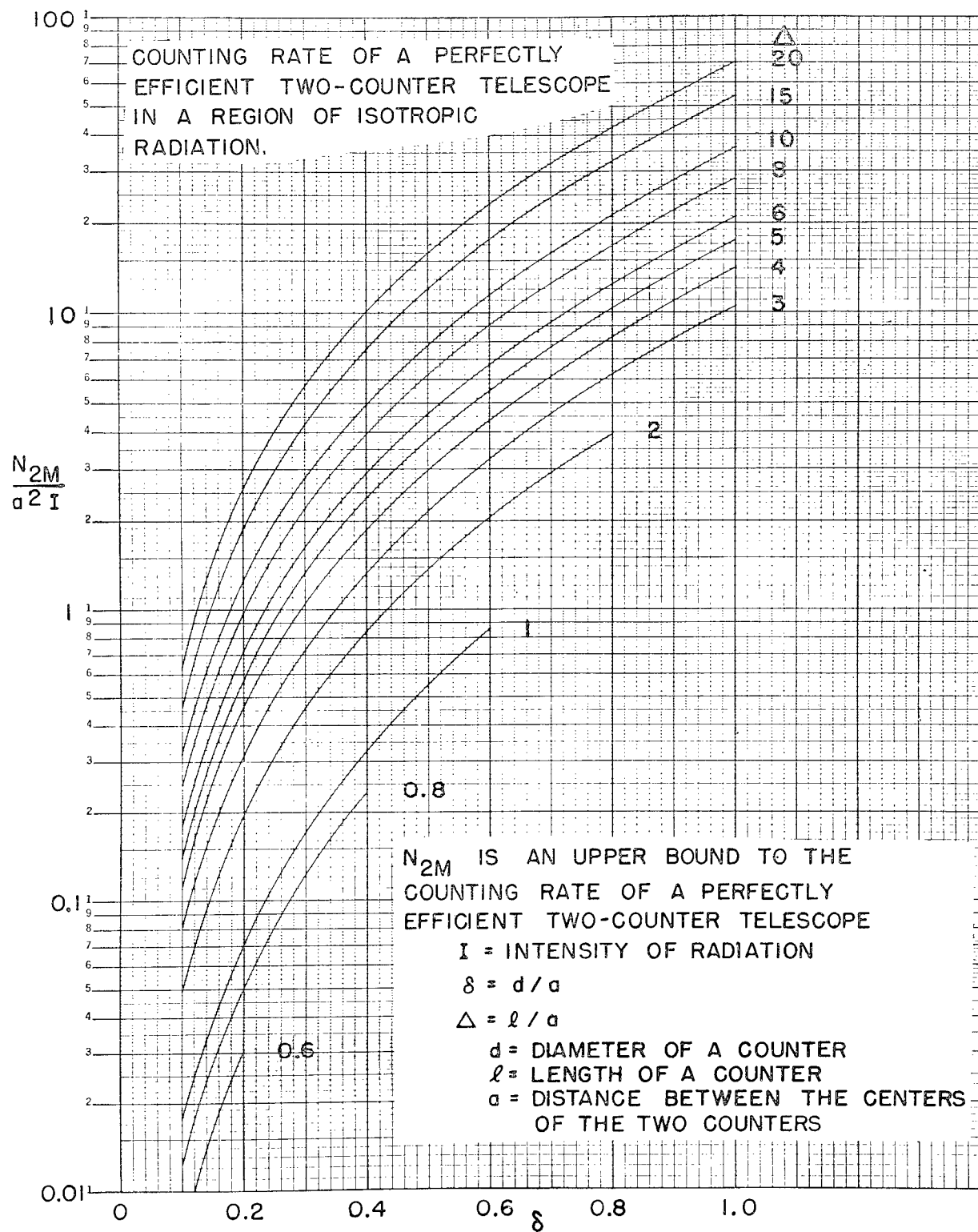


Fig. 45a.

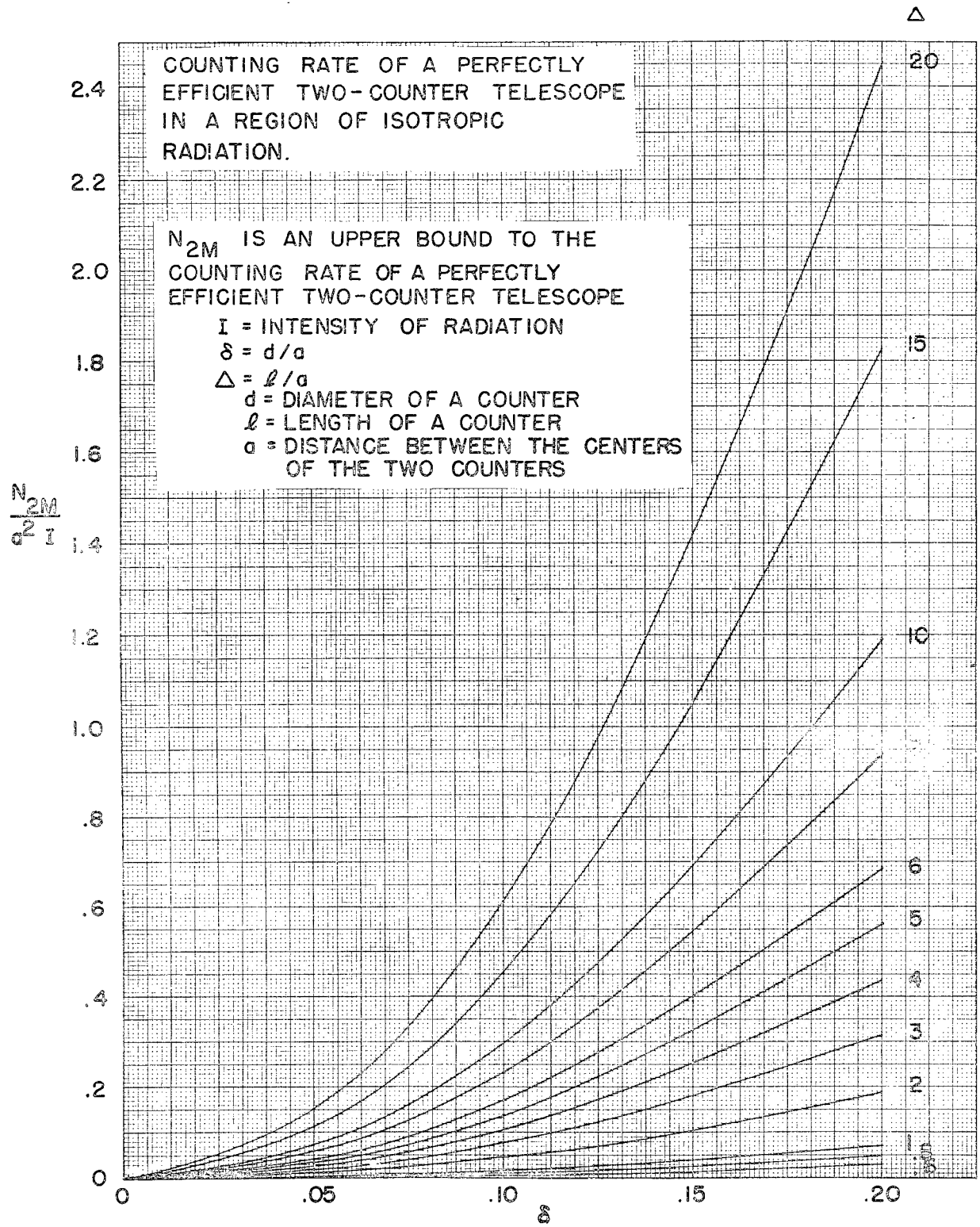


Fig. 45b.

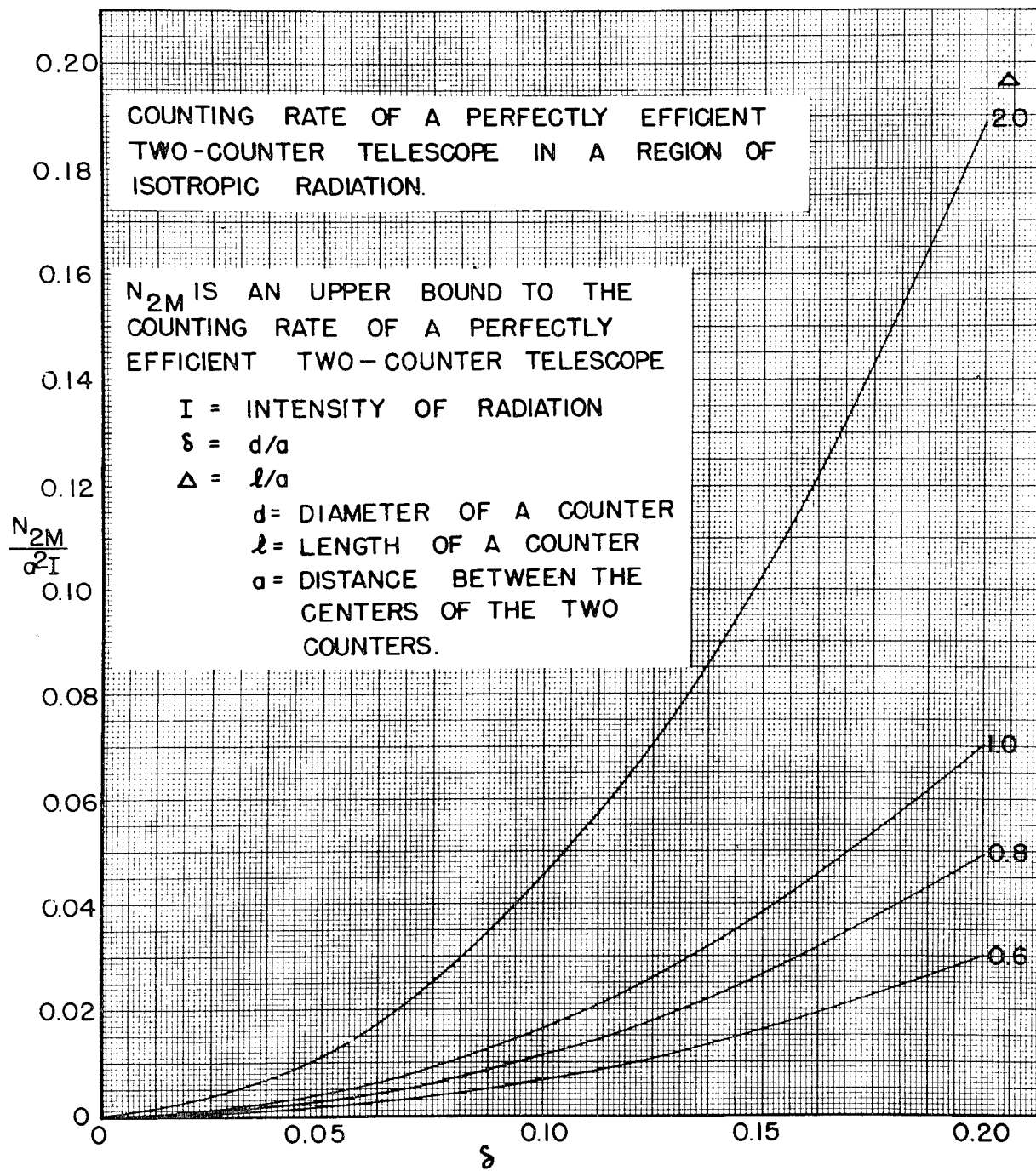
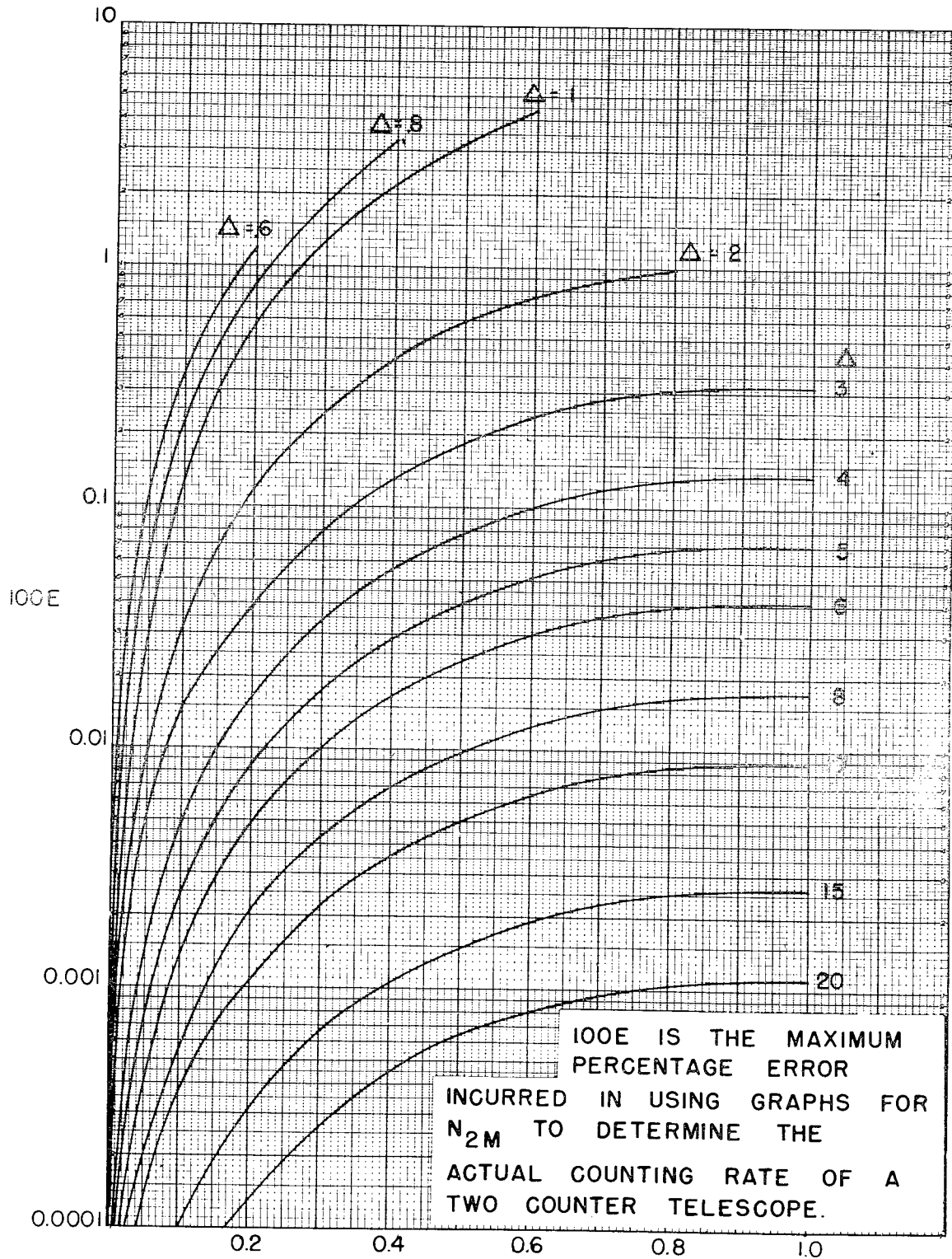


Fig. 45c.



δ

Fig. 46.



CHAPTER VI

ATMOSPHERIC STUDIES AT VERY HIGH ALTITUDES

Introduction

The section's program for the study of the upper atmosphere yielded results up to altitudes of 120 kilometers during the first four cycles of V-2 firings.¹ Further measurements of the pressures in the upper atmosphere were attempted in the V-2 flights of May 15, and July 10, 1947 and January 22, 1948. The first of these rockets exploded prematurely at about 33 kilometers altitude. As a result, no data were obtained in the region of interest above balloon altitudes. The measurements which were made up to 33 kilometers did agree within experimental error with balloon measurements which were made fifteen minutes after the rocket flight. This served as another check on the validity of some of the rocket techniques. The maximum altitude reached by the July 10 V-2, cut down for safety reasons, was only 16 kilometers. While the flight contributed little of direct value to the atmospheric studies, it did serve as the first test of a new wire accelerometer. This instrument is described in Section A. On January 22, for the first time, measurements of atmospheric pressure were made in the winter season at very high altitudes. These midwinter readings are discussed in Section B. They are also compared there with data obtained in previous rocket studies.

¹Cf. Naval Research Laboratory Report No. R-2955, Chapter III, Sections D and E; Naval Research Laboratory Report No. R-3030, Chapter IV, Section B; and Naval Research Laboratory Report No. R-3171, Chapter VII.

CHAPTER VI

ATMOSPHERIC STUDIES AT VERY HIGH ALTITUDES

A. A Wire Accelerometer

by

R. J. Havens and H. E. LaGow

A wire accelerometer was installed in the July 10, 1947 V-2 in order to measure the accelerations experienced by the rocket during the burning period, and to determine as accurately as possible when Brennschluss occurred. Commercial instruments usually employ amplifiers and are not designed to withstand the vibrations and temperatures encountered in a rocket flight. The wire accelerometer was chosen for this application since it was simpler and more rugged, and its time constant (0.5 seconds) was short enough to allow reasonably accurate measurements, yet long enough to filter out the rocket vibrations.

The instrument's principle of operation is simple. Under the proper circumstances, heat is exchanged between a wire and a gas of different temperature by means of convection currents. In general, such currents will exist only in the presence of a field of the gravitational type. The rate at which heat is exchanged is a function of the rate at which the gas is accelerated relatively to the wire. The resistance of the wire is, in turn, a function of its temperature.

The instrument used in the July 10 rocket consisted of a 1 mil platinum wire which was mounted coaxially with a brass cylinder. The cylinder was 6 cm long, had an inner diameter of 1.5 cm, and was sealed at both ends. The chamber contained air at atmospheric pressure. This unit was placed in series with a 94 ohm dropping resistor across a 24 volt battery. The resistance of the platinum wire element, and the voltage drop across it, were functions of the relative accelerations of the wire and the air molecules within the cylinder. This voltage was telemetered to earth.

The instrument was calibrated directly, by means of a centrifuge, for values of the acceleration which lay between 1 g and 8 g. An indirect calibration method was used for accelerations less than 1 g. The wire was maintained at a temperature 300° C above ambient. The resistance was measured at several pressures between 1 atmosphere and 0.5 atmospheres. The radiation and conduction losses were sensibly constant since the temperature difference was constant. The convection losses decreased with the pressure, however. The corresponding curve was extrapolated to zero pressure to furnish an estimate of the resistance of the wire in the absence of convection losses.

The wire accelerometer has several features which render it particularly useful for rocket studies. It does not require an amplifier. It is small, reasonably rugged, and easy to construct and install. Its sensitivity can be increased by filling the cylinder with heavier gases (e.g. argon) at higher pressures. The qualitative data obtained with the accelerometer during the July 10 flight indicate that these advantages are real and that the instrument will perform satisfactorily in the V-2.

CONFIDENTIAL

CHAPTER VI

ATMOSPHERIC STUDIES AT VERY HIGH ALTITUDES

B. The Pressure and Temperature of the Upper Atmosphere on January 22, 1948

by

N. R. Best, D. I. Gale, R. J. Havens
and H. E. LaGow

Pressure measurements were made between the altitudes of 23.9 and 128 kilometers during the January 22 V-2 flight. A considerable number and variety of pressure gages were used in the experiment. The instruments were similar in design and construction to those employed on October 10, 1946 and March 7, 1947.²

Nine of the pressure gages operated satisfactorily and gave good data during the flight. The locations and the pressure ranges of these gages were as follows:

<u>Gage</u>	<u>Pressure Range</u> <u>in mm Hg</u>	<u>Location</u> ³
Pirani	30 - 10	Tail fin I
Pirani	10 - 5	Tail fin I
Pirani	10 - 5	Tail fin III
Pirani	2 - 0.2	Tail fin I
Pirani	2 - 0.2	Tail fin III
Pirani	10^{-1} - 10^{-2}	Tail fin I
Pirani	10^{-1} - 10^{-2}	Tail fin III
Philips	10^{-3} - 10^{-5}	Warhead base
Philips	10^{-3} - 10^{-5}	Warhead base .

²Cf. Naval Research Laboratory Report No. R-2955, Chapter III, Sections D and E; Naval Research Laboratory Report No. R-3030, Chapter IV, Section B; and Naval Research Laboratory Report No. R-3171, Chapter VII.

³The Pirani gages were mounted on a circumference of the rocket 15 centimeters forward of the leading edge of these fins. One of the Philips gages was mounted in the half-plane of tail fin II, the other was mounted in the half-plane of fin IV. The access apertures may be seen in Fig. 14. The warhead surface was truncated conical in this region, the elements making an angle of 11° with the missile axis.

Ionization gages were also mounted on the same circumference as the Philips gages (cf. Fig. 14, Chapter III, Section A). Had the former gages operated, each of the types would have served as a check on the other. The ionization gages were sealed in the Laboratory to prevent the filaments from oxidizing at the relatively high pressures obtaining in the lower atmosphere. The seals were to have been broken at the proper altitude by an automatic device in the rocket. Only one of the seals was broken. The exposed gage gave pressure readings which were much too high, however. This may have been due to air escaping from the warhead into the gage chamber.

The interpretation of the data is made difficult by the fact that the rocket motion after Brennschluss contained an unusual amount of yaw and pitch. The actual motion is not known precisely as yet; hence the results presented here are provisional, particularly for the altitudes above 70 kilometers.

The rocket had a 29 second roll period after Brennschluss. Because of this, the readings of any particular gage of a pair mounted on opposite sides of the rocket were duplicated approximately 14.5 seconds later by the other gage of the pair. The two gave the same readings at certain times during the flight. At certain of the quadrature times, however, the readings of such a pair actually differed between themselves by a factor of 500. This was due to the yaw and pitch of the rocket. The erratic, and as yet not completely known, rocket motion has made it impossible to relate accurately the pressures read at the crossover points to ambient pressures. Estimates of the true pressures may be made, however, on the following basis. The Taylor-Maccoll theory asserts that pressures along a cone are greater than ambient by a factor depending upon the cone angle and the relative velocities involved. The factor appropriate to this experiment was 1.5, provided that the rocket's axis and velocity vector were collinear. This was obviously not the case when gages of a diametrically opposed pair were not reading equal pressures. Therefore the factor was less than 1.5, at crossover points, due to the decrease in ram pressure. During descent observed pressures could be greater or less than ambient by as much as 50%, since the rocket might have been falling either nose first or tail first.

The January 22 V-2 took off at 1:12 P.M., M.S.T. The pressures observed during this flight are shown in Table V and Fig. 47. The considerations of the previous paragraph were not applied in detail to these results since rocket aspect was not known as a function of time. The data were corrected for the time lags of the gages, however. The errors indicated are those associated with the gages themselves and with the interpretation of the telemetering record. Altitudes were determined from radar information and are accurate to about 0.5 km. The points shown at altitudes above 90 kilometers were derived from the Philips gage measurements made at the times when both gages of a diametrically opposite pair read alike. The last three pressures listed were measured while the rocket was descending. For comparison purposes, the pressure curve drawn from the March 7 data is shown in Fig. 47, and values taken from it are given in Table V.

TABLE V

Pressures Observed on March 7, 1947 and January 22, 1948

Altitude in km	Pressure in mm Hg as measured on		Altitude in km	Pressure x 10 ³ in mm Hg as measured on	
	Mar. 7, 1947	Jan. 22, 1948		Mar. 7, 1947	Jan. 22, 1948
1.2	657*	650*	64.6	130	105 ± 5
3.6		490*	65.9		91 ± 5
7.3		300*	67.2	93	76 ± 5
9.4		220*	68.5		60 ± 5
10.7		180*	69.7	62	44 ± 5
12.5		137*	71.0	48	35 ± 3
13.8	106*	112*	72.3	36	30 ± 3
14.4		96*	92.0		1.4 ± 0.03
16.1		77*	112	0.1	0.14 ± 0.01
16.8	66	69*	121	0.035	0.03 ± 0.01
17.7		49*	128		0.005 ± 0.002
20.0	44	41*	118		0.017 ± 0.002
21.7		30*	104		0.29 ± 0.002
22.3		28*			
23.9		27 ± 4			
25.0		20 ± 3			
25.7		14 ± 3			
30.7		7.4 ± 0.4			
31.9		6.3 ± 0.3			
33.0		4.9 ± 0.3			
40.5		2.0 ± .1			
42.0		1.6 ± .1			
43.4		1.33 ± .1			
44.8		1.18 ± .08			
46.3		1.03 ± .05			
47.7	0.88	0.85 ± .05			
49.2		0.80 ± .05			
50.6	0.65	0.65 ± .05			
52.0		0.57 ± .05			
53.4	0.47	0.50 ± .05			
54.8		0.42 ± .04			
56.2		0.31 ± .04			
57.6		0.24 ± .04			

*These pressures were measured from balloons. All other pressures given in this table were measured from V-2 rockets.

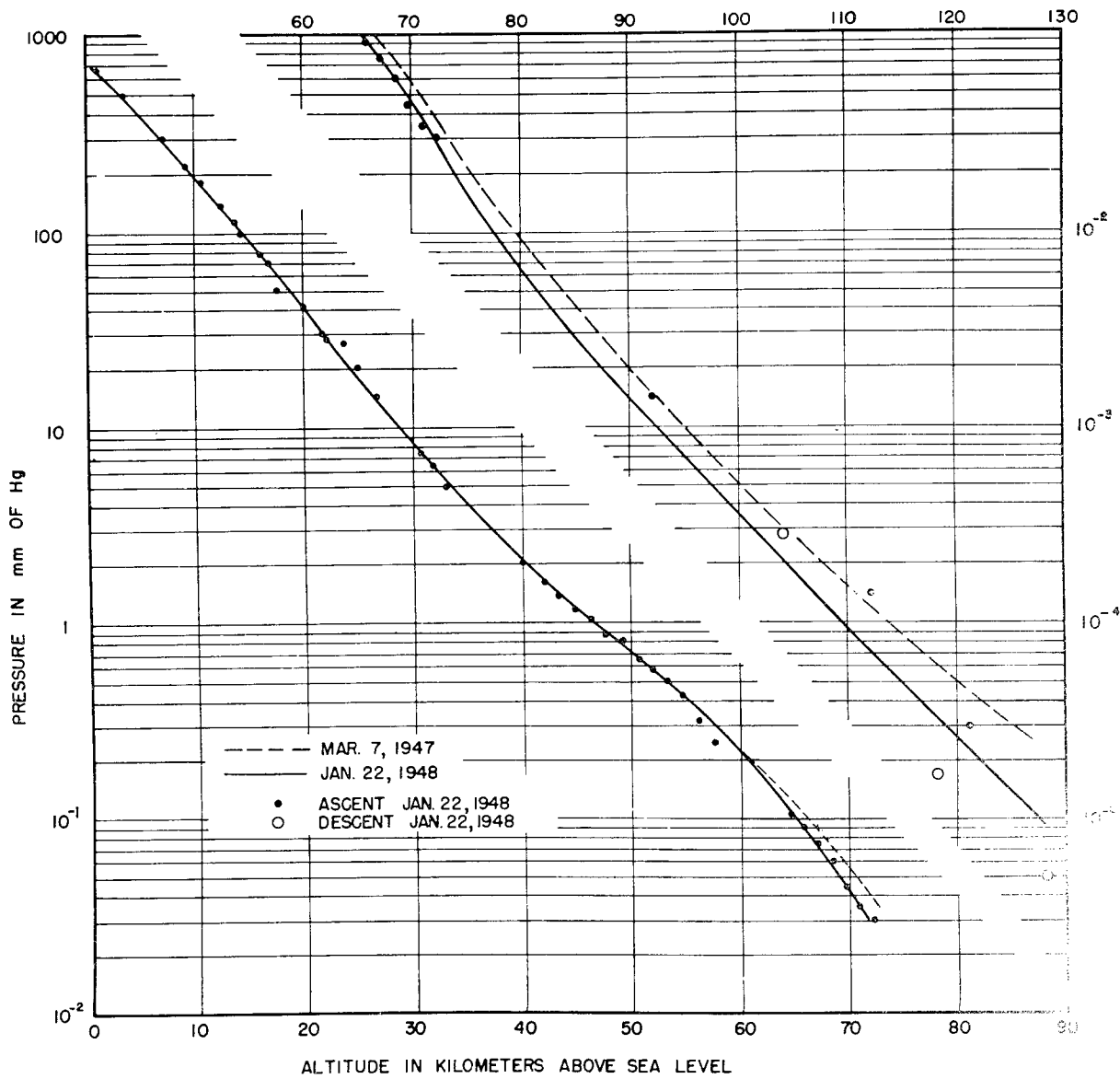


Fig. 47. Pressure as a function of altitude as measured on March 7, 1947 and January 22, 1948.

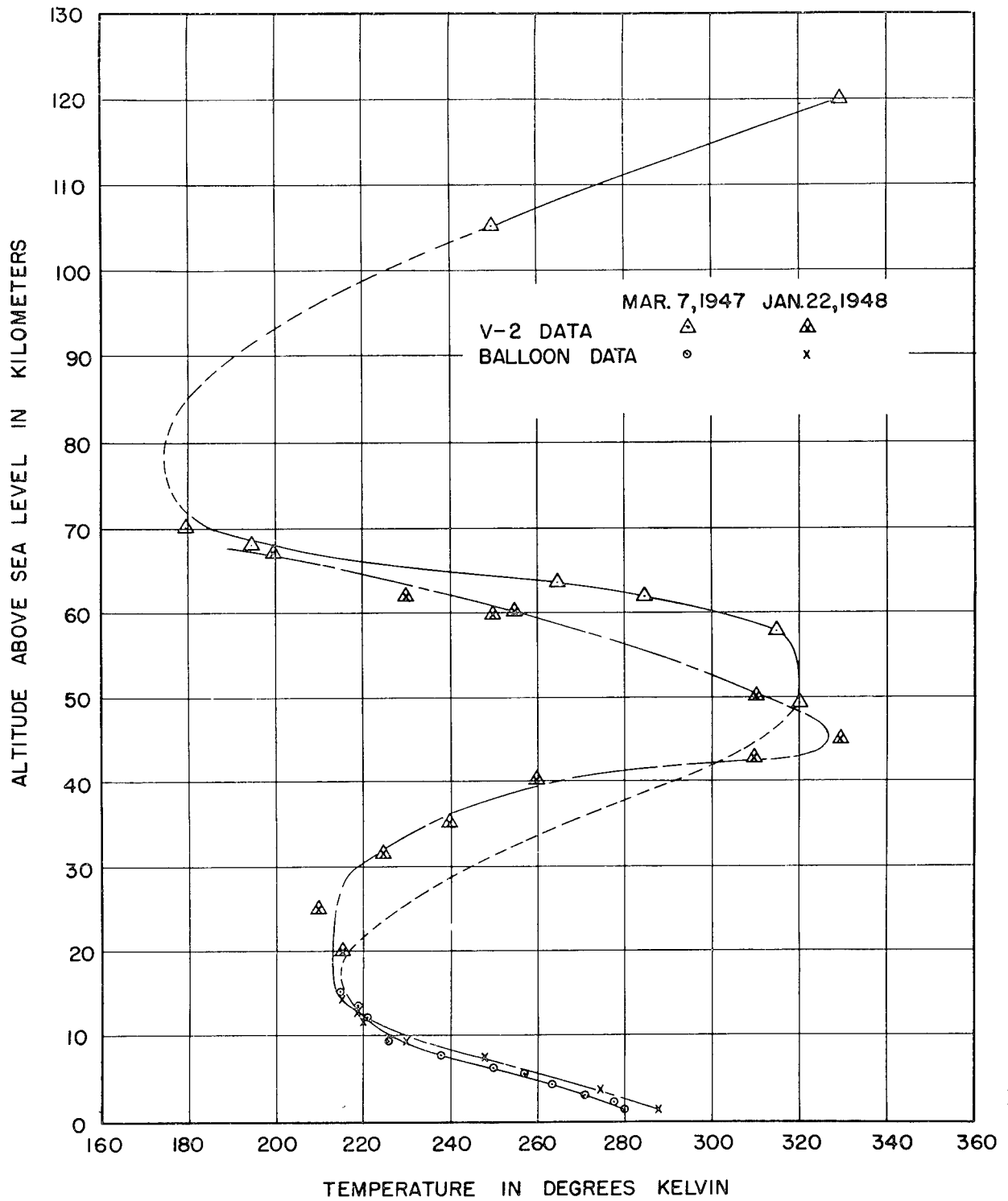


Fig. 48. Temperature as a function of altitude as observed on March 7, 1947 and January 22, 1948.

Two balloons equipped to measure pressures were also released on January 22, one at 7:45 A.M., M.S.T., the other at 1:45 P.M., M.S.T. The latter balloon read pressures up to 14.4 kilometers altitude; the former to 22.3 kilometers altitude. These values are also given in both the table and the figure, together with the results of similar balloon measurements made within an hour of the March 7, 1947 V-2 flight.

Temperatures were determined from the variation of pressure with altitude by means of the following formula:

$$T = \frac{g(H_2 - H_1)}{R \left(\ln \frac{P_1}{P_2} \right)}$$

where P_1 and P_2 were the pressures at altitudes H_1 and H_2 , respectively, and both T and g were referred to the arithmetic mean of these two altitudes. The atmospheric composition at sea level was assumed throughout in the temperature calculations. The temperatures obtained in this way are plotted in Fig. 48. Values for March 7, 1947 are also given. The January 22, 1948 data were insufficient to allow the calculation of temperatures for the strata above 70 kilometers. The mean temperature per kilometer of altitude in the region between 75 and 120 kilometers was calculated, however, and found to be 230° K.

